



Study title:

**Airborne LiDAR Reflective Linear Feature  
Extraction for Strip Adjustment and  
Horizontal Accuracy Determination**

Authors:

Charles Toth<sup>1</sup> and Dorota A. Grejner-Brzezinska<sup>2</sup>  
Center for Mapping<sup>1</sup>  
Department of Civil and Environmental Engineering and  
Geodetic Science<sup>2</sup>  
The Ohio State University

Sponsor name:

Ohio Department of Transportation, Office of Aerial  
Engineering

Prepared in cooperation with the Ohio Department of  
Transportation and the U.S. Department of  
Transportation, Federal Highway Administration

1. Report No. <b>FHWA/OH-2008/15</b>	2. Government Accession No.	3. Recipient's Catalog No.	
4. Title and subtitle <b>Airborne LiDAR Reflective Linear Feature Extraction for Strip Adjustment and Horizontal Accuracy Determination</b>		5. Report Date <b>February 2009</b>	
7. Author(s) <b>Dr. Charles Toth and Dr. Dorota Brzezinska</b>		6. Performing Organization Code	
9. Performing Organization Name and Address <b>The Ohio State University Research Foundation 470 Hitchcock Hall 2070 Neil Ave. Columbus, Ohio 43210-1275</b>		8. Performing Organization Report No.	
12. Sponsoring Agency Name and Address <b>Ohio Department of Transportation 1980 West Broad Street Columbus, Ohio 43223</b>		10. Work Unit No. (TRAIS)	
15. Supplementary Notes		11. Contract or Grant No. <b>134316</b>	
16. Abstract		13. Type of Report and Period Covered	
17. Key Words		14. Sponsoring Agency Code	
18. Distribution Statement No restrictions. This document is available to the public through the National Technical Information Service, Springfield, Virginia 22161			
19. Security Classif. (of this report) Unclassified	20. Security Classif. (of this page) Unclassified	21. No. of Pages	22. Price



Project title:

**Airborne LiDAR Reflective Linear Feature  
Extraction for Strip Adjustment and  
Horizontal Accuracy Determination**

SJN: 134316

Authors:

Charles Toth and Dorota A. Grejner-Brzezinska

Research Agency:  
The Ohio State University

Report date: June 2008  
Revision date: February 2009

Sponsoring Agency  
Ohio Department of Transportation, Office of Aerial  
Engineering

Prepared in cooperation with the Ohio Department of  
Transportation and the U.S. Department of  
Transportation, Federal Highway Administration



## **Disclaimer**

The contents of this report reflect the views of the authors who are responsible for the facts and the accuracy of the data presented herein. The contents do not necessarily reflect the official views or policies of the Ohio Department of Transportation or the Federal Highway Administration. This report does not constitute a standard, specification or regulation.



## Acknowledgments

The authors thank the staff of the ODOT Office of Aerial Engineering for their contributions to this project. In particular, we want to express our gratitude to John Ray, Administrator, Office of Aerial Engineering, for his continuing support and coordination of the system acquisition and the field testing. The authors greatly appreciate the support of Lewis Graham, CEO from GeoCue Corporation, for his collaboration on the interface design and implementation.



## Table of Content

1. Introduction.....	8
2. Research objectives.....	10
3. General description of research.....	11
3.1. LiDAR Strip Adjustment.....	11
3.2. Coordination of concept development and implementation .....	14
3.3. Research Developments to Support OAE LiDAR Operations .....	15
4. Results.....	15
4.1. Curve fitting .....	18
4.2. Curve Matching .....	24
4.3. Pavement Markings Extraction .....	31
4.4. Performance Assessment.....	40
4.5. Software Developments .....	40
5. Conclusions.....	40
6. Implementation plan.....	41
Bibliography.....	42
Appendix A: Publications.....	43
1. Using Pavement Markings to Support the QA/QC of LiDAR data.....	44
2. Quality Assessment of LiDAR Data by Using Pavement Markings.....	50
3. Using Road Pavement Markings as Ground Control for LiDAR Data.....	60
Appendix B: Project Review Presentation.....	66
Appendix C: FMAS Interface Design, .....	85
Appendix D: Software Developments.....	120



## List of Figures and Tables

1. Figure 1. Strip discrepancies observed from four strips.	12
2. Figure 2: Multiple strip overlap (cross-strips at different flying height); square marks building area shown in Fig 1.	12
3. Figure 3. Pavement markings at an intersection in various sensor data; (a) 4k by 4k digital image (orthorectified), (b) LiDAR intensity (gridded), and (c) LiDAR elevation (gridded).	17
4. Figure 4. The curve fitting is done in local coordinate systems, with varying length segments defined on basis that it has only limited curvature; the local coordinate system is oriented to main direction of the segment.	19
5. Figure 5. Piecewise weighted least squares curve fitting method.	20
6. Figure 6. Transfer of slope at connection points.	21
7. Figure 7. Weight based on intensity values.	23
8. Figure 8. Curve fitting to LiDAR and control points.	23
9. Figure 9. Matching straight lines.	26
10. Figure 10. Matching third-order curve from two different positions, (a) and (b).	27
11. Figure 11. Matching a sine wave.	27
12. Figure 12. The effect of point sampling on ICP.	29
13. Figure 13. ICP matched curves; magenta: curves fitted to control points, red: GPS control points, cyan: LiDAR point and curves fitted, and blue: matched points. Change figure for usual intersection figure.	30
14. Figure 3. Histogram distribution of LiDAR intensity values in small area containing pavement markings.	31
15. Figure 4. The separation of pavement markings using different LiDAR intensity thresholds.	32
16. Figure 16. Using a locally optimal threshold in a nearly ideal situation; thresholded image is shown in (a), and the histogram of the original LiDAR intensity data is shown in (b).	33
17. Figure 17. Histograms of various pavement areas; (a-f) concrete and (g-h) asphalt surface.	35
18. Figure 18. Histograms of various grassy and soil areas.	36
19. Figure 19. Data processing block diagram of extracting LiDAR points of pavement markings.	37
20. Figure 20. Mean residuals as a function of the intensity threshold.	38
21. Figure 21. Number of selected points vs. the intensity threshold.	39
22. Figure 22. Extracted pavement marking LiDAR points.	39



## 1. INTRODUCTION

The introduction of airborne LiDAR (Light Detection and Ranging) in the late nineties was followed by a quick proliferation of the technology, and LiDAR is now the primary surface data extraction mapping technique. This remarkable success is mainly due to the fact that LiDAR data are explicit and the processing can be highly automated. Consequently, almost no human intervention is required and the turnaround time is very short. The quality of the LiDAR product is excellent as compared to most of the surface datasets collected in the past. These factors largely contributed to the fast market acceptance of the LiDAR technology.

Early production experiences for most users, however, usually show similar patterns and bring up comparable questions. The two most widely discussed topics in this regard are the horizontal accuracy and the desire to further improve the vertical accuracy. In addition, users generally lack the availability of powerful and user-friendly standardized and widely used software packages; something typical to the conventional large-format aerial camera-based photogrammetry market. This is due to the relative newness of the LiDAR technology, although there are already a few emerging products, such as TerraScan and GeoQue, which are expected to fill the current gap. Therefore, users with stronger in-house R&D capabilities frequently develop their own LiDAR data processing utilities.

The horizontal accuracy of the LiDAR data was not a concern in the early use of this technology. The fact that unprecedented vertical accuracy could be obtained relatively easily satisfied the mapping market for a while. In addition, the applications that fueled the LiDAR technology, such as telecommunications, did not even require the accuracy that was achievable with those early systems. In mapping, orthophoto production was the primary beneficiary of the surface data provided by the new sensor and the requirements for accuracy were not that stringent. The introduction of the LiDAR data created a few quality control and even service/product contracting issues. To address these subjects, the American Society of Photogrammetry and Remote Sensing (ASPRS) initiated an effort to create a recommendation document on LiDAR data, which interestingly dealt with the vertical accuracy (ASPRS, 2004); new ongoing efforts include the horizontal accuracy too.

As the LiDAR market started to grow rapidly, LiDAR vendors could invest more into development, and soon LiDAR systems showed truly phenomenal performance improvements. In less than five years, the pulse rate improved by an order and now 100 and 150 kHz systems are available (Optech, 2006 and Leica, 2006). More importantly, the ranging accuracy for hard surfaces has increased substantially and now stands close to the level of static GPS surveys, i.e., 1-2 cm, and it is almost insignificant to the navigation error budget. In parallel to these developments, users' expectations started to grow; the target vertical accuracy for demanding LiDAR products started to shift from the one foot level to the sub-dm range. The performance of the newer LiDAR systems, combined with better operational techniques, opened the door toward applications where large-scale or engineering-scale accuracy are required. At this point the georeferencing error budget and, to a lesser extent, the sensor calibration quality, are critical to achieving design level accuracy (few cm). Using ground control is an effective way to compensate for georeferencing and sensor





modeling errors. In addition, ground control can provide for independent and highly reliable QA/QC processes. Unfortunately, ground control can be costly, and may present hazard to the field crew in particular, within the transportation network.

The Office of Aerial Engineering (OAE) has been using an Optech 30/70 ALTM airborne LiDAR system for about four years. The introduction of LiDAR technology was a major development towards improving the mapping operations, and the overall experiences are excellent, as evidenced by numerous projects, where highly accurate surface data were produced in an unprecedentedly short time. Similar to the pattern of other users, during the learning period of the new technology, OAE has identified areas for improvements in terms of achieving better accuracy and increasing data processing efficiency. In particular, the following topics required immediate attention:

- To perform a strip adjustment for seamless integration of strips into the final product. Due to navigation solution and sensor calibration anomalies, the surface points in the strip overlap area may differ more than the vertical accuracy range would allow for.
- To improve the horizontal accuracy in order to better characterize the final product; i.e., to provide a measure for the horizontal accuracy similar to the vertical parameters.
- To improve accuracy (both horizontal and vertical), use ground control that is less labor-intense, requires no or limited surveying and imposes less restrictions in normal field operations.

LiDAR-specific ground targets developed by the OSU team in an earlier research project fulfilled the expectation of improving both horizontal and vertical accuracy, as well as providing effective technique for strip adjustment, product characterization, and, in general, for QA/QC. The implementation and operational resources needed, in terms of labor and time constraints imposed on target deployment, however, represented substantial cost, which is generally not available for all the projects OAE executes. Therefore, improvements are needed to reduce the requirements for using ground control. The most obvious extension of the LiDAR target concept introduced earlier was to use existing natural or man-made targets such as reflective pavement markings instead of the deployable LiDAR-specific ones.

The ultimate objective of this research project was to advance the earlier developed LiDAR-specific ground control-based LiDAR data accuracy improvement technique by including existing natural and man-made objects as targets, in particular using pavement markings, and extending the methodology for handling both types of targets in a highly automated way. Obviously, the total elimination of the deployable targets was the desirable long-term research objective. The extended method is expected to support ODOT's urgent production needs by providing a joint solution for strip adjustment, horizontal and vertical products accuracy characterization, and for improved QA/QC process.



## 2. RESEARCH OBJECTIVES

The primary objectives of this research project were as follows:

1. Studying the reflective patterns of objects typically found along road corridors. In particular, road pavement markings and any objects that may have good/distinct reflective characteristics are of interest. The result of this task is a set of objects with good identification potential from LiDAR data.
2. Developing algorithms to automatically identify/extract features/objects from the LiDAR intensity data. A high-level of automation is expected and the false positive rate will be minimized to assure high success rates of the following processes. In addition, the user would be able to select the area(s) of interest using a polygon to define the limits of each area of interest.
3. Developing methods to create best fit lines/curves through the identified features within the selected areas. The “best fit” lines/curves should be centered within the feature such as an edge line pavement marking.
4. Performing a comparison of the control points to the “best fit” line through the identified features. Calculate and report the perpendicular distance from the “best fit” line/curve to the control point, the difference in X, Y directions as well as related statistical information summarized for each control point, all control points within an area, and all control points contained within a project.
5. Using past and new data from the OAE LiDAR database, extensive tests will be performed to assess both the algorithmic performance and the correctness of the original object selection. The algorithms will be refined and the object set could be modified as needed.
6. Investigating the feasibility of extracting image primitives from LiDAR data, including primarily point and linear features. A model library of the primitives will be created; for example, a library of various reflective features, including both radiometric and geometrical description.
7. Developing methods to automatically parameterize objects extracted in (2) and (3) to make their description compatible with the model library of (6). If needed, a parameter optimization will be performed to remove functional correlation of the input parameters.
8. Developing matching technique to match extracted objects with the model library. Once a match is found, the reference location will be determined with high accuracy. This is similar to deriving the center point coordinate of LiDAR specific targets.
9. Extension of the existing LiDAR data correction method to handle the new “target” objects. We expect to keep the existing user interface of the adjustment program and to provide the well-received interactive diagnostic tools for both types of targets.
10. Investigating optimal target density and their geometrical distribution. Based on the results, a test flight will be arranged to validate the suggested spacing and location characteristics in the model. After the data analysis is complete, the parameters will be adjusted if needed. In addition, the results are expected to provide a performance metrics for spacing and point distribution for any given accuracy requirement.

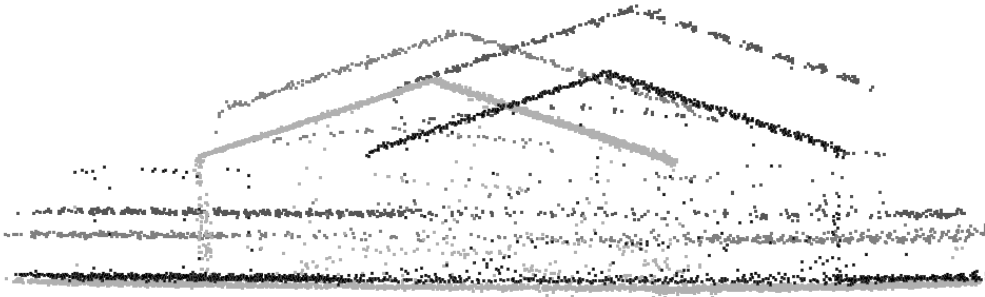


11. Identifying the discrepancies between strips can be corrected in two fundamental ways: either by applying separate corrections to each strip or by adjusting the sensor boresight misalignment; basically the heading, roll, and pitch parameters of the LiDAR sensor with respect to the navigation frame. First, methods to adjust individual LiDAR strips or a set of strips as a group horizontally will be developed. While this method always provides an improvement, provided the strip difference observations are correct, the boresight misalignment approach for correcting strip discrepancies only works if boresight errors exist (the parameters do not reflect the actual spatial relationship). An automated process will be developed to detect the existence of boresight misalignment error, and, if needed, to apply it before the individual strip corrections.
12. Depending on data availability and/or ODOT OAE direction, the performance of the method will be analyzed with respect to various sensor configurations, including flying height, pulse rate, scan rate, field of view, side overlap, etc.
13. Preparing detailed report, operation workflow, and user manual for the developed algorithms and software utilities.

### **3. GENERAL DESCRIPTION OF RESEARCH**

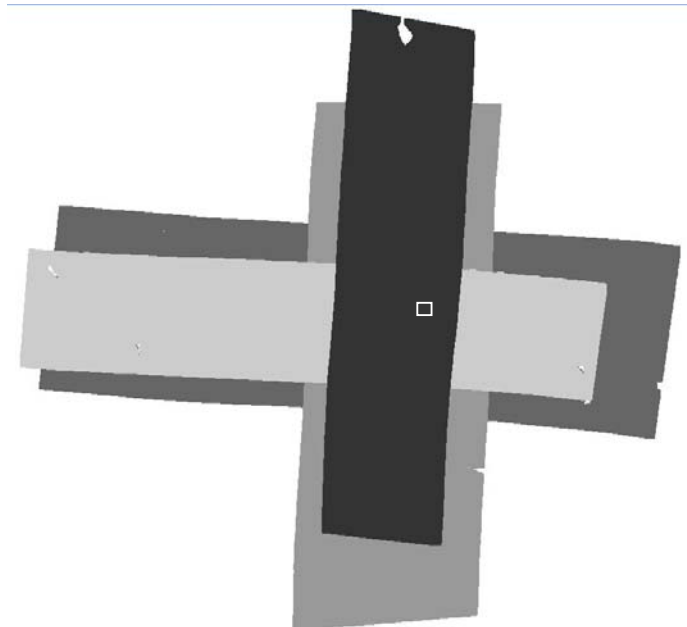
#### **3.1 LiDAR Strip Adjustments**

The primary objective of LiDAR strip adjustment (Shan and Toth, 2008) is to provide quality assurance and quality control (QA/QC) for the final geospatial product by reducing, or ultimately eliminating, discrepancies found in strip overlap areas, and thus create a seamless product. Ideally, there should be no visible or measurable differences between overlapping LiDAR strips, except for sensor noise, mainly caused by varying performance of the georeferencing component. However, strip differences frequently occur. The extent is significantly smaller nowadays than it was when the first generation of commercial LiDAR systems was introduced. At that time, only the vertical accuracy of the LiDAR data was specified and no reference was provided for horizontal precision, consequently strip adjustment was aimed at removing only the height differences. Motivated primarily by the generation of DEMs, the first guidelines to report on LiDAR data quality were only concerned with the vertical accuracy (ASPRS, 2004), but by now, horizontal precision evaluation is part of the process. Strip discrepancies typically show a systematic pattern that provides a basis to model them and subsequently correct them in a strip adjustment process. The differences between various LiDAR strips acquired over the same area are more visible in areas that are rich in objects of simpler geometric shapes, such as man-made objects, like buildings, as shown in Fig. 1; the strip overlap is depicted in Fig. 2.



**Figure 1.** Strip discrepancies observed from four strips.

LiDAR data are collected in strips. In applications, where a rectangular block or corridor is flown in a parallel line pattern, minimal overlap between neighboring strips is typically required to maintain contiguous coverage of the ground. The required margin can vary considerably, although the extent of overlap typically falls in the 10% to 30% range. The amount of variation between strips depends on the flight situation, including flight planning/control, weather conditions, and terrain undulation. Many strip adjustment techniques are based on sensor parameter calibration, and therefore to better support these processes, cross strips are also frequently flown. The reliability of earlier sensor systems necessitated frequent sensor calibration, which required additional dedicated data collection, such as flying cross-strips over an airport or parking areas before and after the survey, resulting in multiple overlap data.



**Figure 2.** Multiple strip overlap (cross-strips at different flying height); square marks building area shown in Fig 1.

LiDAR users recognized very early the advantage of strip overlap and methods were developed to assess the discrepancies between strips, and then apply corrections to the



data. Early developments in strip adjustment techniques were further influenced by other factors, such as the LiDAR point density. In the late 1990s, the LiDAR point density was modest compared to current systems. The pulse rate (10 kHz PRF) was an order of magnitude less than that of current state-of-the-art systems (100 kHz PRF), so one approach to increase point density was to fly larger overlaps, say 50%, which essentially provided double coverage of the surveyed area (i.e., doubling the effective point density).

The general concept of the LiDAR strip adjustment process is simple: first, differences should be identified and measured between two overlapping strips, and then, using a geometric model, the parameters of a suitable transformation must be determined that can be subsequently applied to correct/adjust the strips. Unfortunately, the implementation of strip adjustment is not straightforward, as establishing the required correspondence between two strips is rather difficult. This difficulty comes primarily from the irregular distribution of points in the LiDAR point cloud, which means that the same object space is randomly sampled in the spatial domain in every strip, and thus, there are no conjugate points between the two point clouds (even if there were observations of the same object from different strips, they would not be recognized as such, because LiDAR points have no identifiers). Therefore, either interpolation of data is needed (e.g., conversion to a common grid), or shape-based techniques (based on features extracted from a group of points) should be used instead of conventional point-based methods.

The complexity of the object space, including terrain undulation with additional natural and man-made objects, has a significant effect on the process of finding matching primitives in the two point clouds. If the object space (terrain) variations are large, the spatial spectrum of the object space has high spatial frequency components, and thus the LiDAR point density is most likely not sufficient to meet the Nyquist criterion, and consequently, the point cloud in this case is not adequate to fully describe the object space, making the correspondence problem an ill-posed one.

LiDAR systems have undergone remarkable developments since their introduction in the late-1990s and the development of the first strip adjustment techniques. The laser ranging accuracy for hard surfaces has approached the static surveying accuracy, about 1-2 cm ( $1\sigma$ ), and the use of multiple returns, the intensity signal have become wide-spread, and multi-pulse systems have been introduced recently. More importantly has increased by an orders of magnitude, allowing for better spatial sampling and improved object space reconstruction. Developments in the georeferencing component of LiDAR systems are also significant as the navigation solution is currently the most significant term in the overall LiDAR error budget. Typical topographic LiDAR surveys provide point densities in the 2-5 pts/m<sup>2</sup> range, although for some applications, such as helicopter-based transmission line surveys, 20+ pts/m<sup>2</sup> densities are reported. Note that the along and across spatial sampling rates vary depending on the scanning mechanism used in the LiDAR system and the scanning parameter controls; although the parameter settings are generally optimized for approximately even spatial sampling.

LiDAR strip adjustment methods have evolved over time, and there is a variety of algorithmic approaches and techniques customized to specific conditions. From a



conceptual point of view, the strip adjustment methods can be categorized based on several not totally independent characteristics, with the most important one is whether it is based on co-registration or calibration, as the strip discrepancies can be eliminated/reduced either by applying an adequate transformation to the LiDAR strips or by introducing a correction to the sensor parameters, and then recreating the LiDAR point cloud from corrected sensor data. Conceptually, the strip adjustment methods fall into two categories. The techniques in the first group are a type of rubber-sheeting co-registration solution, which tries to minimize the differences between strips for a given transformation model; this technique is also called “data driven,” as it is not based on a physical model and is focused only on removing the discrepancies between strips. In contrast, the second approach is concerned with the source of the errors and aims to reduce the strip discrepancies by modifying/adjusting the parameters of the sensor models and/or sensor orientation, thus basically implements an in situ calibration of the multi-sensor system. The boresight calibration of LiDAR sensors is the most frequently used approach if sensor model-based strip adjustment is performed. This project is focused on a data-driven solution and no attempt was directed to use the measured discrepancies to model sensor/boresight errors although it is possible.

### **3.2 Coordination of concept development and implementation**

To exploit research results in practice is always a challenge, as there is the usual gap between a research prototype system and a commercial product. Obviously, the ODOT OAE needs products, as it is primarily a production environment. Therefore, various implementation options were considered at the beginning of the project, and the decision was made to integrate the expected research results into the GeoCue product, which is the workhorse of LiDAR project management in the OAE. This solution has several advantages such as it clearly separates the algorithmic design and the user interface, provides the usual interface to the operator, and ultimately requires the least effort in system development costs.

Shortly after the official project start, frequent interactions with ODOT personnel as well as with GeoCue Corporation took place with discussions focused on the integration of the research results into ODOT OAE processing workflow through the GeoCue product. After the preparations reached the required level, a project coordination meeting was held at the Center for Mapping, OSU, on April 12, 2007; the persons attending were John Ray, Jeff Syar and Rachel Lewis from ODOT; Lewis Graham and Derek Morris from GeoCue Corporation, Chris Gard from TEC, and Dr. Charles Toth and Eva Paska from OSU. The technical content of the discussion was on the development of the interface concept and its implementation. As the main outcome of this productive meeting was the release of Version 3.0 of the LIDAR Featuring Matching & Adjustment System (FMAS). As a follow-up, during the ASPRS Annual Conference in Tampa, FL, May 7-11, 2007, John Ray, Lewis Graham, Charles Toth and Eva Paska had several informal discussions on the project component that is related to the GeoCue interface and on the development of a new XML data passing protocol. There were several discussions between ODOT and OSU personnel, the most important one was on August 2, 2007, when several important questions were clarified at the project meeting at The Center for Mapping, OSU, with





John Ray and Jeff Syar from ODOT, and Dr. Charles Toth and Eva Paska from OSU attending.

To support algorithmic research and system developments, a test dataset was acquired on May 11, 2007, including LiDAR data flown by ODOT OAE over a small town and country roads. The dataset included GPS VRS-surveyed pavement markings data for several intersections and other areas of interest. The availability of this dataset was essential during the course of this project, as it satisfied most of the project needs; in fact, there was no need for additional test flights.

### **3.3 Research Developments to Support OAE LiDAR Operations**

The accomplished research tasks were primarily concerned with the development of introducing manual and automated pavement markings measurements in the GeoCue environment to improve horizontal strip adjustment performance as well as QA/QC processes, and thus, to support the LiDAR-based map production system to achieve the accuracy requirements required by the specifics of OAE operations. The algorithmic developments, techniques researched, and programs developed are discussed in the Results section.

## **4. RESULTS**

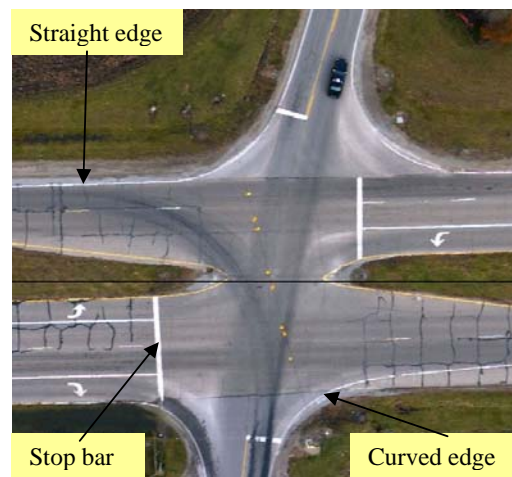
The foundation behind the idea of using pavement markings as ground control to support the QA/QC of LiDAR data rests on two main conditions. First, the general availability of the LiDAR intensity signal, which is essential to extract location information over relatively flat surfaces, should be mentioned. Second, a technology is required to quickly measure pavement markings at good accuracy, which is safe for the crew and present limited hazard with respect to traffic.

The introduction of airborne LiDAR in the late nineties was followed by a quick proliferation of the technology, and LiDAR became the primary surface data extraction mapping technique. Yet, the general availability of the intensity signal is a rather recent development. The primary driving motivation for using intensity signals in the LiDAR production is simply the fact that the intensity data provides a quite good visualization tool, which was in a way missed for a long time by users who always wanted to see what was behind the point cloud (this was reason while video and small format cameras have been accompanying LiDAR sensors from the very beginning). Fig. 3 shows a comparison between optical imagery and LiDAR intensity and elevation data. It must be noted that the use of the intensity signal for feature extraction has been limited primarily for research, as the intensity signal is a relative measurement, which is quite different from the explicitness of the LiDAR range data, and thus the automated processing present more challenges.

Concerning the pavement marking measurements, the rapidly broadening use of real-time GPS correction services, based on the use of the CORS network, provides the necessary infrastructure to perform the survey of pavement markings in a quick and accurate manner. Practically, the 10-20 m stretches of road pavement markings can be

accomplished in a few minutes.

This work proposes a method to use road pavement markings as ground control to assess the quality of the LiDAR data as well as to improve the point cloud accuracy by post-processing. The idea behind using pavement markings is that they are widely available on the road network, albeit quality may vary at a larger scale. Their spatial distribution is nearly optimal as they are used nearly evenly on the road surface. Equally importantly, road pavement markings have distinct reflective characteristics relative to the road pavement, which is essential from the feature extraction perspective, as the LiDAR elevation data is identical for the road surface regardless whether it is painted or not. Figs. 4.x a-c show simultaneously acquired digital orthorectified image, LiDAR intensity and LiDAR elevation image, respectively, of an intersection. The LiDAR point density was about 4 pts/m<sup>2</sup> with a foot print size of 15 cm. The pavement markings in the LiDAR intensity image are quite visible and distinct from the pavement. Note that LiDAR intensity image is rather inferior in quality with respect to the optical imagery. Clearly, the affect of coarser sampling and the larger footprint is quite noticeable. Nevertheless, the extraction of pavement markings seems to be feasible and thus they can be used as ground controls, provided they are surveyed, and consequently can support the QA/QC processes of the LiDAR data themselves. Note that this approach can improve both horizontal and vertical accuracy of the LiDAR data, and provide for the first time a measure of the horizontal accuracy. As a result, it enables to evaluate the horizontal accuracy of LiDAR data as well as quantify the horizontal and vertical product accuracies.

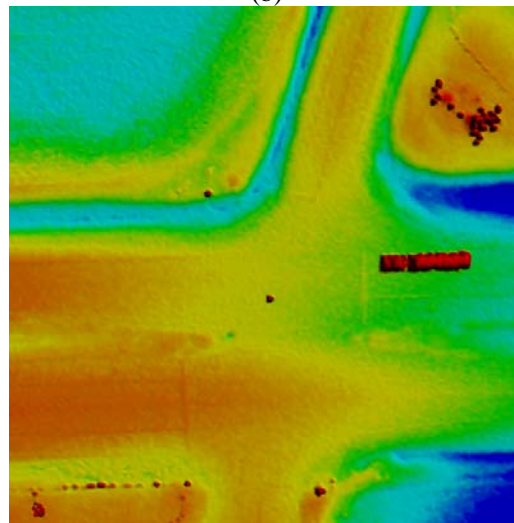


(a)





(b)



(c)

**Figure 3.** Pavement markings at an intersection in various sensor data; (a) 4k by 4k digital image (orthorectified), (b) LiDAR intensity (gridded), and (c) LiDAR elevation (gridded).

In summary, the proposed method based on using reflective pavement markings instead of the deployable LiDAR-specific targets offers the same accuracy performance potential but it is less expensive, there is no need for deployment of sizeable targets around the road, the surveying requirements are simpler, as measurement of the road surface is easier and faster compared to the elevated targets, and the risk for the crew is consequently much lower. A clear advantage of the pavement markings is that they can be reused in subsequent mapping missions, as long as their quality allows for it; in time, the pavement markings wear out due to traffic and weather. In addition, the availability of the pavement marking positions can significantly improve the traffic flow extraction processes, as it accurately confines the search space. Furthermore, based on the measurement of the pavement markings at the road edges, can be used to extract the lane separator pavement markings, as their geometry is closely known, so again using the LiDAR intensity



data they can be extracted with high success rate. This, in turn, enables for better vehicles extraction on a lane bases, which can provide for better traffic flow patterns.

The scientific progress has been continuously documented in journal papers and conference proceeding papers. All the relevant and related papers are included in Appendix A. In addition, a presentation given at the last ELGR Summer meeting is included in Appendix B, as it provides an overview of the final phase of the project.

#### **4.1 Curve fitting**

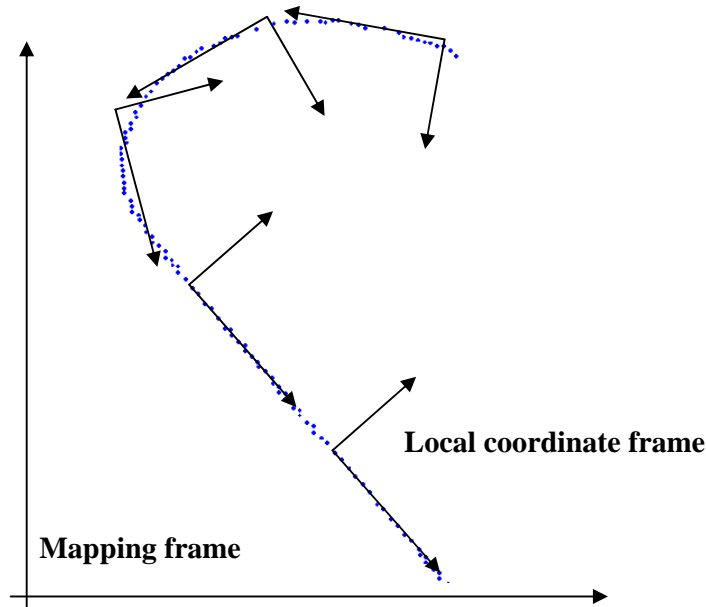
The pavement markings can be either surveyed by GPS, such as using the ODOT VRS system, or measured from LiDAR data on a workstation. In both cases, shape of the pavement markings is sampled at random distances; the distance between the sampled points varies. For these sample points, the geometry of the pavement markings should be reconstructed for processing and visualization. While it is not a difficult task in general, the universal nature of the pavement markings, such as that could be of any shape and in any combinations, requires the use of piecewise curve fitting methods. Note that the curve fitting method is essential for both operator-based and manual measurements.

The primary purpose of the curve fitting process is to reconstruct the shape of the pavement markings, which can be equally applied to automatically extracted LiDAR points as well as to the reference points obtained by GPS surveying. Of course, there is a significant difference in the two representations, as the reference points are quite accurate, in fact, they can be considered almost error-free if compared to the horizontal accuracy of the LiDAR points. In addition, their sampling is probably adequate to properly describe the shape as the surveyors know quite well what point density is required for proper representation of linear features. In contrast, the pavement marking points extracted from LiDAR are distributed over a larger range in both directions, along and across the pavement marking centerline. Therefore, finding a curve that represents an optimal fit in some terms is a challenge. The higher sampling rate (LiDAR point density) has a positive impact on the curve fitting process, as better error cancellation can be expected. The section describes the curve fitting method that was developed based on the original concept introduced in (Ichida and Kiyono, 1977). The technique (basic idea) was adopted, modified and extended to the specifics of the LiDAR point cloud and control points. The fitted curve can be described both analytically and numerically, such as a dense polyline representation, which could provide for performance advantages in certain implementations.

##### Introduction of a local coordinate system

The shape defined by the extracted LiDAR points of the pavement markings should be modeled as linear features in order to be matched with their controls; the most generic format is a 3D curve. The selected method to create best fit lines/curves through the extracted LiDAR points is a piecewise weighted least squares curve fitting based on cubic (third-order polynomial) model, which seemed to be adequate for our conditions, based on a priori experimental results. In the following, the 2D case will be discussed, although the implementation is based on the full 3D model. To

handle any kind of curves, defined as the locus of points  $f(x, y) = 0$  where  $f(x, y)$  is a polynomial, the curve fitting is performed for smaller segments in local coordinate systems, which are defined by the end points of the curve segments. The primary advantage of using a local coordinate system is to avoid problems when curves become vertical in the mapping coordinate system, i.e., when there are more than one  $y$  values for an  $x$  value. Fig. 4 shows the concept of the local coordinate system used for curve fitting. The fitting results as well as the fitting constraints are always converted forth and back between the local and mapping coordinate frames. In the following, the core curve fitting for a single segment in a local coordinate system is discussed.



**Figure 4.** The curve fitting is done in local coordinate systems, with varying length segments defined on basis that it has only limited curvature; the local coordinate system is oriented to main direction of the segment.

The notation used to describe the main steps of the piecewise cubic fitting (PCF) process is introduced in Fig. 5. To achieve a smooth curve, the curve fitting to any segment is constrained by enforcing identical slope of the curves' tangent at the segment connection points; in other words, the PCF polynomials are continuous with their first derivatives at the connection points, such as  $x=s$ ,  $x=t$ , etc. Eqns. (1) and (2) describe the third-order polynomial, with the constant, 1<sup>st</sup>, 2<sup>nd</sup>, and 3<sup>rd</sup>-order terms,  $c_k$ ,  $d_k$ ,  $a_k$  and  $b_k$ , respectively, and its first derivative for curve  $S_k$ , placing the coordinate system's origin to the connection point  $s$ :

$$\begin{aligned}
 S_k(x) &= c_s + d_s \cdot (x-s) + a_s \cdot (x-s)^2 + b_s \cdot (x-s)^3 \\
 m_k(x) = slope &= S_k'(x) = d_s + 2 \cdot a_s \cdot (x-s) + 3 \cdot b_s \cdot (x-s)^2
 \end{aligned}
 \tag{1), (2)}$$

Since

$$y_s = y_k(s) = S_k(x=s) = c_s + d_s \cdot (s-s) + a_s \cdot (s-s)^2 + b_s \cdot (s-s)^3 = c_s$$

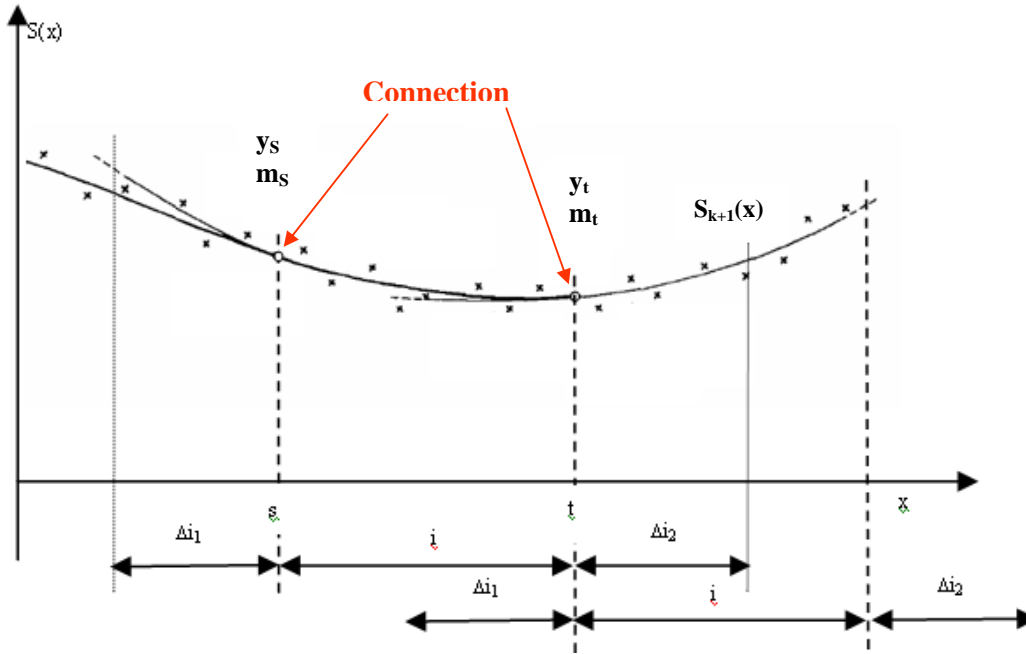
$$m_s = m_k(s) = S'_k(x=s) = d_s + 2 \cdot a_s \cdot (s-s) + 3 \cdot b_s \cdot (s-s)^2 = d_s$$

Therefore

$$S_k(x) = y_s + m_s \cdot (x-s) + a_s \cdot (x-s)^2 + b_s \cdot (x-s)^3$$

$$\text{slope} = S'_k(x) = m_s + 2 \cdot a_s \cdot (x-s) + 3 \cdot b_s \cdot (x-s)^2$$

The constant and the 1<sup>st</sup>-order term of the third-order polynomial are equal to the value of the curve,  $y_s$ , at the origin, as well as the slope of the curve's tangent at the origin, respectively. As the curve's value and slope are kept fixed at the connection points, when computing the coefficients of the third-order polynomial piece, only the 2<sup>nd</sup> and 3<sup>rd</sup> order terms are the unknowns in the least squares adjustment, and the constant and 1<sup>st</sup>-order terms are treated as constant (non-random) variables or fixed constraints, except for the first segment, when all the coefficients are treated as unknown values.



**Figure 5.** Piecewise weighted least squares curve fitting method.

$$\rightarrow x = s$$

$$S_k(x) - y_s - m_s \cdot (x-s) = a_s \cdot (x-s)^2 + b_s \cdot (x-s)^3$$

Step 1

Unknown parameters are :  $a_s, b_s$

$$\text{LS for points in interval } (\Delta i_1 + i + \Delta i_2)_k \Rightarrow \hat{a}_s, \hat{b}_s \rightarrow a_s = \hat{a}_s, b_s = \hat{b}_s$$

$$\Rightarrow S_k(x) = y_s + m_s \cdot (x-s) + a_s \cdot (x-s)^2 + b_s \cdot (x-s)^3$$

---


$$x = t$$

Step 2  $y_t = S_k(t) = y_s + m_s \cdot (t-s) + a_s \cdot (t-s)^2 + b_s \cdot (t-s)^3$

$$m_t = S'_k(t) = m_s + 2 \cdot a_s \cdot (x-s) + 3 \cdot b_s \cdot (x-s)^2$$


---


$$\rightarrow x = t$$

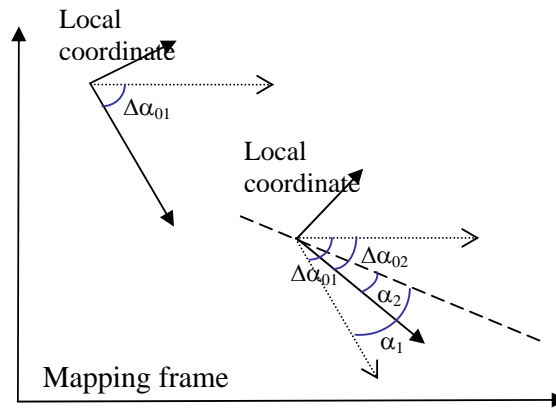
$$S_{k+1}(x) - y_t - m_t \cdot (x-t) = a_t \cdot (x-t)^2 + b_t \cdot (x-t)^3$$

Step 3 Unknown parameters are :  $a_t, b_t$

LS for points in interval  $(\Delta i_1 + i + \Delta i_2)_{k+1} \Rightarrow \hat{a}_t, \hat{b}_t \rightarrow a_t = \hat{a}_t, b_t = \hat{b}_t$

$$\Rightarrow S_{k+1}(x) = y_t + m_t \cdot (x-t) + a_t \cdot (x-t)^2 + b_t \cdot (x-t)^3$$

When the orientation of the subsequent local coordinate system is different from the previous one, the constraints (value and slope) at the connection point need to be computed into the new system. Fig. 6 shows the notation used in the computation, described by Eq. (3) and the transformation between local and global frames is defined by Eq. (4).



**Figure 6.** Transfer of slope at connection points.

$$m_2 = \tan(\alpha_2) = \tan(\alpha_1 + \Delta\alpha_{01} - \Delta\alpha_{02}) \quad (3)$$

where  $\alpha_1 = \text{atan}(m_1) * 180 / \pi$

Where

- $m_1$  The slope of the curve's tangent at the connection point in the local coordinate system 1
- $m_2$  The slope of the curve's tangent at the connection point in the local coordinate system 2
- $\alpha_1$  The angle between the curve's tangent and the x axis of the local coordinate system 1
- $\alpha_2$  The angle between the curve's tangent and the x axis of the local coordinate system 2
- $\alpha_{01}$  The angle between the axes of local coordinate system 1 and the mapping



frame  
 $\alpha_{02}$  The angle between the axes of local coordinate system 2 and the mapping frame

$$\begin{aligned} X_0 &= R_{01}^{-1} \cdot X_1 + T_{01} \\ X_2 &= R_{02} \cdot (X_0 - T_{02}) = R_{02} \cdot (R_{01}^{-1} \cdot X_1 + T_{01} - T_{02}) \end{aligned} \quad (4)$$

Where

- $X_0$  The coordinates of the fitted curve at the connection point in the mapping frame
- $X_1$  The coordinates of the fitted curve at the connection point in local coordinate system 1
- $X_2$  The coordinates of the fitted curve at the connection point in local coordinate system 2
- $T_{01}$  The translation in the mapping frame between the origins of the mapping frame and local coordinate system 1
- $T_{02}$  The translation in the mapping frame between the origins of the mapping frame and local coordinate system 2

The discussion so far has considered all the LiDAR points with the same weight, which ignores the possible differences among the LiDAR points. While this model provides good results in most cases, improvements can be expected if the LiDAR points are weighted according to their location with respect to the pavement marking. For example, there is quite a difference in shape between a regular lane pavement marking and a stop bar, as the second one has a larger width that is comparable to its length, consequently, the estimation of the two lines could be quite different. The answer to the question on what basis the LiDAR points can be weighted is the intensity value. As shown in Fig. 7, with varying overlap between the pavement marking and the LiDAR point footprint, the intensity value is somewhat proportional, as it was discussed earlier. Using the intensity value as a weight allows for better line extraction as shown in Fig. 8. The simplest way is to use the reciprocal of the intensity, or a somewhat more non-linear mapping function. Note if the pavement marking is long enough, not the case of the stop bar, then there is a statistically good distribution of the intensity values as well as good spatial distribution, and therefore the intensity-weighted and not weighted solutions will be similar.





## 4.2 Curve Matching

Various matching techniques were considered for matching the different representations of pavement markings, before the Iterative Closest Point (ICP) algorithm was selected. The primary reason for ICP was the fact that it does not require any point correspondence and its robustness. Using the polyline curve representation of the curve fitting results, the ICP matching of free-form curves can be directly applied; the two point sets, adequately describing the curves, have no point-to-point correspondence. ICP can be applied in any dimensions, in 2D or 3D, and the correspondence between two curves is iteratively established as well as the transformation parameters of the geometrical model are estimated. ICP is sensitive to initial approximation and outliers too. A modification was proposed to the standard ICP method to deal with the various lengths of the different representations of the same pavement marking that could lead to false results when searching for correspondences between point sets if not properly treated. In the developed algorithm, this situation is properly handled and thus unacceptable errors are avoided.

For the sake of simplicity, the ICP technique will be discussed for the 2D case, as the generalization for 3D is straightforward. Note that in our application this is generally the case, as the road surface is almost flat although not necessarily horizontal but for smaller areas can be almost always modeled by a plane. Also, the ICP can determine different models of the geometrical relationships between two data sets, but in our case, only the rigid body model is considered, as any deformation between the two data sets can be ruled out.

The Iterative Closest Point (ICP) method in 2D is used to find the best correspondence between two curves (point sets) by iteratively determining the translations and rotation parameters of a 2D rigid body transformation. The ICP algorithm can be summarized as follows:

- 1) Establish correspondence between pairs of features based on proximity.
- 2) Estimate the rigid transformation that best maps the first member of the pairs onto the second, based on minimizing the following expression

$$\min_{(R,T)} \sum_i \|M_i - (RD_i + T)\|^2$$

where  $R$  is a 2\*2 rotation matrix,  $T$  is a 2\*1 translation vector and subscript  $i$  refers to the corresponding points of the sets  $M$  (model) and  $D$  (data).

- 3) Apply the estimated transformation to all features in the first/previous structure.
- 4) Repeat steps 1 – 3 until convergence is reached.

ICP assumes that the closest points are in correspondence, and during the repeated processing, the data sets get closer and closer, and ultimately, they converge to the correct answer. The 2D rigid body transformation used in the discussion can be described with three parameters, two translations, and one rotation, as shown in Eq. (5)





and Eq. (6) where the transformation matrix includes both the translation and rotation components in homogenous format.

$$\begin{bmatrix} X_C \\ Y_C \end{bmatrix} = \begin{bmatrix} \Delta X \\ \Delta Y \end{bmatrix} + \begin{bmatrix} \cos \alpha & -\sin \alpha \\ \sin \alpha & \cos \alpha \end{bmatrix} \cdot \begin{bmatrix} X_D \\ Y_D \end{bmatrix} \quad (5)$$

$$\begin{bmatrix} X_C \\ Y_C \\ 1 \end{bmatrix} = \begin{bmatrix} \cos \alpha & -\sin \alpha & \Delta X \\ \sin \alpha & \cos \alpha & \Delta Y \\ 0 & 0 & 1 \end{bmatrix} \cdot \begin{bmatrix} X_D \\ Y_D \\ 1 \end{bmatrix} \quad (6)$$

where  $X_C$  and  $Y_C$  are the mapping coordinates of the control feature points;  $X_D$  and  $Y_D$  are the mapping coordinates of the conjugate digitized feature points;  $\Delta X$  and  $\Delta Y$  are the translation parameters between the two sets; and  $\alpha$  is the rotation angle.

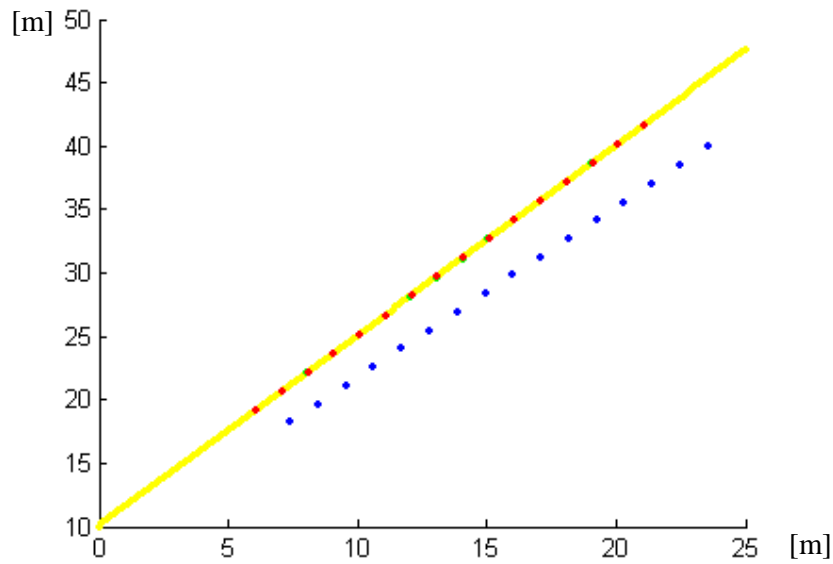
The ICP method is rather robust in general provided that good approximations are available to start the process. This is certainly the case for the pavement markings, as the two representations of the same linear feature are quite close in geometrical terms. However, the relatively coarse sampling and varying overlap needs additional attention, as the potential for a mismatch cannot be ruled out. To avoid these situations, two extensions were added to our ICP implementation. First, one curve was represented in a very dense polyline structure; in actual numbers, at 1 mm sampling rate. This way, the closest points needed to form the pairs are guaranteed to be from the closet point on the curve. Second, in a preliminary analysis, a threshold was estimated to provide a maximum value for distances between the two point sets. Applying this threshold to all pairs, point pairs with excessive distance, which are likely to be erroneous, are eliminated from the processing. The ICP method, customized to the matching of different pavement marking representations was implemented in Matlab and has been tested with both simulated and real data.

#### ICP performance test with simulated data

To assess the performance potential as well as the implementation correctness of the ICP methods, various tests were initially executed using simulated data. These tests were aimed to determine the effectiveness with respect to shape and noise content. Given the typical shape of the pavement markings, straight line, 3<sup>rd</sup> order polynomial curve, and sine wave were selected for our investigation.

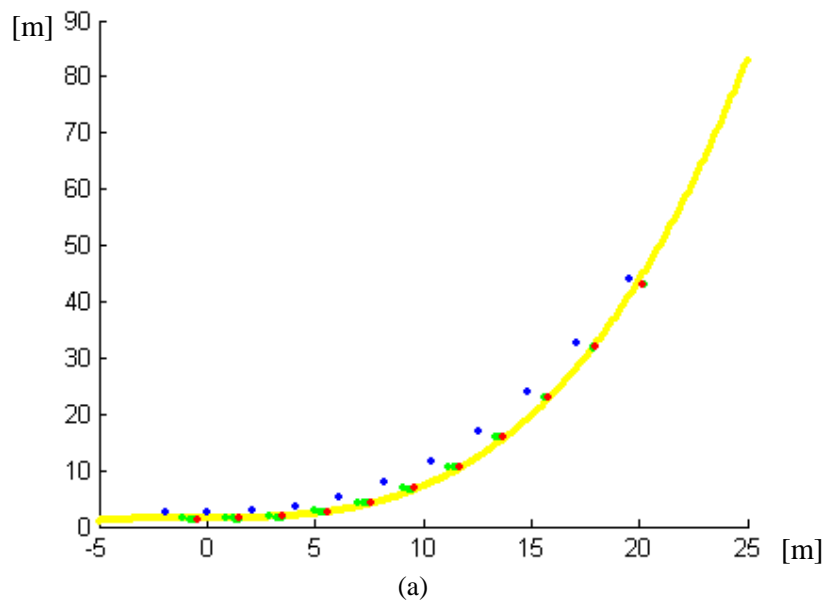
Straight lines are probably the most frequently occurring pavement markings and so they are of high importance. Furthermore, the matching between two straight lines is an ill-posed problem due to the uncertainty in one direction (along the line), resulting in infinite number of solutions for the shift parameters. Consequently, using only straight lines to determine the parameters of the 2D transformation, a group of lines with various orientations is needed to counter the deficiency of matching lines. Fig. 9 shows an example matching two straight lines, where the yellow is the reference, the dense polyline representation, blue points are the points to be matched to the curve,

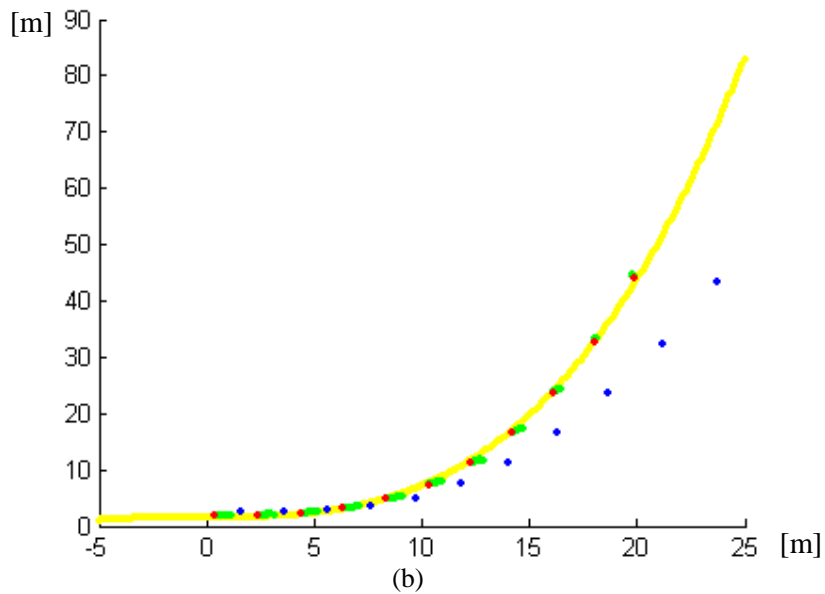
red points are the results of the ICP, and the green points show the results of each iteration step. Note the difference in orientation between the two lines.



**Figure 9.** Matching straight lines.

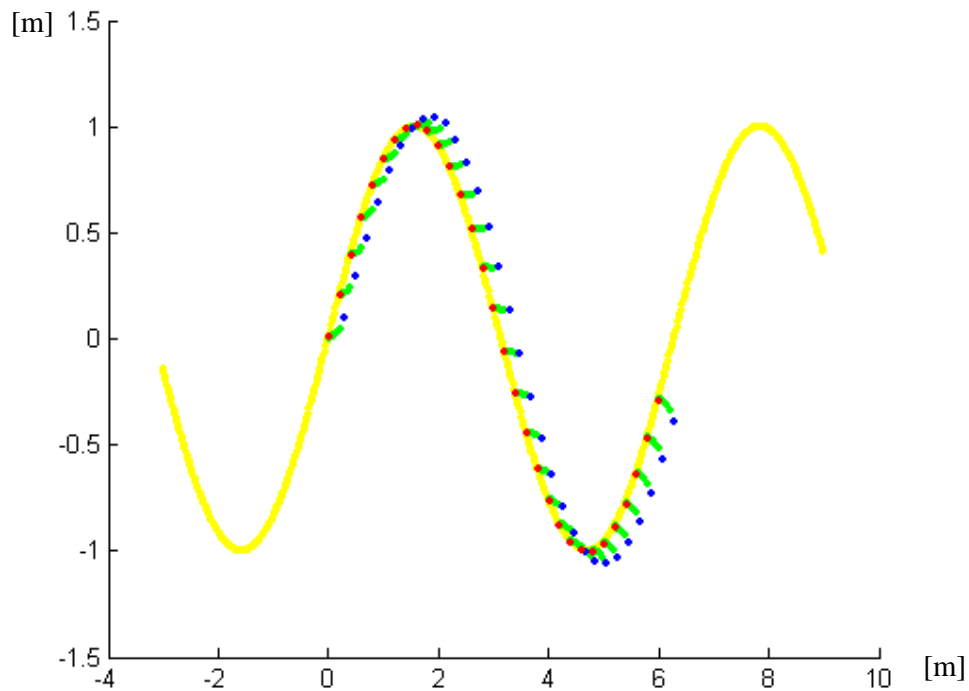
Fig. 10 shows a curve modeled by a 3<sup>rd</sup> order polynomial and two different point sets that were ICP matched; the same color scheme is used to mark the point status. Although, it is difficult to judge visually, but both points sets get matched to the same and correct location. Clearly, the shape of the curve, varying curvature, helps to the ICP method to properly match the point sets to the curve.





**Figure 10.** Matching third-order curve from two different positions, (a) and (b).

More complex curves are rare in practice and can come in variety of shapes, so they have no typical shape. Therefore, a sine wave, approximating a good spatial point distribution, was simulated, as shown in Fig. 11.



**Figure 11.** Matching a sine wave.

The numerical results of these examples are listed in Table below.

Curve type	Number of iterations	Transformation parameters [m]	Accuracy estimates [m]
Straight line	3	$\Delta x = 0.296$ $\Delta y = -0.631$ $\alpha = 0.052$	$\sigma_{\Delta x} = 0.008$ $\sigma_{\Delta y} = 0.004$ $\sigma_{\alpha} = 0.0002$
3 <sup>rd</sup> order polynomial (a)	9	$\Delta x = -1.516$ $\Delta y = 1.173$ $\alpha = 0.021$	$\sigma_{\Delta x} = 0.001$ $\sigma_{\Delta y} = 0.0009$ $\sigma_{\alpha} = 0.00005$
3 <sup>rd</sup> order polynomial (b)	17	$\Delta x = 1.071$ $\Delta y = 0.803$ $\alpha = 0.064$	$\sigma_{\Delta x} = 0.009$ $\sigma_{\Delta y} = 0.008$ $\sigma_{\alpha} = 0.0004$
Sine wave	12	$\Delta x = 0.282$ $\Delta y = 0.093$ $\alpha = 0.032$	$\sigma_{\Delta x} = 0.0001$ $\sigma_{\Delta y} = 0.0002$ $\sigma_{\alpha} = 0.00006$

The curve fitting process has a low-pass filtering effect on the curve representation, which is more significant for the LiDAR point data, as its horizontal accuracy is about an order worse compared to the reference points, determined by GPS. Therefore, noise is not expected to be an issue for the ICP method. Table below shows results when various amounts of random noise were added to the sine wave curve for the ICP testing.

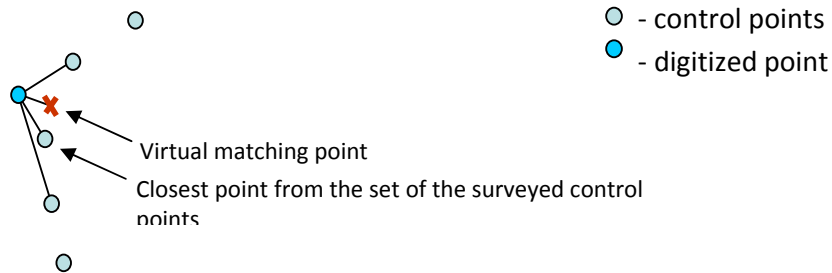
Noise Std [m]	Num of iterations	Coordinate difference (Reference-ICP) [m]	
		Mean (dx, dy)	Std ( $\sigma_{dx}, \sigma_{dy}$ )
<b>0.00</b>	3	-1.036	0
		-1.554	0
<b>0.05</b>	3	-1.055	0.011
		-1.545	0.007
<b>0.10</b>	3	-1.064	0.016
		-1.541	0.011
<b>0.20</b>	3	-1.075	0.024
		-1.536	0.0164

The simulation data based tests confirmed that the ICP method works well for all the typical shapes used in the pavement marking practice; obviously, it works better for curves with strong shapes, defined as good 2D spatial extent. The noise tolerance of the ICP method is remarkable; the transformation parameters were practically unchanged and only their accuracy terms changed a little.

#### ICP performance test with real data

From the logic of the ICP method, the original points describing the same pavement marking are not properly sampled. Note this should not be mixed with the sampling theory, as the point density for the usual LiDAR data and ground control certainly

satisfies the Nyquist criterion. The problem for ICP is that when selecting the closest point from one set to a point in the other set, most likely the chosen point would be the closest one only from the set, but not the actual closest point in the curve described by the point set. Fig. 12 illustrates the situation, why we need the curve fitting,



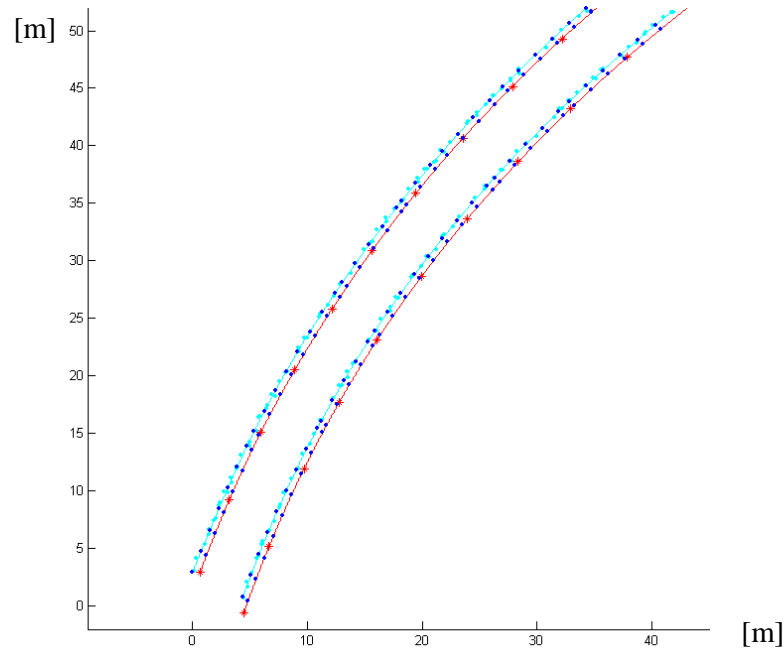
to find the actual closest point. The closest point from the original point set would give a false closest point.

**Figure 12.** The effect of point sampling on ICP.

By densifying one point set, the control points in our case, the ICP will match to the correct point, as instead of the distance between pairs formed from the original points, the distance to the interpolated point will be considered; the one from where the line in the perpendicular direction to curve contains the digitized point. This is the reason why the option for dense polyline representation in the curve fitting was introduced. Another option could be if both curves are fitted and have dense representation. Obviously, this requires significantly more computing power, as the point pair formation will drastically increase.

To investigate the various options with respect to robustness, accuracy and execution speed, the following three combinations were considered:

1. Both, LiDAR and GPS control points are curve-fitted before running ICP; it is invariant which one is used as reference and as data.
2. Only GPS control points are curve-fitted before running ICP.
3. Only LiDAR points are curve-fitted before running ICP.



**Figure 13.** ICP matched curves; magenta: curves fitted to control points, red: GPS control points, cyan: LiDAR point and curves fitted, and blue: matched points.  
Change figure for usual intersection figure.

In the test data, the LiDAR point spacing varied in the 1-3 pts/m range, and the horizontal accuracy of the GPS-surveyed points, provided by a VRS system was 1-2 cm horizontally.

The transformation parameters between these two point sets (the original LiDAR-derived points and their corresponding points on the control curve) are calculated in a least squares adjustment. Table below shows the 2D transformation parameters for the three different cases, clearly indicating the robustness of the ICP method with respect to noisy data, such as using the original LiDAR points. The differences between curves and residuals after ICP matching for the three cases are shown in the second Table below. The 2 cm horizontal precision is realistic, given the fact that the GPS-surveyed points are known at a 1-2 cm-level accuracy, and the LiDAR-based pavement marking positioning accuracy is estimated at the few cm range. The 9-10 cm precision terms in case 2 correspond to the use of the noisy LiDAR data (no curve-fitting applied to smoothly model the pavement markings).

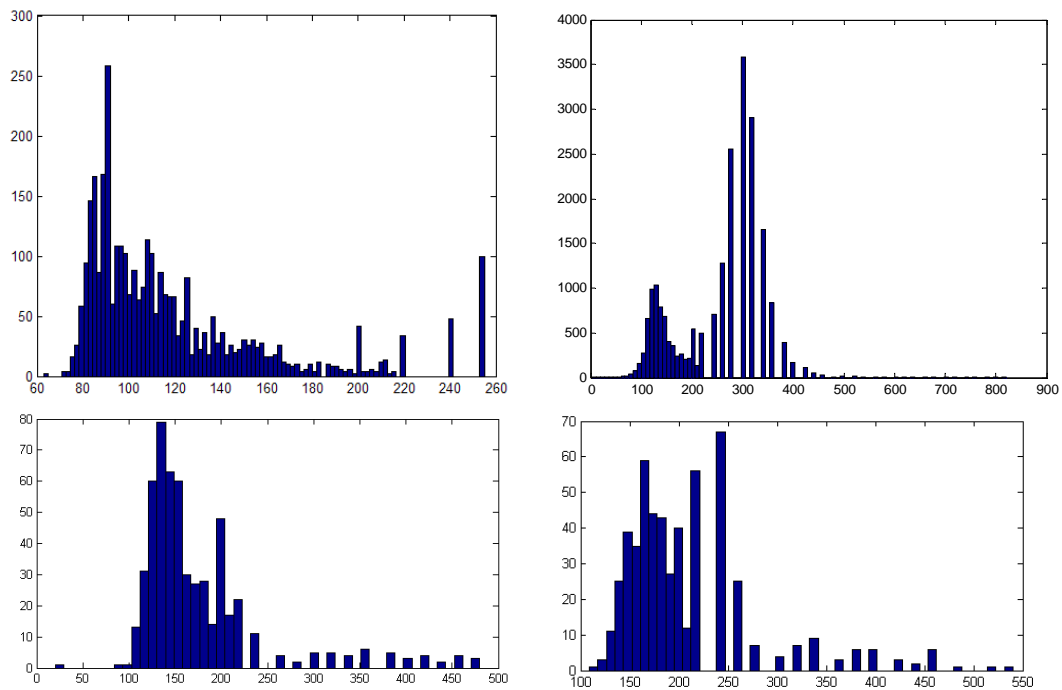
ICP input data	ICP-adjusted transformation parameters		
	$\Delta X$ [m]	$\Delta Y$ [m]	$\phi$ [°]
Both, LiDAR and GPS points are curve-fitted	0.153	-0.114	0.000
No fitting of LiDAR points, GPS points curve-fitted	0.150	-0.114	0.000
No fitting of GPS points, LiDAR points curve-fitted	0.158	-0.116	0.000

Case	Differences/Residuals							
	X [m]				Y[m]			
	Before		After		Before		After	
	mean	Std	mean	std	mean	std	mean	Std
1	0.16	0.02	0.00	0.02	-0.11	0.02	0.00	0.02
2	0.16	0.10	0.00	0.10	-0.12	0.09	0.00	0.09
3	0.16	0.02	0.00	0.02	-0.12	0.01	0.00	0.01

### 4.3 Pavement Markings Extraction

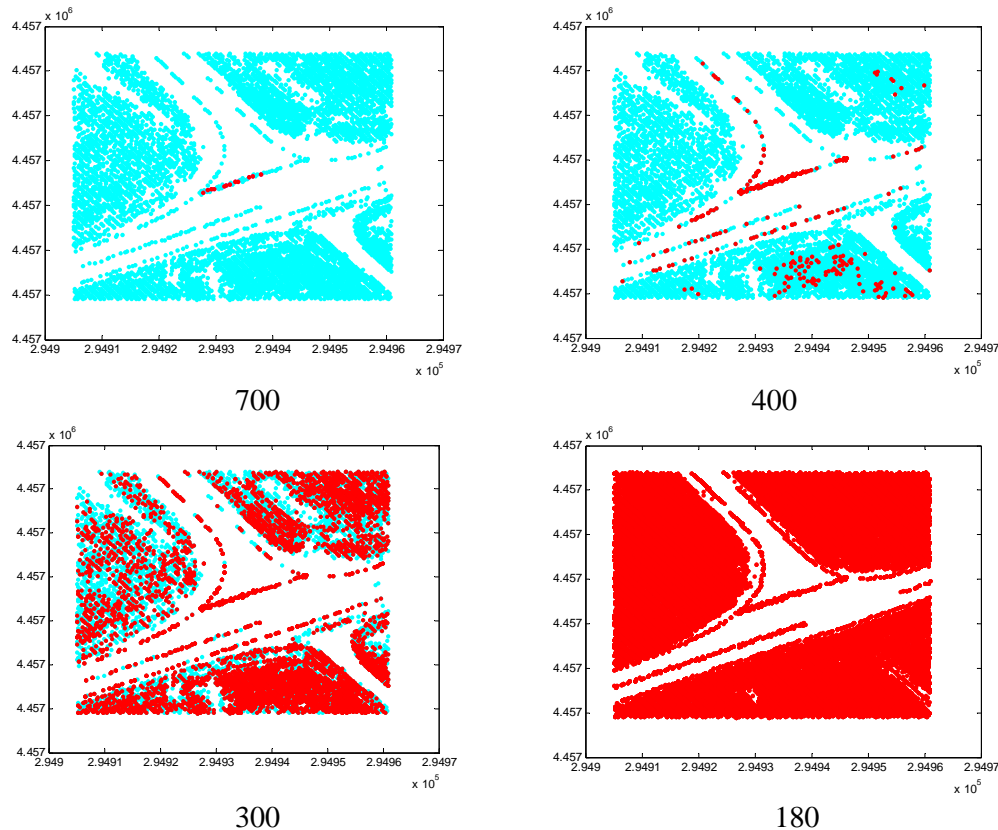
The automated extraction of the pavement markings from LiDAR intensity data presented a formidable challenge for the project. By definition, the LiDAR intensity data stand for a relative measure; thus, different materials from different flying heights may produce identical intensity values. Therefore, the intensity can be only applied on a local basis and with sufficient care. In preparation, several datasets flown under various conditions were analyzed to establish a statistical basis for the pavement marking extraction process. After the evaluation, the conclusion was reached that a multiphase adaptive method should be developed to achieve the minimum performance level required. Some sample figures below show the difficulties of the automated pavement marking extraction.

The relative nature of the LiDAR intensity signal is demonstrated in Fig. 14, where the histograms of areas around pavement markings, defined by a 1m envelop, are shown. Note the wide range of intensity signal values and location of the region around the first local maximum.



**Figure 14.** Histogram distribution of LiDAR intensity values in small area containing pavement markings.

The performance of using a global threshold is illustrated in Fig. 15, showing the separation of the pavement markings at various intensity threshold levels.

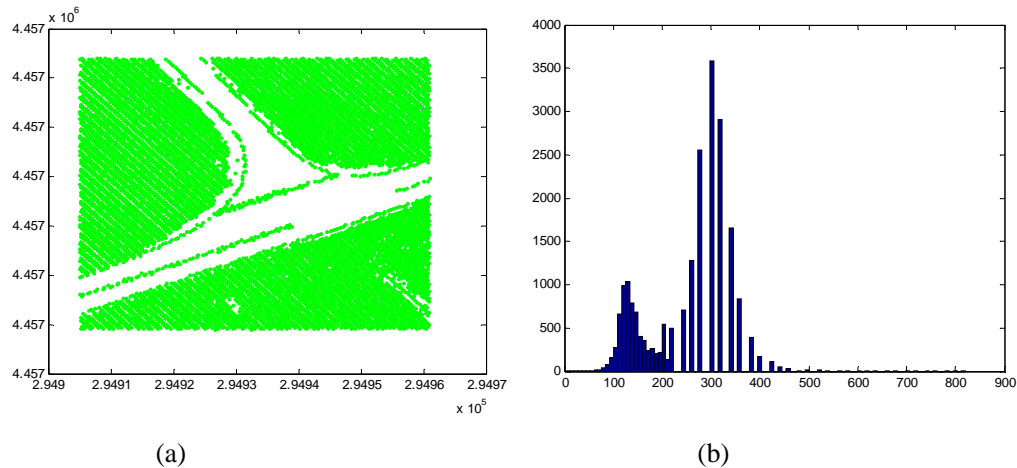


**Figure 15.** The separation of pavement markings using different LiDAR intensity thresholds.

The objective of the pavement marking extraction is to identify the LiDAR points reflected off from the pavement markings that will serve as input to subsequent processing, such as curve fitting and matching. The pavement markings shown in Fig. 16 are quite visible but that is not always the case, as road surface material and quality, the condition of the pavement markings and other factors may reduce the illustrated sharp contrast between the road surface and markings in the LiDAR intensity data under varying circumstances. Therefore, a simple `global_threshold` applied to the intensity to separate pavement markings is not a directly applicable method in the general case. Furthermore, even for a given situation, such as the intersection shown in Fig. 16, where there is a good separation, there exists no single absolute threshold value; for example, LiDAR data acquired at different flying heights over the same area would have different intensity values. Hence, an adaptive method is proposed here, which was based on the statistical evaluation of various datasets. The basic idea is to find a locally optimal threshold that will separate the pavement markings from the pavement and the underlying assumption is that the relative relationship of the intensity values for different materials is generally preserved. It must be emphasized again that the availability of the reference data (GPS-surveyed representation of



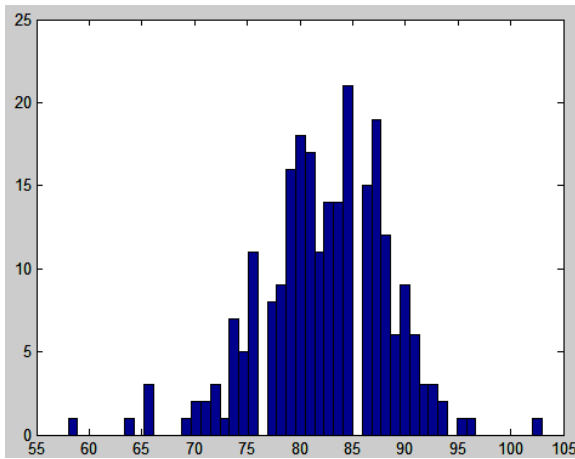
pavement markings) provides an enormous help to accomplish this task, as it defines a rather narrow search space to find pavement markings. Note that as a potential follow-up, pavement markings without reference data can be extracted in nearby areas based on road geometry and parameters settings adjusted to the location.



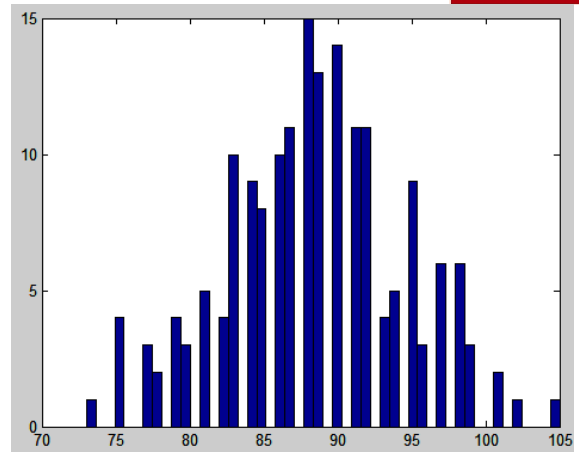
**Figure 16.** Using a locally optimal threshold in a nearly ideal situation; thresholded image is shown in (a), and the histogram of the original LiDAR intensity data is shown in (b).

In Fig 4.x, a threshold of 180 was applied, which was determined as the optimal value to separate the two slightly overlapping intensity distributions of the road surface and all the other objects, including pavement markings and grassy area. The peak at the low intensity values reflects pavement, while the peak at the medium range reflects grassy/soil area, and the high values come from pavement markings. Note as the number of pavement marking returns is relatively low, there is no peak visible. Applying the search window defined by the reference data, clearly, the pavement markings can be easily extracted. Note that the intensity values above 220 are quantized differently, as the lower digits are ignored (set to zeros), so there are gaps in the vertical axis of the histogram above that value.

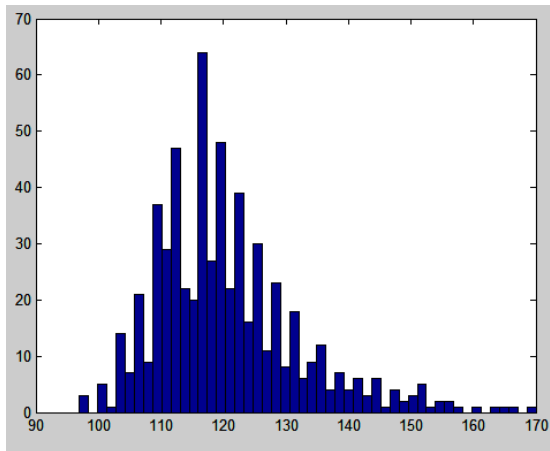
To develop a better understanding of the intensity signal behavior, LiDAR data acquired by different systems and under various conditions were analyzed. The histogram of the intensity signal was evaluated for areas of interest to this investigation, such as road surfaces, pavement markings and grassy areas/soil that are typical around roads. The areas were manually selected and attempted to be a good representation of the three object categories. Fig. 17 shows eight histograms that were selected from three different areas. Note that relatively “clean” road surfaces were identified by the operator to achieve a good estimate of the intensity distribution.



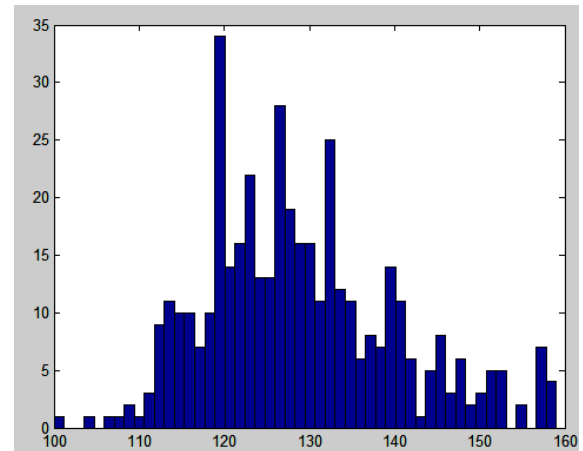
(a) Area 1, sub-area 1



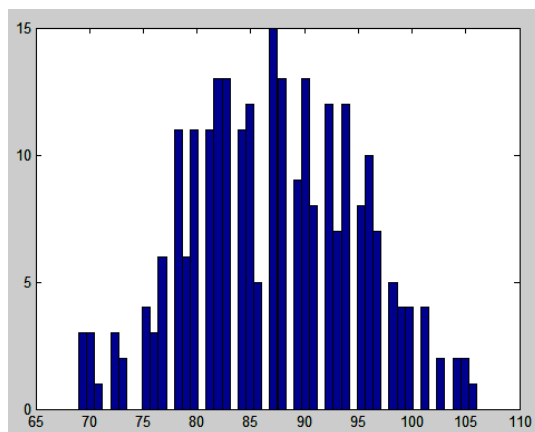
(b) Area 1, sub-area 2



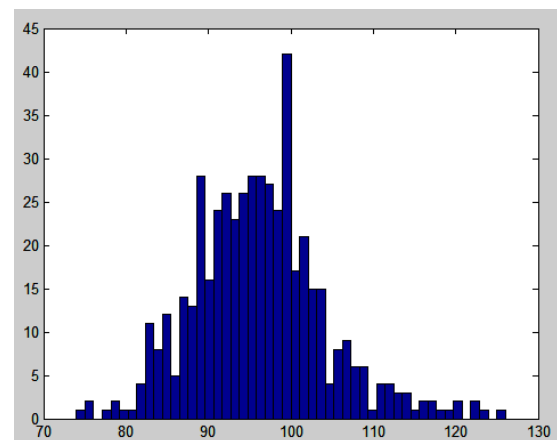
(c) Area 3, sub-area 1



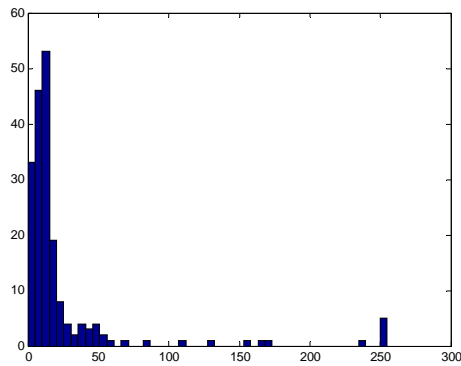
(d) Area 3, sub-area 2



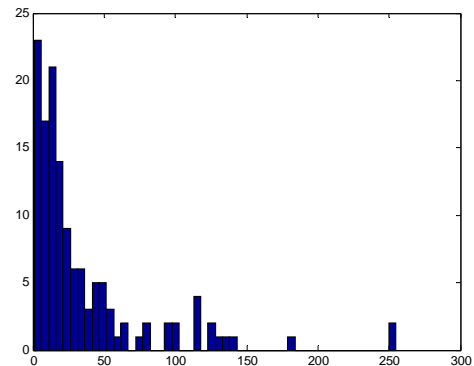
(e) Area 3, sub-area 3



(f) Area 5, sub-area 1



(g) Area 7, sub area 1

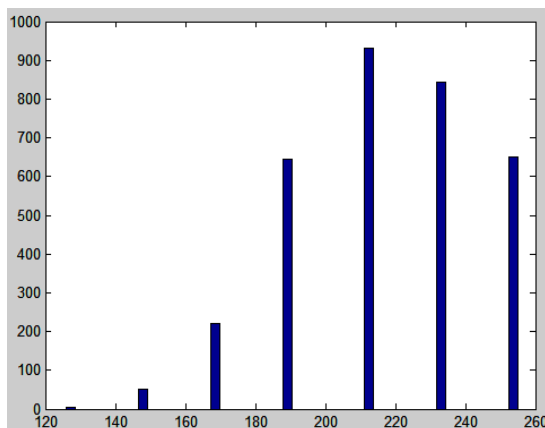


(h) Area 7, sub area 2

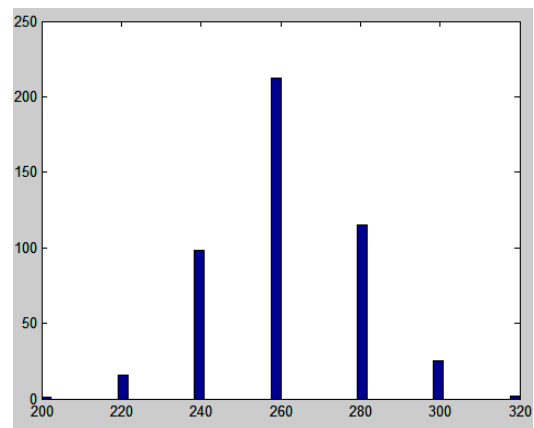
**Figure 17.** Histograms of various pavement areas; (a-f) concrete and (g-h) asphalt surface.

The various histograms in Fig. 17 clearly demonstrate that the intensity varies by missions and within one mission too. Note all the concrete data are from one long mission, but taken from different areas with different road quality. An additional observation is that even along a short stretch of 100 m, the intensity values can noticeable change. Also, the distributions show some variations; note the fact the fresh asphalt may not provide returns. The mean of the samples varies over the range of 85 and 125.

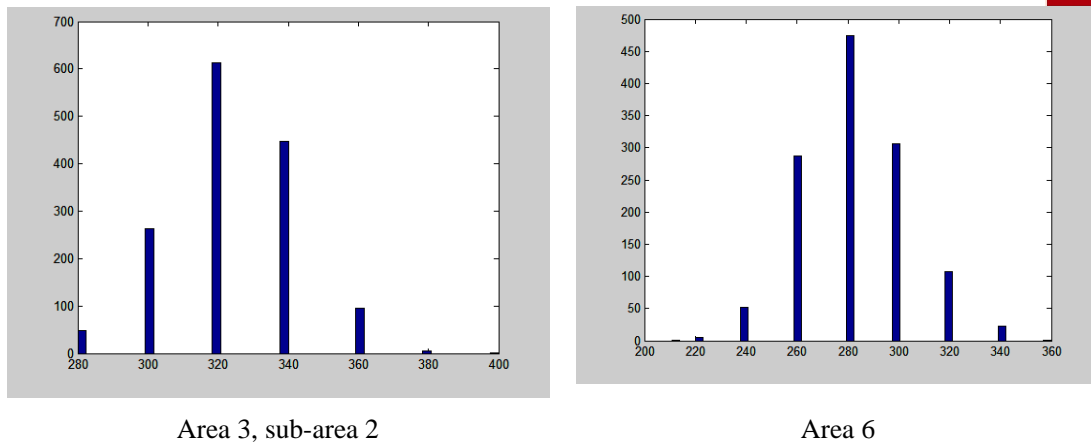
Grassy and soil areas were analyzed in the next step. Fig. 18 shows four grassy/soil areas. The results show a clear separation from the pavement.



Area 1



Area 3, sub-area 1

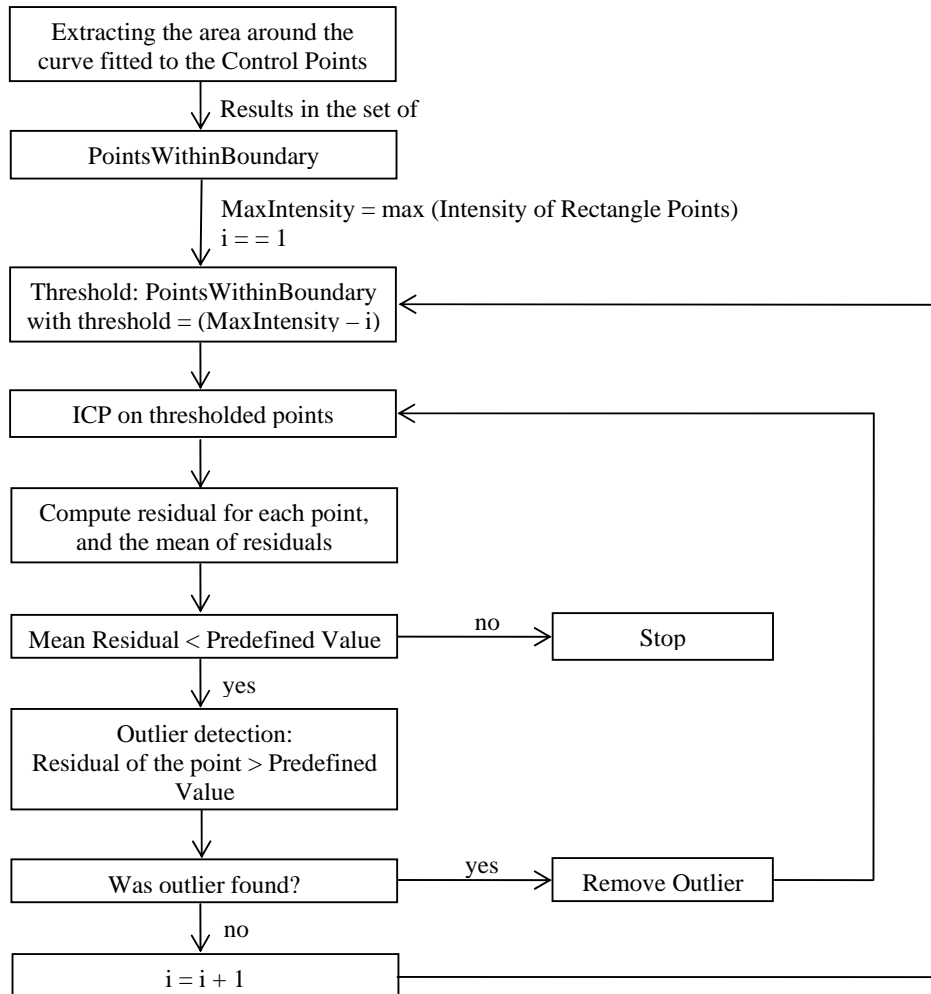


**Figure 18.** Histograms of various grassy and soil areas.

In the last step, pavement markings were evaluated. Unfortunately, the histograms of the pavement markings are overlapping with that of both the pavement and grassy/soil areas, with more overlap with the second group. This is a bit contradicting to expectation, as the dark road surface and bright pavement markings should be at the opposite end of the intensity range. The reason why the pavement markings intensity distribution has unexpectedly lower values is explained by the specifics of the spatial sampling of the LiDAR data. Due to beam divergence, the LiDAR pulse has non-negligible footprint, ranging from a few cm to close to a meter, depending on flying height and sensor aperture. Therefore, the LiDAR footprint is generally larger than the width of a typical pavement marking, which means that the reflection will jointly come from both areas (the pavement marking and the pavement), and thus, the final intensity value is a combination of the high intensity return from the pavement markings and the low intensity return from the pavement, proportional to the footprint overlaps of the two features. Fig. 7 shows the illustration based on actual LiDAR data.

An additional attribute of the intensity signal is that there is no agreement in the industry concerning the definition and the suggested range of the intensity value; note the different range of the figures above. Furthermore, the formation of the intensity value could be different and is not necessarily proportional to the relative energy of the reflected pulse, as it could additionally include another value, which is an expression of the shape or change in shape of the returned pulse. Therefore, it is not a surprise that different LiDAR manufacturers use different intensity ranges, such as [0-255] or [0-4095]. Further complicate the case, some systems come with AGC (automated gain control), so the receiver electronics adjusts the absolute intensity range according to a slowly changing average signal strength and provides intensity values relative to that value in the same intensity range.

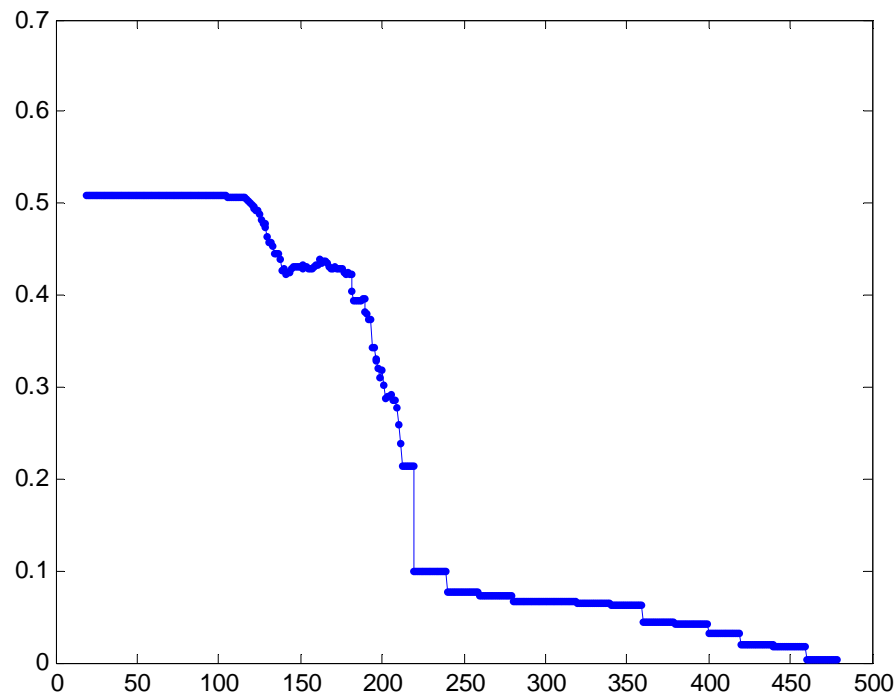
Based on the histogram analysis and the impact of the LiDAR footprint, a method was developed that is not only adaptive but brings in object space constraints in terms of applying the shape of the pavement markings to improve the point selection. Fig. 19 shows the block diagram of the proposed method. Note that some components such as curve fitting and ICP (Iterative Closest Point) are discussed in subsequent sections.



**Figure 19.** Data processing block diagram of extracting LiDAR points of pavement markings.

The process starts once the search spaces around the pavement markings have been extracted. The survey data of the control features, pavement markings, are provided as point observations along the centerline of the markings. Pavement markings can be easily surveyed using GPS VRS technology; the process is fast, typically it takes less than a minute to survey a point, and the accuracy, in general, is about 2-3 and 3-6 cm horizontally and vertically, respectively. In most cases survey data are available for the pavement markings along the edge lines which can be very quickly and efficiently surveyed. The overall accuracy of the LiDAR system can be estimated from the sensor/system and the flying parameters. Adding a margin, the maximum error envelopes can be computed, and thus, LiDAR points in the vicinity of the pavement markings can be extracted; the typical distance value is about 1 m or less in most situations.

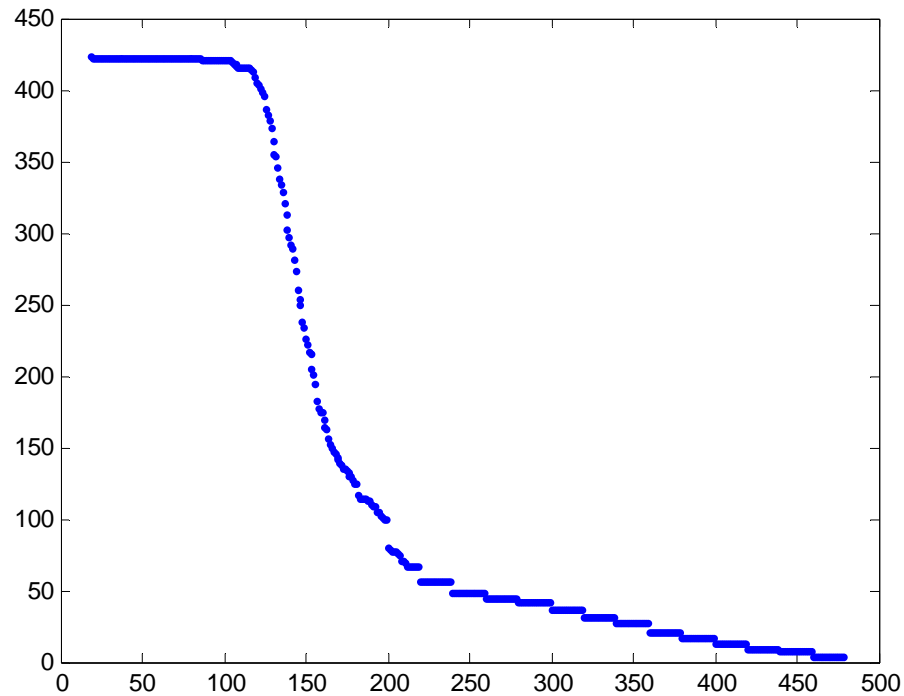
The method was implemented in Matlab and a large number of tests were performed to assess the performance of the extraction process; note that other modules developed to support the curve fitting and ICP processes were also used. Fig 20 shows how the mean residual of the selected points with respect to the reference drops at the optimal intensity value.



**Figure 20.** Mean residuals as a function of the intensity threshold.

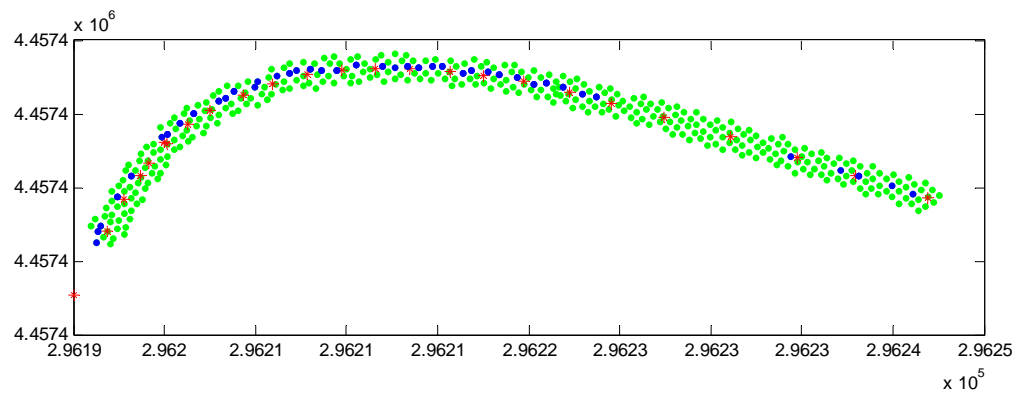
Although, with higher intensity threshold the mean residual continues to decrease, this improvement is minor and more importantly it is less stable, as the number of selected points will go down too, as shown in Fig. 21. Therefore, the final threshold will be selected when the mean residual falls below a predefined value, to assure that the good residual value is based on a reliable number of points. The threshold value of allowed individual residuals mentioned in the block diagram are determined based on

the pavement width and footprint size, and it is the maximum allowed value that a marking point could be far away from the curve's center.



**Figure 21.** Number of selected points vs. the intensity threshold.

The results of a typical pavement markings extraction is shown in Fig. 22; green points are the extracted points based on the search window, defined by the estimated maximum error envelop, red points are the reference points from the GPS survey, and blue points are the identified LiDAR points bounced off from the pavement markings.



**Figure 22.** Extracted pavement marking LiDAR points.



In the developed method there was no assumption on the distribution of the LiDAR points with respect to the orientation of the pavement markings. In reality, however, LiDAR missions over roads are typically flown along the road line, so in most cases the LiDAR profiles, points collected in one swing of the oscillating (or rotating) mirror, fall across the main direction of the pavement markings. This geometrical situation can be exploited, as one-dimensional search techniques can be applied. Note that spacing is usually denser along the profile lines. The footprint of the profile for short distances can be always modeled as a straight line, so it can be easily intersected with the pavement markings centerline. The conjugate LiDAR point of the intersection does not exist in general, but analyzing the intensity profile along the profile, such as fitting a curve and determining the maximum, can provide the matching virtual LiDAR point. This approach leads to a slightly different processing, since a point-to-point correspondence is established right away, and thus, the transformation can be directly computed. This avenue was not further investigated in this effort.

#### **4.4 Performance Assessment**

The initial performance assessment included all the processing steps, including the automated pavement marking extraction. The attached publication (Appendix A.3) provides a complete review of the performance validation. Additional results may be added to the final report.

#### **4.5 Software Developments**

During the course of the project extensive code developments were carried out. Matlab environment represented the basic platform for algorithmic implementation and testing, and all the statistical analyses and simulations were carried out in Matlab. Then, once the techniques had settled, a wrapper interface in Microsoft Visual Studio, C++ environment was developed that the processes can be called from C++. The benefit of this approach is that the C++ code can be accessed from the GeoCue application, the data transfer and conversion are simpler in C++. A large number of Matlab routines are available in different categories such as curve fitting, ICP, least square adjustments, various 3D transformations, etc. Most of the macros can be easily reused for other purposes. In addition a basic Java interface was created to export and import XML, which is the basic data passing protocol for the GeoCue product. The program manual is in Appendix C.

### **5. CONCLUSIONS**

LiDAR technology can routinely deliver accuracy sufficient to meet the requirements of mainstream (basic) mapping— typical quoted vertical accuracy is about 50 cm at 90% CEP level, but 10-20 cm is also achievable under well-controlled circumstances. For large-scale mapping, such as engineering scale mapping of transportation corridors, however, additional effort is needed to achieve the required accuracy, including careful flight planning, adequate processing and QA/QC methods. Because of the nature of LiDAR, navigation-based direct orientation of an active imaging





sensor, there is no feedback in the processing loop that could provide for assessment of the absolute accuracy, and therefore the use of ground control is always necessary. The developed technique in this research project, which is based on using road pavement markings, has shown good automation potential and attractive performance as tool to validate the horizontal accuracy and/or to provide for strip corrections, if needed. Except for the automated pavement markings extraction component, all the other processing steps exhibit a rather robust performance. In summary, based on our test results, the horizontal accuracy terms can be obtained around 5 cm precision for typical transportation corridor projects, at engineering scale, flown by the ODOT OAE LiDAR system.

## **6. IMPLEMENTATION PLAN**

The OSU-developed code in Matlab, wrapped in C++ has been passed to GeoCue Corporation for integration in two phases; the curve fitting and matching part was already delivered in December 2007. We expect to collaborate on the integration, so the developed technique can be used as a standard production tool in GeoCue in the ODOT OAE production environment.



## BIBLIOGRAPHY

1. ASPRS LiDAR Committee, 2004. ASPRS Guidelines Vertical Accuracy Reporting for LiDAR Data  
[http://www.asprs.org/society/committees/lidar/Downloads/Vertical\\_Accuracy\\_Reporting\\_for\\_Lidar\\_Data.pdf](http://www.asprs.org/society/committees/lidar/Downloads/Vertical_Accuracy_Reporting_for_Lidar_Data.pdf)
2. Kozo Ichida and Takeshi Kiyono: Curve Fitting by a One-Pass Method With a Piecewise Cubic Polynomial. ACM Transactions on Mathematical Software, Vol 3. No 2, June 1977, Pages 164-174.
3. Leica Geosystems, ALS50, <http://gis.leica-geosystems.com>
4. Optech International, 2004. ALTM 30/70/100 User Manual. Toronto, Canada.
5. Optech, ALTM 3100AE, 2006,  
<http://www.optech.ca/pdf/Brochures/ALTM3100EAspecsfnl.pdf>
6. Maas, H.G. (2002). Methods for Measuring Height and Planimetry Discrepancies in Airborne Laserscanner Data. *Photogrammetric Engineering & Remote Sensing*, 68(9):933-940.
7. Topographic Laser Ranging and Scanning: Principles and Processing, Eds: Shan, J., and Toth, C., Taylor and Francis 2008 (under publishing).



## APPENDIX A

### Publications

1. Toth, C., Paska, E., Grejner-Brzezinska, D.A. (2007): Using Pavement Markings to Support the QA/QC of LiDAR Data, proceedings of *Photogrammetric Image Analysis (PIA 2007)*, *International Archives of Photogrammetry and Remote Sensing*, Vol. XXXVI, 3/W49B, pp. 173-178.
2. Toth, C., E. Paska and D. Brzezinska, (2008): Quality Assessment of LiDAR Data by Using Pavement Markings, ASPRS Annual Conference, Portland, Oregon, April 28 – May 2.
3. Toth, C., E. Paska and D. Brzezinska, (2008): Using Road Pavement Markings as Ground Control for LiDAR Data, XXI ISPRS Congress, Beijing, China, July 3–11, 2008.

# USING ROAD PAVEMENT MARKINGS AS GROUND CONTROL FOR LIDAR DATA

C. Toth<sup>a,\*</sup>, E. Paska<sup>a</sup>, D. Brzezinska<sup>b</sup>

<sup>a</sup> Center for Mapping, OSU, 1216 Kinnear Road, Columbus, OH 43212 USA - (toth, eva-paska)@cfm.ohio-state.edu

<sup>b</sup> Dept. of Civil and Environmental Engineering and Geodetic Science, OSU, dbrzezinska@osu.edu

## Commission I, WG I/2

**KEY WORDS:** LiDAR, LiDAR intensity, Feature extraction, QA/QC

### ABSTRACT:

LiDAR technology, the primary source of highly accurate surface data at large scale, has seen remarkable developments in recent years. Specifically, the accuracy of the laser ranging has reached the few cm level for hard surfaces, close to static survey performance, and the point density has increased significantly, as a result of higher pulse rates, such as 150 kHz PRF for multipulse LiDAR systems. The high ranging accuracy of the laser sensor also means that the overall accuracy of the point cloud is now predominantly determined by the quality of the navigation solution (typically based on GPS/IMU sensor integration), which is also advancing. All these developments allow for better surface representation in terms of denser point cloud with highly accurate point coordinates. Furthermore, because of the increased point density, the horizontal accuracy has become an equally important part of the product characterization. In parallel to these developments, the demand for better QA/QC is also growing, and now the characterization of the LiDAR products includes the horizontal accuracy. Except for relative measures, there is no reliable way to assess the positioning quality of the data captured by any imaging sensor system, which is based on direct georeferencing, and therefore, using some ground control is almost mandatory if high accuracy is required. This paper introduces a method to use road pavement marking as ground control that could be used for QA/QC. These linear features are widely available in urban areas and along transportation corridors, where most of the government and commercial mapping takes place, and an additional advantage of using pavement markings is that they can be quickly surveyed with various GPS technique (RTK, VRS, post-processed).

## 1. INTRODUCTION

The evolution of ground control used for product QA/QC is closely related to the improvements in the LiDAR point density. When sparsely distributed points were available, the vertical accuracy was the only concern (ASPRS Guidelines, 2004). In fact, the horizontal characterization was greatly ignored at the introduction of LiDAR technology. Obviously, from a theoretical point of view, points separated by a few meters did not allow for adequate surface characterization in general, except for flat areas. To assess the vertical accuracy of the point cloud, flat horizontal surfaces with precisely known elevations can be used. Once the vertical difference was measured, usually based on the statistics derived from a sufficient number of points over flat surface patches, either a simple vertical shift was applied as a correction, or a more complex model could be used that factored in surface differences observed at several (well distributed) locations.

As the LiDAR market started to grow rapidly, soon the LiDAR systems showed truly phenomenal performance improvements. In less than five years, the pulse rate improved by an order, and now 100 and 150 kHz systems are widely used (Optech, 2006 and Leica, 2006); in addition multi-pulse systems are also available. More importantly, the ranging accuracy has increased substantially and now stands close to the level of static GPS or short baseline kinematic surveys, i.e., 1-2 cm for hard surfaces, which is practically negligible to the typical navigation error budget. This remarkable performance potential of the newer LiDAR systems, combined with better operational techniques, opened the door toward applications where large-scale or

engineering-scale accuracy is required. At this point, the georeferencing error budget and, to a lesser extent, the sensor calibration quality, are critical to achieving engineering design level accuracy (few cm). Using ground control is an efficient way for independent and highly reliable QA/QC processes and, if needed, to compensate for georeferencing and sensor modeling errors.

The errors in laser scanning data can come from individual sensor calibration or measurement errors, lack of synchronization, or misalignment between the different sensors. Baltsavias (1999) presents an overview of the basic relations and error formulae concerning airborne laser scanning. Schenk (2001) provides a summary of the major error sources for airborne laser scanners and error formulas focusing on the effect of systematic errors on point positioning. More recently, Csanyi May (2007) presents a comprehensive analysis on LiDAR error modeling. In general, LiDAR sensor calibration includes scan angle and range calibration, and intensity-based range correction. The LiDAR sensor platform orientation is always provided by a GPS/IMU-based integrated navigation system. The connection between the navigation and LiDAR sensor frames is described by the mounting bias, which is composed of the offset between the origin of the two coordinate systems and the boresight misalignment (the boresight misalignment describes the rotation between the two coordinate systems, and is usually expressed by roll, pitch and heading angles). To achieve optimal error compensation that assures the highest accuracy of the final product, all of these parameters should be calibrated. Since not all of the parameters can be calibrated in a laboratory environment, a combination of

---

\* Corresponding author.

laboratory and in situ calibrations is the only viable option for LiDAR system calibration. Typical anomalies in the LiDAR data indicating system calibration errors are: edges of the strips could bend up or down (scan angle error), horizontal surfaces have a visible mismatch between the known and the LiDAR point-defined surfaces (boresight misalignment or navigation error), vertical coordinates of LiDAR points over flat areas do not match the known vertical coordinate of the area (ranging or navigation error), objects, such as pavement markings made of retro reflective coatings, may show up above the surface level, although they should practically have identical vertical coordinates (lack of intensity correction of the range data), etc.

The techniques to detect and ultimately compensate for errors fall into two broad categories based on whether they use absolute control or not. The first group includes most of the strip adjustment techniques and some of the sensor and boresight calibration methods. The ground control-based techniques encompass comparisons to reference surfaces, such as parking lots and buildings, and methods using LiDAR-specific control targets. Another categorization of the techniques is whether they only aim to remove observed differences, also called data driven methods, or they try to achieve the same objective through the sensor model, in other words, to calibrate the sensor model parameters.

The use of dedicated LiDAR targets is a basic method to observe LiDAR point cloud differences at reference points and, consequently, to estimate errors. One of the first approaches to use LiDAR-specific ground targets was developed at OSU (Csanyi and Toth, 2007). The circular targets, optimized for a point density of 3-4 pts/m<sup>2</sup> and above, had a diameter of 2 m and used a different reflective coating on the center circle and outer ring. At the required point cloud density, the number of points returned from the targets allowed for accurate estimation of both vertical and horizontal differences. The technique has been used in several projects and provided highly accurate ground control for QA/QC (Toth *et al.*, 2007a). In a similar implementation, small retro reflectors are placed in a certain shape of similar size, in which case the construction of the target is simpler while the processing is more complicated. Although, these solutions provide excellent results, their use is somewhat limited by economic factors; i.e., the installation and the necessary survey of the targets could be quite labor-intensive. Note that the processing of the LiDAR-specific ground targets is highly automated, and human intervention is only needed for the final evaluation of the results.

To advance the use of ground targets for transportation corridor surveys, an economic method is proposed here that can achieve results comparable to using LiDAR-specific ground targets (Toth *et al.*, 2007b). The use of pavement markings as ground control offers the advantage of being widely available in excellent spatial distribution, and require no installation. Certainly, the surveying of the targets is still needed, but it becomes less difficult with the increasing use of GPS VRS systems that can provide cm-level accuracy in real-time. The other condition of using pavement markings is the availability of LiDAR intensity data that is hardly a restriction with modern LiDAR systems. Note that the distinct appearance of the pavement markings in the LiDAR intensity image is essential to the proposed method, see Figure 1. The main steps of using pavement marking as ground control are briefly described in this paper.

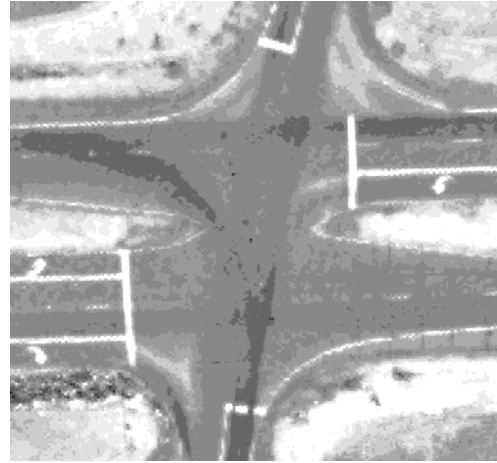


Figure 1. Typical pavement markings at an intersection (LiDAR point density was about 4 pts/m<sup>2</sup>).

## 2. THE CONCEPT

The concept of the proposed method, including pavement marking extraction together with the parameterization of the marks based on LiDAR intensity data, the comparison with ground truth, and the determination of a transformation to correct the point cloud, analysis of the result, etc., is shown in Figure 2. The GPS-surveyed data of the pavement markings, represented in a series of points with cm-level accuracy are assumed to be available. For sensor calibration and/or strip adjustment, sufficient number of pavement markings with good spatial distribution is required to achieve good performance. Currently, only the most commonly found types of pavement markings are considered, such as stop bars, straight edge lines and curved edge lines. In each case, the survey data of the pavement markings are provided as point observed along the centerline of the markings. The LiDAR data, including range and intensity components, are assumed to be of a reasonable quality; i.e., with no gross errors, and thus, the point cloud accuracy is better than a meter.

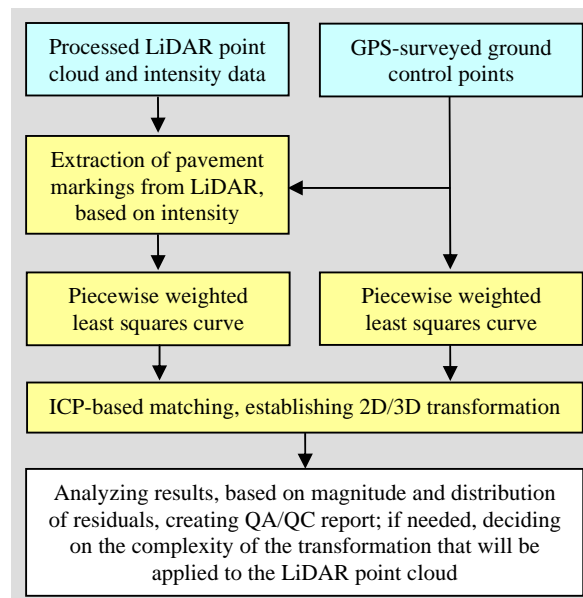


Figure 2. Overall workflow of the proposed method.

Based on the comparison of the two representations of pavement markings, one obtained from the GPS survey and the other one from LiDAR intensity and range data, 2D/3D offset and orientation differences can be detected. Since the road surfaces are predominantly flat and mostly horizontal, the horizontal and vertical discrepancies can be separated in most of the cases. Analyzing the magnitudes of the observed differences and their spatial distribution, the LiDAR data quality can be assessed and, if needed, corrections can be applied to the LiDAR point cloud to improve the point position accuracy. The methodology for the correction could be based on either introducing a spatial transformation to reduce the differences at the controls, or trying to adjust the sensor parameters to achieve the same objective. In most of the cases, a 3D similarity transformation is applied, and the accuracy terms for both data sets are needed to properly characterize the data quality after applying the correction. Note that assessing the horizontal accuracy of the LiDAR point cloud is difficult, as it is mainly defined by the footprint of the laser pulse, which depends on the flying height and beam convergence; in addition, the impact of object surface characteristics could be also significant. In the following sections, the three key components of the proposed method, pavement marking extraction, curve fitting and matching, are discussed in detail.

### 3. EXTRACTING PAVEMENT MARKINGS

One of the first attempts on using LiDAR intensity data was demonstrated by Maas (2001), who describes the extension of a TIN-based matching technique using reflectance data (LiDAR intensity data) to replace surface height texture for the determination of planimetric strip offsets in flat areas with sufficient reflectance texture. Later, research interest steered toward conventional classification use of the intensity data. Song *et al.* (2002) proposed a technique to use intensity data for land-cover classification. A comprehensive study on processing both range and intensity data is provided by Sithole (2005). Kaasalainen *et al.* (2005) provides a review on intensity data as applied to calibration. Finally, Ahokas *et al.* (2006) presents the results of a calibration test on intensity data using the Optech ALTM 3100. All these demonstrations emphasize the relative nature of the LiDAR intensity data; namely, different surfaces, data from different flying heights, and different surface orientations can produce exactly the same intensity values. Therefore, techniques to normalize or calibrate the intensity data, such as to reference the intensity and range values with respect to each other started becoming more common.

The extraction of the pavement markings is based on the typically significant difference in the LiDAR intensity values between road surfaces and pavement markings, as illustrated in Figure 1. The selection of LiDAR points obtained from the pavement markings is greatly simplified by the availability of GPS survey data of the pavement markings, which can drastically reduce the search window. Figure 3 shows a typical case, where the GPS survey points are overlaid on the LiDAR image; note the minor, yet visible, mismatch between the pavement marking and the survey points.

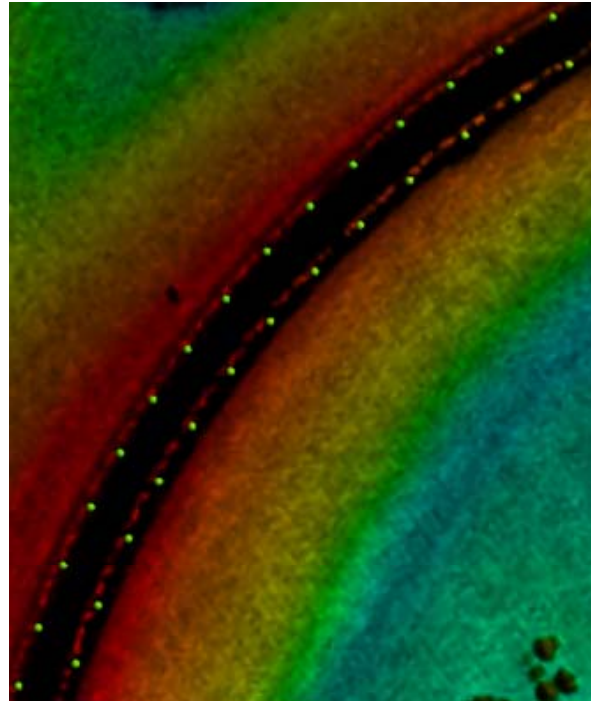


Figure 3. Freeway ramp with pavements markings and GPS-surveyed points (green).

Depending on the overall LiDAR data quality, more precisely the horizontal accuracy of the point cloud, the actual search area is typically a narrow patch along the GSP-surveyed points with a width of less than 1 m. Ideally, an extracted patch should only contain points of road surfaces and pavement markings, with two dominant intensity ranges. Figure 4 depicts the histogram of the LiDAR intensities in such an area. The distribution shows a typical shape, characterized by most of the points clustered at lower intensities with slowly decreasing frequencies toward the higher intensities of the pavement markings. The reason why there is no clear separation between the points of the road surface and pavement markings is illustrated in Figure 5, which shows that the points falling on the boundary regions between the two areas have varying intensity values; note that the LiDAR footprint size is comparable to the pavement markings' dimension.

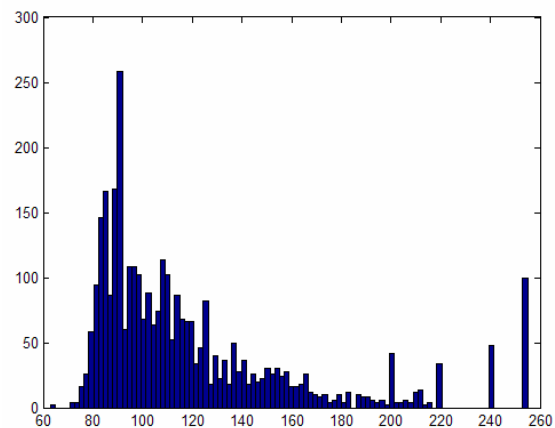


Figure 4. Intensity histogram of a narrow area around pavement markings.

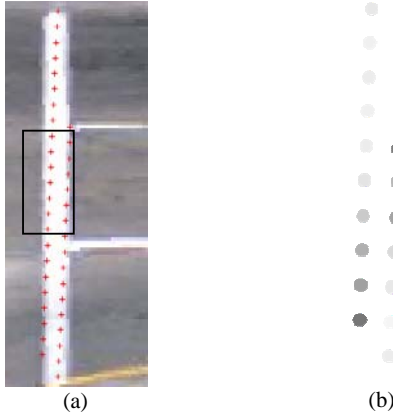


Figure 5. Changes of intensity values along pavement markings: LiDAR point locations overlaid on optical image (a) and intensity values (b).

Unfortunately, the relative nature of the LiDAR intensity signal does not allow for a general parameterization of the intensity values for pavement surfaces and pavement markings, and thus, there is no absolute threshold that would separate the two areas. Therefore, first the distribution of the intensity signals in the search window should be analyzed to determine an optimal threshold for separating pavement and pavement marking points. In our approach, the point, where the curve of the pavement surface points levels out, was selected as a threshold, and subsequently used for extraction of the pavement marking points. The points extraction based on this threshold could result in errors, such as marking points are omitted or pavement points are included. Therefore, further checks are needed, which is accomplished by curve fitting and matching, described below, where the availability of object space information, such as curvature of the pavement markings, can be utilized. Figure 6 shows the pavement markings extracted for the area pictured in Figure 3; the threshold was 180.

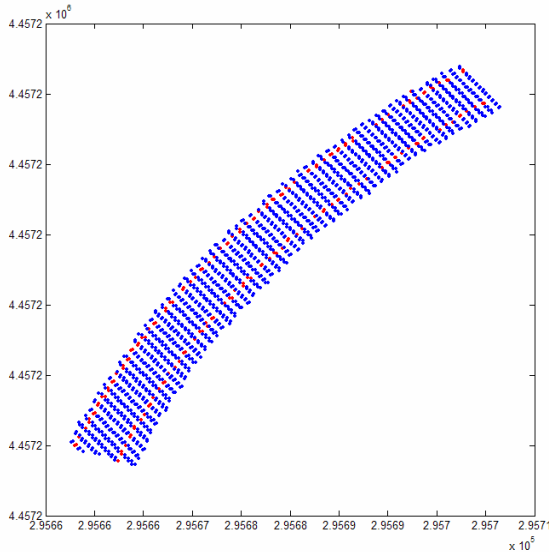


Figure 6. Pavement markings extracted by thresholding.

#### 4. CURVE FITTING

The extracted pavement marking and GPS-surveyed points have no point-to-point correspondence, and thus, a point-based transformation is directly not applicable. However, their shape

can be matched, on condition that the two representations provide an adequate description of the same linear feature. In this case, the problem is simply how to match two free-shape curves. In the following, the key steps of curve fitting are presented, while the matching is discussed in the next section.

The purpose of curve fitting is twofold: first, it provides a validity check for the pavement marking points extracted, and second, it allows for modeling both pavement marking descriptions as linear features, so they can be matched to each other. The selected curve fitting method is an extended version of the algorithm, originally proposed by Ichida and Kiyono in 1977, and is a piecewise weighted least squares curve fitting based on cubic (third-order polynomial) model, which seemed to be adequate for our conditions, such as linear features with modest curving. To handle any kind of curves, defined as the locus of points  $f(x, y) = 0$ , where  $f(x, y)$  is a polynomial, the curve fitting is performed for smaller segments in local coordinate systems, which are defined by the end points of the curve segments. The primary advantage of using a local coordinate system is to avoid problems when curves become vertical in the mapping coordinate system. Obviously, the fitting results as well as the fitting constraints are always converted forth and back between the local and mapping coordinate frames, for details, see (Toth *et al.*, 2007).

The main steps of the piecewise cubic fitting (PCF) process are shortly discussed below; the notation used in the discussion is introduced in Figure 7. To achieve a smooth curve, the curve fitting to any segment is constrained by its neighbors by enforcing an identical curvature at the segment connection points; in other words, PCF polynomial is continuous with its first derivative at connection points  $x=s$ ,  $x=t$ , etc. The equations describing the 3rd polynomial and its first derivative are:

$$S_k(x) = y_s + m_s \cdot (x - s) + a_s \cdot (x - s)^2 + b_s \cdot (x - s)^3$$

$$\text{slope} = S'_k(x) = m_s + 2 \cdot a_s \cdot (x - s) + 3 \cdot b_s \cdot (x - s)^2$$

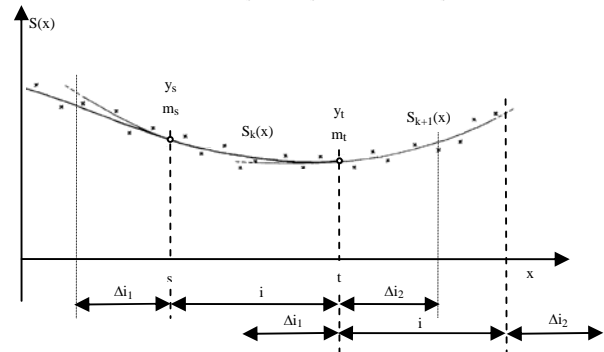


Figure 7. Piecewise weighted least squares curve fitting method.

The core processing includes the following steps: 1)  $a_s$  and  $b_s$ , the coefficients of the second and third order terms of the fitted curve for interval 'i' are estimated; consider the constant term ( $y_s$ ) and the coefficient of the first order term ( $m_s$ ) fixed, known from the curve fitting from the previous segment. In the adjustment, the points in interval  $\Delta i_2 + i + \Delta i_1$  (past, present, and future data points) are used, 2) the value ( $y_t$ ) and the slope ( $m_t$ ) at  $x=t$  are computed; these values are used as fixed constraints in the curve fitting for the next segment, and 3) step 1 is repeated to process the next segment. Additional details can be found in (Toth *et al.*, 2007). Curves fitted to pavement markings' and GPS-surveyed points are shown in Figure 8; the LiDAR scanlines are readily visible.



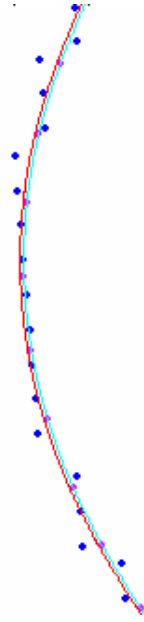


Figure 8. Curve fitting, LiDAR and GPS-surveyed points (blue and magenta) and fitted curves (red and cyan)

### 5. MATCHING CURVES

The objective of curve matching is to find the spatial relationship between two data representations of the pavement markings, the curve-fitted pavement markings and the GPS surveyed points. Assuming that the two representations, such as the curve fitted ones, provide an adequate description of the same shape, the free-shape curve matching techniques can be applied. Since the pavement markings' descriptions in both original and curve-fitted representations for both LiDAR and GPS-surveyed points are spatially close to each other, the well-known Iterative Closest Point (ICP) algorithm (Besl and McKay, 1992; Madhavan *et al.*, 2005) was selected to perform this task.

Iterative registration algorithms are increasingly used for registering 2D/3D curves and range images. Due to its consistent performance, the ICP algorithm was adopted here to match curves describing pavement markings obtained from LiDAR intensity and GPS measurements. The ICP algorithm finds the best correspondence between two curves (point sets) by iteratively determining the translations and rotations parameters of a 2D/3D rigid body transformation.

$$\min_{(R,T)} \sum_i \|M_i - (RD_i + T)\|^2$$

Where  $R$  is a  $2 \times 2$  rotation matrix,  $T$  is a  $2 \times 1$  translation vector, and subscript  $i$  refers to the corresponding points of the sets  $M$  (model) and  $D$  (data). The ICP algorithm can be briefly summarized as follows:

1. For each point in  $D$ , compute the closest point in  $M$
2. Compute the incremental transformation ( $R, T$ )
3. Apply incremental transformation from step (2) to  $D$
4. If relative changes in  $R$  and  $T$  are less than a given threshold, terminate, otherwise go to step (1)

ICP can be applied to individual pavement markings or to a group of pavement markings. Figure 9 shows an intersection where four lines were matched.

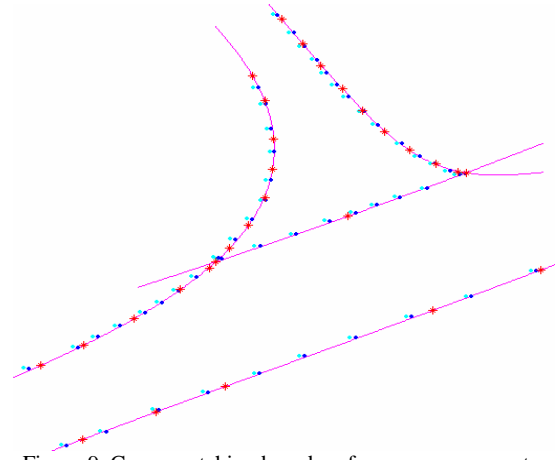


Figure 9. Curve matching based on four curves; magenta: curves fitted to control points, red: GPS control points, cyan: curve points derived from LiDAR, and blue: transformed curve points after ICP.

The ICP algorithm was implemented in Matlab and space-scale optimization was incorporated to reduce execution time.

### 6. EXPERIMENTAL RESULTS

Initial performance tests of the proposed method were performed using typical intersection and freeway ramp data from a recently flown LiDAR survey, where GPS-surveyed pavement markings were available, both were provided by the Ohio Department of Transportation. The LiDAR point spacing varied in the 1-3 pts/m range, and the horizontal accuracy of the GPS-surveyed points, provided by a VRS system was 1-2 cm.

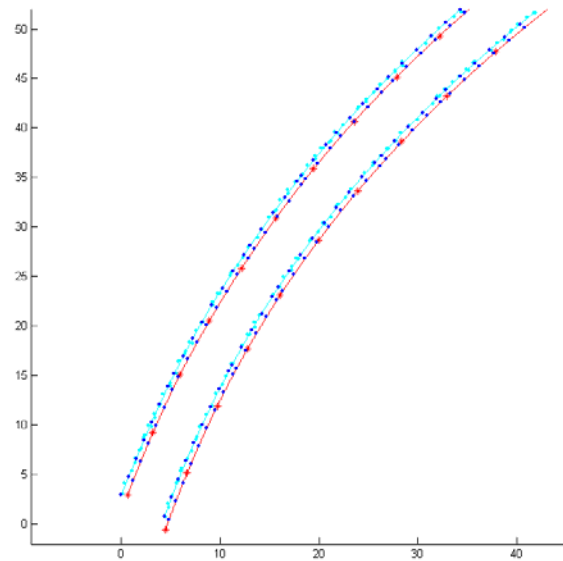


Figure 10. ICP matched curves; magenta: curves fitted to control points, red: GPS control points, cyan: LiDAR point and curves fitted, and blue: matched points.

In the curve fitting process both data representations were fitted, with a point spacing of 1 cm, and various combinations were processed by the ICP-based curve matching in 2D and 3D. In order to assess the accuracy of the transformation, the correspondence between the LiDAR-derived curve and the



control curve was established. Since the two curves, in general, are not entirely identical, even after the final ICP iteration, the transformed LiDAR point-derived curve is close but not necessarily falls on the control curve. However, the location of the transformed LiDAR-derived points represents the best fit to the control curve in the least squares sense. Therefore, these points are projected to the closest points of the control curve, and then they are considered as conjugate points. Figure 10 shows the results for the ramp area pictured in Figure 3. The transformation parameters between these two point sets (the original LiDAR-derived points and their corresponding points on the control curve) are calculated in a least squares adjustment. Table 1 shows the 2D transformation parameters for three different cases, clearly indicating the robustness of the ICP method with respect to noisy data, such as using the original LiDAR points. The differences between curves and residuals after ICP matching for the three cases are shown in Table 2. The 2 cm horizontal precision is realistic, given the fact that the GPS-surveyed points are known at a 1-2 cm-level accuracy, and the LiDAR-based pavement marking positioning accuracy is estimated at the few cm range. The 9-10 cm precision terms in case 2 correspond to the use of the noisy LiDAR data (no curve-fitting applied to smoothly model the pavement markings).

ICP input data	ICP-adjusted transformation parameters		
	$\Delta X$ [m]	$\Delta Y$ [m]	$\phi$ [°]
Both, LiDAR and GPS points are curve-fitted	0.153	-0.114	0.000
No fitting of LiDAR points, GPS points curve-fitted	0.150	-0.114	0.000
No fitting of GPS points, LiDAR points curve-fitted	0.158	-0.116	0.000

Table 1. Transformation results (2D).

Case	Differences/Residuals							
	X [m]				Y [m]			
	Before		After		Before		After	
	mean	Std	mean	std	mean	std	mean	Std
1	0.16	0.02	0.00	0.02	-0.11	0.02	0.00	0.02
2	0.16	0.10	0.00	0.10	-0.12	0.09	0.00	0.09
3	0.16	0.02	0.00	0.02	-0.12	0.01	0.00	0.01

Table 2. Original differences and residuals after ICP (2D).

## 7. CONCLUSION

The new method that introduced the use of pavement markings as LiDAR ground control delivered encouraging initial results. The performance of the three main processing steps, including the extraction of pavement markings, curve fitting, and ICP-based matching has been validated. Using a dataset acquired over a transportation network by a state-of-the-art LiDAR system, pavement markings from several intersections and freeway ramps have been processed delivering robust results. In particular, the performance of the ICP matching algorithm is noteworthy.

### Acknowledgement

The authors would like to thank the Ohio Department of Transportation for the GPS survey of pavement markings and flying LiDAR surveys to acquire essential data for this research.

### References:

- Ahokas, E., Kaasalainen, S., Hyypää, J. and Suomalainen, J., 2006. Calibration of the Optech ALTM 3100 Laser Scanner Intensity Data Using Brightness Targets, Proceedings of ISPRS Commission I. Symposium.
- ASPRS LiDAR Committee, 2004. ASPRS Guidelines Vertical Accuracy Reporting for LiDAR Data [http://www.asprs.org/society/committees/lidar/Downloads/Vertical\\_Accuracy\\_Reporting\\_for\\_Lidar\\_Data.pdf](http://www.asprs.org/society/committees/lidar/Downloads/Vertical_Accuracy_Reporting_for_Lidar_Data.pdf)
- Baltsavias, E.P., 1999. Airborne Laser Scanning: Basic Relations and Formulas. ISPRS Journal of Photogrammetry & Remote Sensing, Vol. 54: 199-214.
- Besl, P. J. and McKay, N. D. A method for registration of 3-d shapes. IEEE Trans. Pat. Anal. and Mach. Intel. 14(2), pp 239-256, Feb 1992.
- Csanyi N, Toth C., Grejner-Brzezinska D. and Ray J., 2005. Improving LiDAR data accuracy using LiDAR-specific ground targets, ASPRS Annual Conference, Baltimore, MD, March 7-11, CD-ROM.
- Csanyi May, N., 2007. A Rigorous Approach to Comprehensive Performance Analysis of State-Of-The-Art Airborne Mobile Mapping Systems, PhD dissertation, The Ohio State University.
- Csanyi, N. and Toth, C., 2007. Improvement of LiDAR Data Accuracy Using LiDAR-Specific Ground Targets, Photogrammetric Engineering & Remote Sensing, Vol. 73, No. 4, pp. 385-396.
- Ichida, K. and Kiyono, T. 1977. Curve Fitting with One-Pass Method with a Piecewise Cubic Polynomial, ACM Transactions on Mathematical Software, Vol. 3, No. 2, pp. 164-174.
- Leica Geosystems, ALS50, <http://gis.leica-geosystems.com>
- Maas, H.-G., 2001. On the Use of Pulse Reflectance Data for Laserscanner Strip Adjustment. International Archives of Photogrammetry, Remote Sensing and Spatial Information Sciences, 33 (Part 3/W4): 53-56.
- Madhavan, R., Hong, T., Messina, E. Temporal Range Registration for Unmanned Ground and Aerial Vehicles, Journal of Intelligent and Robotic Systems, Vol. 44, No. 1, September, 2005, pp. 47-69.
- Optech, ALTM 3100AE, 2006, [www.optech.ca/pdf/Brochures/ALTM3100EAWspecsfnl.pdf](http://www.optech.ca/pdf/Brochures/ALTM3100EAWspecsfnl.pdf)
- Schenk, T., 2001. Modeling and Analyzing Systematic Errors in Airborne Laser Scanners. Technical Notes in Photogrammetry, vol. 19. The Ohio State University, Columbus, USA.
- Sithole, G., 2005. Segmentation and Classification of Airborne Laser Scanner Data, Publication of Geodesy 59, Nederlandse Commissie voor Geodesie, Delft (184 pages).
- Song, J-H., Han, S-H., Yu, K, and Kim, Y., 2002. Assessing the Possibility of Land-Cover Classification Using LiDAR Intensity Data, International Archives of Photogrammetry, 34. pp. 4.
- Toth C., Csanyi N. and Grejner-Brzezinska D. 2002. Automating the Calibration of Airborne Multisensor Imaging Systems, Proc. ACSM-ASPRS Annual Conference, Washington, DC, April 19-26, CD ROM.
- Toth, C., D. Brzezinska, N. Csanyi, E. Paska and N. Yastikly, (2007a). LiDAR Mapping Supporting Earthquake Research of the San Andreas Fault, ASPRS Annual Conference, Tampa, Florida, May 7-11, CD ROM.
- Toth, C., Paska, E., Grejner-Brzezinska, D.A. (2007b): Using Pavement Markings to Support the QA/QC of LiDAR Data, PIA 2007, International Archives of Photogrammetry and Remote Sensing, Vol. XXXVI, 3/W49B, pp. 173-178.

## QUALITY ASSESSMENT OF LIDAR DATA BY USING PAVEMENT MARKINGS

**Charles Toth, Eva Paska**

Center for Mapping  
The Ohio State University  
Columbus, OH 43212  
[toth@cfm.ohio-state.edu](mailto:toth@cfm.ohio-state.edu)

**Dorota Brzezinska**

Department of Civil and Environmental Engineering and Geodetic Science  
The Ohio State University  
Columbus, OH 43212

### ABSTRACT

LiDAR technology has seen remarkable developments in recent years. In particular, the accuracy of the laser ranging has reached the few cm level for hard surfaces, close to static survey performance, and the point density has increased significantly, reaching 150 kHz PRF for multipulse LiDAR systems. These developments allow for better surface representation and exploitation of the 3D nature of the point cloud; in other words, the horizontal accuracy has become an equally important part of the product characterization. The high ranging accuracy of the laser sensor means that overall accuracy of the point cloud is predominantly determined by the quality of the navigation solution (typically based on GPS/IMU sensor integration). Despite recent significant advancements in navigation technologies, to achieve and sustain a high accuracy navigation solution of an airborne platform for longer flight lines over extended time is still a difficult task, as positional drift frequently occur. Moreover, there is no reliable way to assess the positioning quality of the data captured by the laser sensor within the LiDAR system, which is based on direct georeferencing. Therefore, using some ground control is almost mandatory if high accuracy is required. This paper introduces a method to use road pavement marking as ground control that could be used for QA/QC. These linear features are widely available in urban areas and along transportation corridors, where most of the government and commercial mapping takes place.

### INTRODUCTION

Since its introduction in the late 90s, LiDAR has seen remarkable developments, mainly driven by technology. For the user, it means higher point density, or better surface representation, and improving accuracy. The state-of-the-art is that the laser sensor can provide 1-2 cm ranging accuracy for so-called hard surfaces at normal flying heights; which means that the georeferencing term accounts primarily for the accuracy of the LiDAR product. Despite consistent advancement of the GPS/IMU-based georeferencing technology for longer flight lines, the performance of the navigation solution could change, resulting in a varying accuracy of the LiDAR point cloud. The main effect is that strip overlap areas could show varying amount of discrepancies; typically, described as drift. While a strip adjustment can eliminate the strip differences, the absolute accuracy is not necessarily improved as a result of the applied correction. Therefore, ground control is always needed as there is no other way to independently validate the accuracy of the LiDAR product, including both the vertical and horizontal terms. The methodology to characterize a LiDAR product using ground control includes several components, such as the determination of the differences between LiDAR data and reference surfaces, requirement for the number of ground control areas, analysis of the distribution of the differences, statistical method used, specification and qualification of the results, etc. This paper is only addressing the measurements of discrepancies.

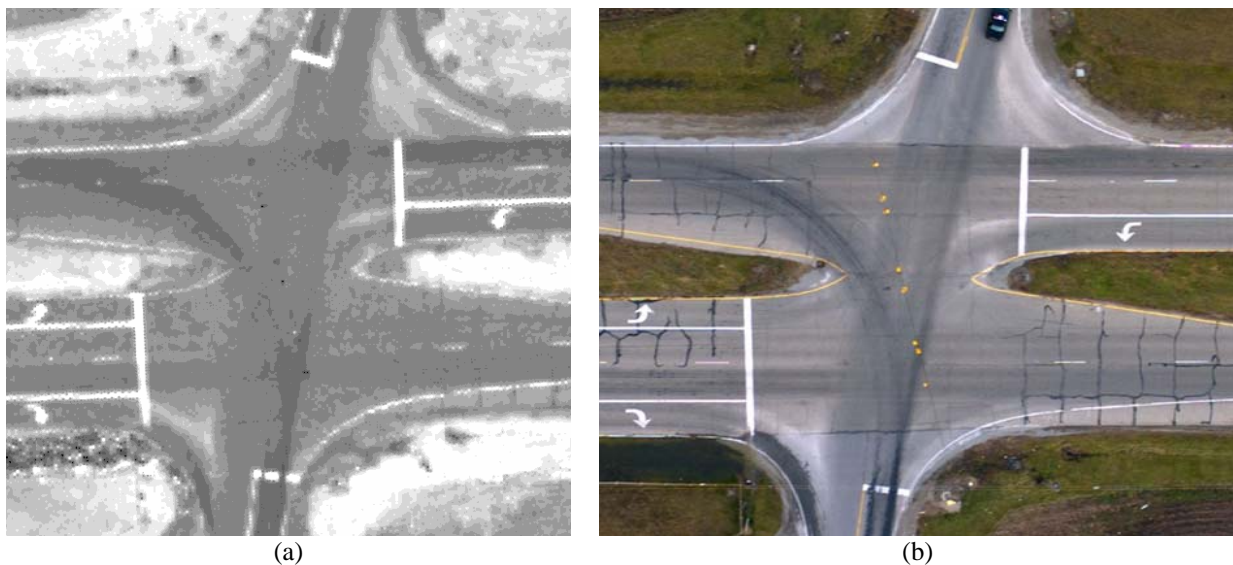
The evolution of ground control used for product QA/QC is closely related to the improvements in the LiDAR point density. When sparsely distributed points were available, the vertical accuracy was the only concern (ASPRS Guidelines, 2004). In fact, the horizontal characterization was greatly ignored at the introduction of LiDAR technology. Obviously, from a theoretical point of view, points separated by a few meters did not allow for adequate surface characterization in general, except for flat areas. To assess the vertical accuracy of the point cloud, flat horizontal surfaces with precisely known elevation can be used. Once the vertical difference was measured, usually based on the statistics derived from a sufficient number of points over flat surface patches, either a simple vertical

shift was applied as correction or a more complex model could be used that factored in surface differences observed at several (well distributed) locations.

As density increased, however, the need for characterizing the point cloud in 3D terms became important, which ultimately required the measurements of 3D surface discrepancies. Methods were soon developed to determine surface discrepancies that could be applied to both LiDAR strips and reference surfaces. Obviously, 3D observations are only available if there is sufficient terrain relief, in which case the problem is solved by surface matching (e.g., Besl and McKay, 1992; Gruen and Akca, 2005). There is a variety of methods that can handle any kind of surfaces or can use a number of planar surface patches with different surface normal vectors. A practical aspect of the surface matching is that it is rather difficult to precisely survey ground surfaces of any shape in general, although terrestrial laser scanning is becoming a viable solution for this purpose. Using man-made objects, such as buildings, provides an easier approach to develop a reference test range with many differently oriented planar surfaces. In fact, airport areas are frequently used for laser sensor calibration.

The use of dedicated LiDAR targets is another alternative to observe LiDAR point cloud differences at reference points and, consequently, to estimate errors. One of the first approaches to use LiDAR-specific ground targets was developed at OSU (Csanyi and Toth, 2007). The circular-shaped targets, optimized for a point density of 3-4 pts/m<sup>2</sup> and above, had a diameter of 2 m and used a different reflective coating on the center circle and outer ring. At the required point cloud density, the number of points returned from the targets allowed for accurate estimation of both vertical and horizontal differences. The technique has been used in several projects and provided highly accurate ground control for QA/QC (Toth *et al.*, 2007a). In a similar implementation, small retro reflectors are placed in a certain shape of similar size, in which case the construction of the target is simpler while the processing is more complicated. Although, these solutions provide excellent results, their use is somewhat limited by economic factors; i.e., the installation and the necessary survey of the targets could be quite labor-intensive. Note that the processing of the LiDAR-specific ground targets is highly automated, and human intervention is only needed for the final evaluation of the results.

To advance the use of ground targets for transportation corridor surveys, an economic method is proposed here that can achieve comparable results using LiDAR-specific ground targets (Toth *et al.*, 2007b). The use of pavement markings as ground control offers the advantage of being widely available in excellent spatial distribution, and requires no installation. Certainly, the surveying of the targets is still needed, but it becomes less difficult with the increasing use of GPS VRS systems that can provide cm-level accuracy in real-time. The other condition of using pavement markings is the availability of LiDAR intensity data that is hardly a restriction with modern LiDAR systems. Note that the distinct appearance of the pavement markings in the LiDAR intensity image is essential for the proposed method, see Figure 1. The main steps of using pavement marking as ground control are briefly described in this paper.



**Figure 1.** Pavement marking appearance in LiDAR intensity image (a) and reference optical image (b).

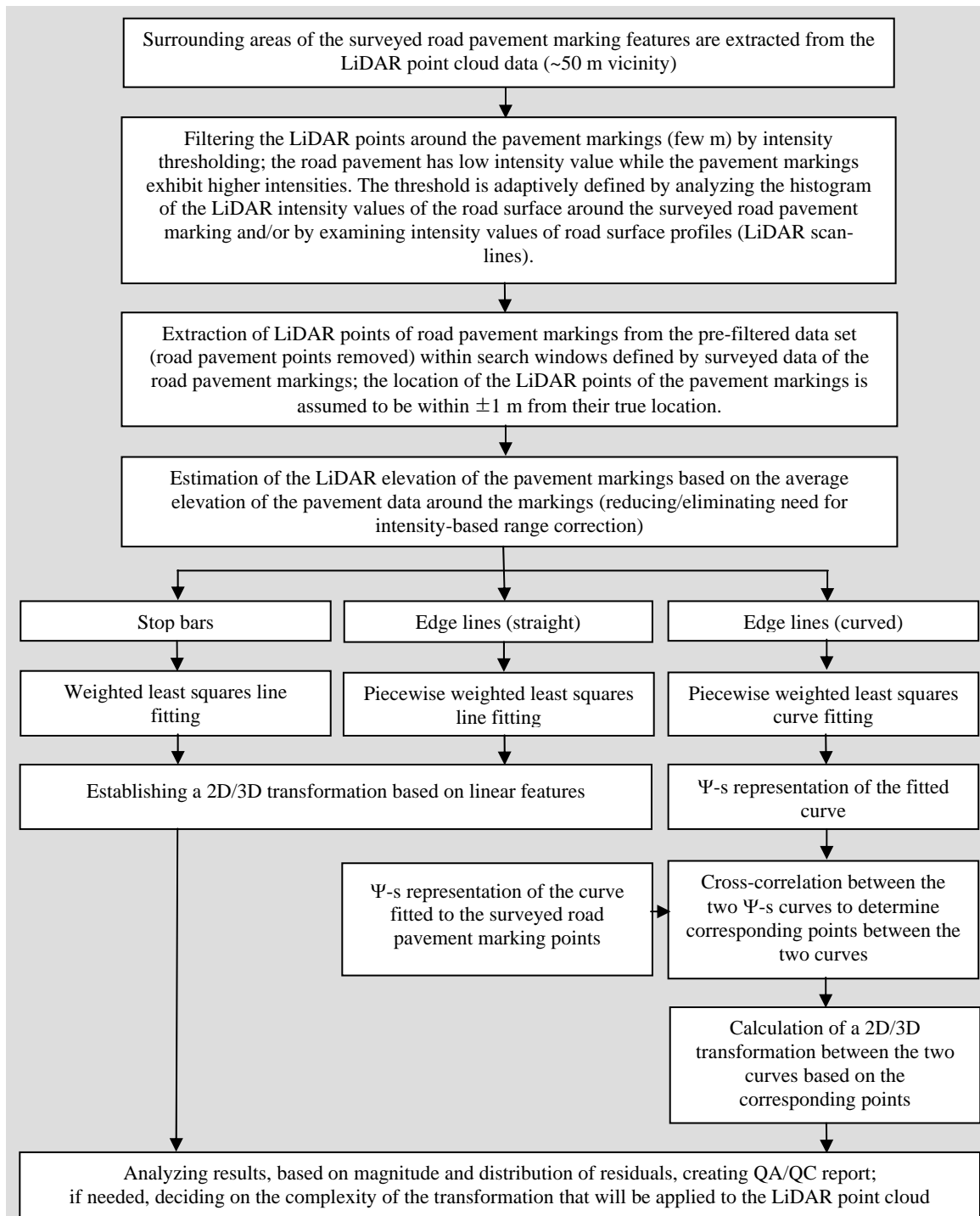
## USING PAVEMENT MARKINGS AS GROUND CONTROL

The concept of the proposed method, including pavement marking extraction together with the parameterization of the marks based on LiDAR intensity data, the comparison with ground truth, and the determination of a transformation to correct the point cloud, analysis of result, etc., is shown in Figure 2. The GPS-surveyed data of the pavement markings, represented in a series of points with cm-level accuracy is assumed to be available. For sensor calibration and/or strip adjustment, sufficient number of pavement markings with good spatial distribution is required to achieve good performance. Currently, only the most widely found types of pavement markings are considered: Stop bars, straight edge lines and curved edge lines. In each case, the survey data of the pavement markings is provided as point observations along the centerline of the markings. The LiDAR data, including range and intensity components, are assumed to be of reasonable quality; i.e., no gross errors and thus the point cloud accuracy is better than a meter.

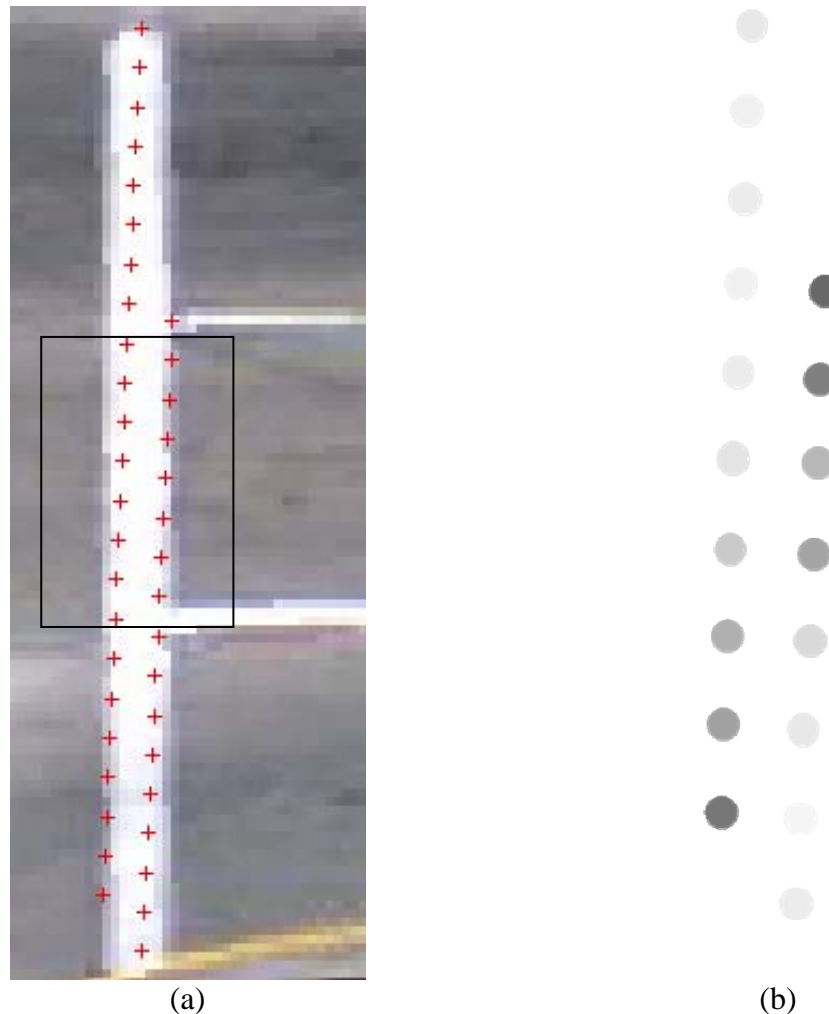
Based on the comparison of the two descriptions of pavement markings, one obtained from the GPS survey and the other one from LiDAR intensity and range data, 2D/3D offset and orientation differences can be detected. Since the road surfaces are predominantly flat and mostly horizontal, the horizontal and vertical discrepancies can be separated in most of the cases. Analyzing the magnitude of the observed differences and their spatial distribution, the LiDAR data quality can be assessed and, if needed, corrections can be applied to the LiDAR point cloud to improve the point position accuracy. The methodology for the correction could be based on either introducing a spatial transformation to reduce the differences at the controls or trying to adjust the sensor parameters to achieve the same objective. In most of the cases, a 3D similarity transformation is applied and the accuracy terms for both data sets are needed to properly characterize the data quality after applying the correction. Note that assessing the horizontal accuracy of the LiDAR point cloud is difficult, as it is mainly defined by the footprint of the laser pulse, which depends on flying height and beam convergence; in addition, the impact of object surface characteristics could be also significant. In the following, the three key components of the proposed method, pavement marking extraction, curve fitting and matching are discussed at detail.

### Extraction of Pavement Markings

The extraction of the pavement markings is based on the significant difference in the LiDAR intensity values between road surfaces and pavement markings. Furthermore, the availability of GPS survey data of the pavement markings drastically reduces the search window for the extraction process (the selection of LiDAR points obtained from the pavement markings). Depending on the overall LiDAR data quality, more precisely the horizontal accuracy of the point cloud, the actual search area is typically a narrow patch with a width of less than 1 m. Unfortunately, the relative nature of the LiDAR intensity signal does not allow for a general parameterization of the intensity values for pavement surfaces and pavement markings. Therefore, first the distribution of the intensity signals in the search window should be analyzed to determine an optimal threshold for separating pavement and pavement marking points. The points extraction based on the threshold could result in errors such as marking points are omitted or pavement points are included. Therefore, further checks are needed, which is accomplished by curve fitting, described below, where the availability of object space information can be utilized, such as curvature of the pavement markings. To illustrate the difficulty of the extraction process, Figure 3 shows the troubling case when the LiDAR scan line is near parallel to the pavement marking.



**Figure 2.** Concept of extracting pavement markings and using them as ground control.



**Figure 3.** Changes of intensity values along pavement markings: LiDAR point locations overlaid on optical image (a) and intensity values (b).

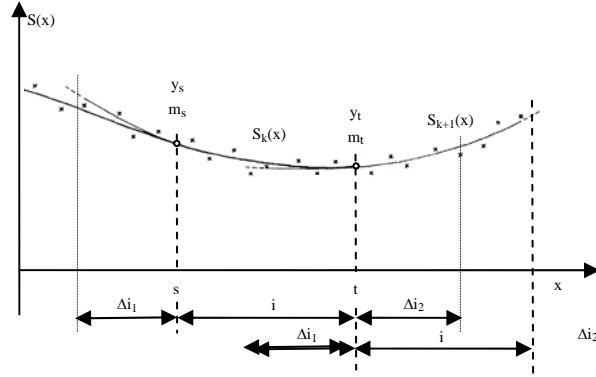
### Curve Fitting

The purpose of curve fitting is twofold: first, it provides a validity check for the pavement marking points extracted, and second, it allows for modeling both pavement marking descriptions as linear features, so they can be matched to each other. The selected curve fitting method is an extended version of the algorithm, originally proposed by Ichida and Kiyono in 1977, and is a piecewise weighted least squares curve fitting based on cubic (third-order polynomial) model, which seemed to be adequate for our conditions, linear features with modest curving. To handle any kind of curves, defined as the locus of points  $f(x, y) = 0$  where  $f(x, y)$  is a polynomial, the curve fitting is performed for smaller segments in local coordinate systems, which are defined by the end points of the curve segments. The primary advantage of using a local coordinate system is to avoid problems when curves become vertical in the mapping coordinate system. Obviously, the fitting results as well as the fitting constraints are always converted forth and back between the local and mapping coordinate frames.

The main steps of the piecewise cubic fitting (PCF) process are shortly discussed below; the notation used in the discussion is introduced in Figure 4. To achieve a smooth curve, the curve fitting to any segment is constrained by its neighbors by enforcing an identical curvature at the segment connection points; in other words, PCF polynomial is continuous with its first derivative at connection points  $x=s$ ,  $x=t$ , etc. The equations describing the third-order polynomial and its first derivative are:

$$S_k(x) = y_s + m_s \cdot (x - s) + a_s \cdot (x - s)^2 + b_s \cdot (x - s)^3$$

$$\text{slope} = S'_k(x) = m_s + 2 \cdot a_s \cdot (x - s) + 3 \cdot b_s \cdot (x - s)^2$$



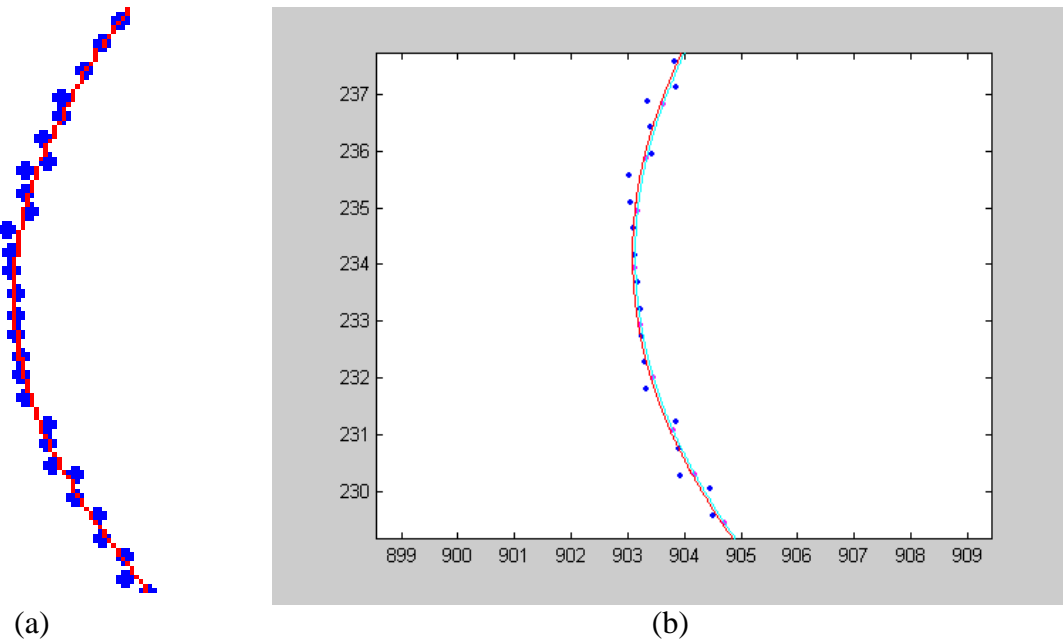
**Figure 4.** Piecewise weighted least squares curve fitting method.

The core processing includes the following steps: 1)  $a_s$  and  $b_s$ , the coefficients of the second and third order terms of the fitted curve for interval ‘ $i$ ’ are estimated; consider the constant term ( $y_s$ ) and the coefficient of the first order term ( $m_s$ ) fixed, known from the curve fitting from the previous segment. In the adjustment, the points in interval  $\Delta i_2 + i + \Delta i_1$  (past, present, and future data points) are used, 2) the value ( $y_t$ ) and the slope ( $m_t$ ) at  $x=t$  are computed; these values as fixed constraints are used in the curve fitting for the next segment, and 3) step 1 is repeated to process the next segment.

	$y - y_s - m_s \cdot (x - s) = a_s \cdot (x - s)^2 + b_s \cdot (x - s)^3$
Step 1	LS for points in interval $\Delta i_1 + i + \Delta i_2 \Rightarrow \hat{a}_s, \hat{b}_s$ $\Rightarrow S_k(x) = y_s + m_s \cdot (x - s) + \hat{a}_s \cdot (x - s)^2 + \hat{b}_s \cdot (x - s)^3$ $\rightarrow x = t$
Step 2	$\hat{y}_t = S_k(t) = y_s + m_s \cdot (t - s) + \hat{a}_s \cdot (t - s)^2 + \hat{b}_s \cdot (t - s)^3$ $\hat{m}_t = S_k'(t) = m_s + 2 \cdot \hat{a}_s \cdot (x - s) + 3 \cdot \hat{b}_s \cdot (x - s)^2$ $\rightarrow y_t = \hat{y}_t$ and $m_t = \hat{m}_t$
Step 3	$S_{k+1}(x) - y_t - m_t \cdot (x - t) = a_t \cdot (x - t)^2 + b_t \cdot (x - t)^3$ LS for points in interval $\Delta i_1 + i + \Delta i_2 \Rightarrow \hat{a}_t, \hat{b}_t$

The curve fitting allows for a polyline representation of both data types, LiDAR or GPS, with a user-defined spacing and thus can effectively curve fitting. Figure 5 shows curve fitted to LiDAR points as well as a case where both data data sets were modeled by curves.





**Figure 5.** Curve fitting:  
 (a) LiDAR points (blue) and fitted curve (red)  
 (b) LiDAR data and GPS-surveyed points (magenta) and fitted curve (cyan).

### Curve Matching

The objective of curve matching is to find the spatial relationship between two data representations of the pavement markings. Because there is no point-to-point correspondence between the two data sets, point-based transformations are directly not applicable. Furthermore, the somewhat modest horizontal accuracy of the LiDAR points is an additional disadvantage. Using linear features, however, presents a solution that is less sensitive compared to point-based methods. Assuming that the two representations, such as the curve fitted ones, provide an adequate description of the same shape, the problem is simply how to match two free-shape curves. The pavement markings descriptions in both original and curve-fitted format are spatially close to each other, the well-known Iterative Closest Point (ICP) algorithm (Besl and McKay, 1992; Madhavan et al., 2005) was selected to perform that task.

Iterative registration algorithms are increasingly used for registering 2D/3D curves and range images recently. The ICP algorithm is adopted here to match curves describing pavement markings obtained from LiDAR intensity and GPS measurements. The ICP algorithm finds the best correspondence between two curves (point sets) by iteratively determining the translations and rotations parameters of a 2D/3D rigid body transformation.

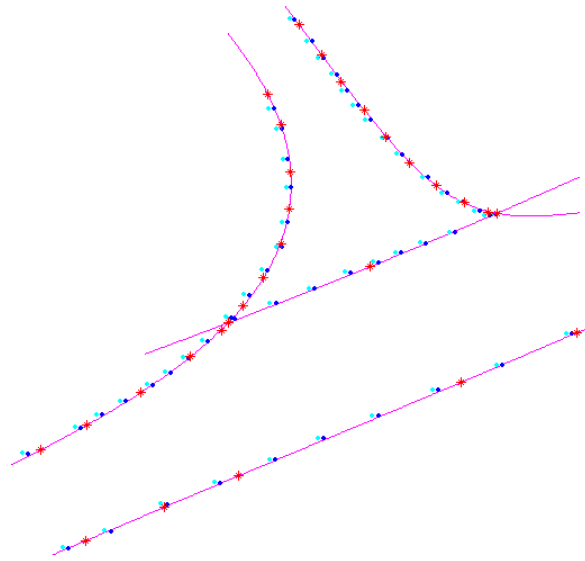
$$\min_{(R,T)} \sum_i \|M_i - (RD_i + T)\|^2$$

where  $R$  is a 3\*3 rotation matrix,  $T$  is a 3\*1 translation vector and subscript  $i$  refer to the corresponding points of the sets  $M$  (model) and  $D$  (data). The ICP algorithm can be summarized as follows:

1. For each point in  $D$ , compute the closest point in  $M$
2. Compute the incremental transformation  $(R, T)$
3. Apply incremental transformation from step (2) to  $D$
4. If relative changes in  $R$  and  $T$  are less than a given threshold, terminate, otherwise go to step (1)

ICP can be applied to individual pavement markings or to a group of pavement markings. Figure 6 shows an intersection where four lines were matched.

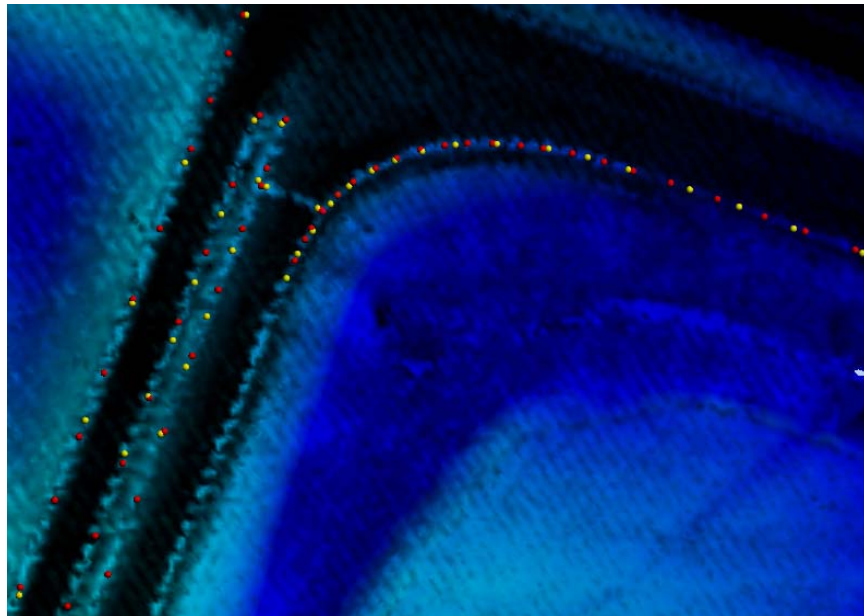




**Figure 6.** Curve matching based on four curves; magenta: curves fitted to control points, red: GPS control points, blue: curve points derived from LiDAR, and cyan: transformed curve points after ICP.

## EXPERIMENTAL RESULTS

To support performance testing of the proposed method, the Ohio Department of Transportation surveyed several intersections in an area which was recently LiDAR surveyed. The pavement markings were surveyed using a VRS system with about 1-2 cm horizontal and 2-5 cm vertical accuracy; the point spacing varied in the 1-3 pts/m range. Figure 7 shows an area with linear pavement markings measured from the LiDAR intensity data as well as the GPS points; for better illustration only the operator-measured LiDAR points, which were considered as reference, are shown. Note the small yet clearly visible misfit between the two point sets.



**Figure 7.** Intersection with pavements markings measured from LiDAR intensity data (points marked yellow) and GPS-surveyed points (blue).

In the curve fitting process both data representations were fitted, with a point spacing of 1 cm, and various combinations were processed by ICP-based curve matching in 2D and 3D. In order to assess the accuracy of the transformation, the correspondence between the LiDAR-derived curve and the control curve were established. Since the two curves in general are not totally identical, even after the final ICP iteration, the transformed LiDAR-derived points are close but not necessarily fall on the control curve. However, the location of the transformed LiDAR-derived points represents the best fit to the control curve in least squares sense. Therefore, these points are projected to the closest points of the control curve, and then they are considered as conjugate points. The transformation parameters between these two point sets (the original LiDAR-derived points and their corresponding points on the control curve) are calculated in a least squares adjustment. In this computation, the 2D transformation parameters for a representative test data set were estimated at  $\sigma_{\Delta X} = \pm 0.013\text{m}$ ,  $\sigma_{\Delta Y} = \pm 0.010\text{m}$ , and  $\sigma_{\text{angle}} = \pm 1.95$  arcmin, indicating that a good match was found with the ICP method. The numerical values, including the transformation parameters and error terms, are listed in Tables I and II.

**Table 1.** Transformation results (2D).

Transformation parameter	ICP-adjusted results [m, °]	Estimated accuracy [cm, °]
$\Delta X$	0.041	0.013
$\Delta Y$	-0.023	0.010
$\phi$	-0.000	0.03

The ~2 cm horizontal accuracy could be considered excellent given the fact that the GPS-surveyed points are known, at best, 1 cm-level accuracy and the LiDAR-based pavement marking positioning accuracy is estimated at the few cm range.

Since the overall LiDAR data quality used for testing was quite good, the discrepancies found at several intersections were rather small, a simulated error was introduced to test the method for less than ideal situations. Using the same data set, a 16 and -4 cm horizontal offset was added to the X and Y coordinates of the LiDAR point measurements, respectively. Tables II and III show the residuals measured at the pavement markings before and after the correction.

**Table 2.** Initial residuals.

	$\Delta X$ [m]	$\Delta Y$ [m]
Mean	0.158	-0.036
STD	0.048	0.045

**Table 3.** Residuals after correction.

	$\Delta X$ [m]	$\Delta Y$ [m]
Mean	0.000	-0.000
STD	0.048	0.045

## CONCLUSION

The introduced method to use pavement markings as ground control showed good initial performance. Using a data set acquired by a state-of-the-art LiDAR system, the performance of the three main processing steps was validated. In all the cases, the curve fitting and ICP-based matching delivered robust results. The extraction of pavement markings, however, has experienced difficulties in some cases where the intensity data were noisier. A key advantage of using pavement markings is that they can be quickly surveyed with GPS VRS technique.

## ACKNOWLEDGEMENTS

The authors would like to thank the Ohio Department of Transportation for the GPS survey of pavement markings and flying LiDAR surveys to acquire essential data for this research.

## REFERENCES

- ASPRS LiDAR Committee, 2004. ASPRS Guidelines Vertical Accuracy Reporting for LiDAR Data, [http://www.asprs.org/society/committees/lidar/Downloads/Vertical\\_Accuracy\\_Reporting\\_for\\_Lidar\\_Data.pdf](http://www.asprs.org/society/committees/lidar/Downloads/Vertical_Accuracy_Reporting_for_Lidar_Data.pdf).
- Besl, P. J. and McKay, N. D., 1992. A method for registration of 3-d shapes, *IEEE Trans. Pat. Anal. and Mach. Intel.* 14(2), pp 239-256, Feb 1992.
- Burman, H., 2002. Laser strip adjustment for data calibration and verification, *International Archives of Photogrammetry and Remote Sensing*, 34 (Part 3A): 67-72.
- Csanyi N, Toth C., Grejner-Brzezinska D. and Ray J., 2005. Improving LiDAR data accuracy using LiDAR-specific ground targets, In *Proceedings of the ASPRS 2005 Annual Conference*, Baltimore, MD, March 7-11, CD-ROM.
- Csanyi, N. and Toth, C., 2007. Improvement of LiDAR data accuracy using LiDAR-specific ground targets, *Photogrammetric Engineering & Remote Sensing*, Vol. 73, No. 4, pp. 385-396.
- Gruen, A., Akca, D., 2005. Least squares 3D surface and curve matching, *ISPRS Journal of Photogrammetry and Remote Sensing*, 59 (3), 151-174.
- Hasegawa, H., 2006. Evaluations of LiDAR reflectance amplitude sensitivity towards land cover conditions, *Bulletin of the Geographical Survey Institute*, Vol. 53.
- Ichida, K. and Kiyono, T. 1977. Curve fitting with one-pass method with a piecewise cubic polynomial, *ACM Transactions on Mathematical Software*, Vol. 3, No. 2, pp. 164-174.
- Kager, H. and Kraus, K., 2001. Height discrepancies between overlapping laser scanner strips, In *Proceedings of Optical 3D Measurement Techniques V*, Vienna, Austria: 103-110.
- Maas, H.-G., 2001. On the use of pulse reflectance data for laserscanner strip adjustment, *International Archives of Photogrammetry, Remote Sensing and Spatial Information Sciences*, 33 (Part 3/W4): 53-56.
- Madhavan, R., Hong, T., Messina, E., 2005. Temporal range registration for unmanned ground and aerial vehicles, *Journal of Intelligent and Robotic Systems*, Volume 44, Number 1 / September, 2005, pp. 47-69.
- Toth, C., D. Brzezinska, N. Csanyi, E. Paska and N. Yastikly, 2007a. LiDAR mapping supporting earthquake research of the San Andreas fault, In *Proceedings of the ASPRS 2007 Annual Conference*, Tampa, Florida, May 7-11, CD ROM.
- Toth, C., Paska, E., Grejner-Brzezinska, D.A., 2007b. Using pavement markings to support the QA/QC of LiDAR data, *Photogrammetric Image Analysis (PIA 2007)*, *International Archives of Photogrammetry and Remote Sensing*, Vol. XXXVI, 3/W49B, pp. 173-178.

# USING PAVEMENT MARKINGS TO SUPPORT THE QA/QC OF LIDAR DATA

C. Toth<sup>a,\*</sup>, E. Paska<sup>a</sup>, D. Brzezinska<sup>b</sup>

<sup>a</sup> Center for Mapping, OSU, 1216 Kinnear Road, Columbus, OH 43212 USA - (toth, eva-paska)@cfm.ohio-state.edu

<sup>b</sup> Dept. of Civil and Environmental Engineering and Geodetic Science, OSU, dbrzezinska@osu.edu

## Commission I, WG I/2

**KEY WORDS:** LiDAR, LiDAR intensity, Feature extraction, QA/QC

### ABSTRACT:

LiDAR technology became an indispensable airborne mapping tool in recent years and is the primary source of highly accurate surface data at large scale. Although, the ranging accuracy of the laser sensor strongly depends on the surface characteristics, by and large, it falls in to the few cm range. This also implies that the achieved accuracy of a LiDAR system, defined in terms of the absolute accuracy of the laser points, is predominantly determined by the quality of the navigation solution (typically based on GPS/IMU sensor integration). Despite significant advancements in navigation technologies recently, to achieve and sustain a high accuracy navigation solution of an airborne platform for extended time is still a difficult task. Furthermore, there is no reliable way to assess the positioning quality of the data captured by any imaging sensor systems, which are based on direct georeferencing. Therefore, using some ground control is almost mandatory if high accuracy is required. This paper introduces a method to use road pavement marking as ground control that could be used for QA/QC. These linear features are widely available in urban areas and along transportation corridors, where most of the government and commercial mapping takes place. A key advantage of using pavement markings is that they can be quickly surveyed with GPS VRS technique.

## 1. INTRODUCTION

The introduction of airborne LiDAR (Light Detection And Ranging) in the late nineties was followed by a quick proliferation of the technology, and LiDAR is now the primary surface data extraction mapping technique. This remarkable success is mainly due to the fact that LiDAR data are explicit and the processing can be highly automated plus that an unprecedented vertical accuracy could be obtained relatively easily. The horizontal accuracy of the LiDAR data was not a concern in the early use of this technology. In fact, the first LiDAR data QA/QC and product characterization effort did only deal with the vertical accuracy (ASPRS, 2004).

As the LiDAR market started to grow rapidly, soon the LiDAR systems showed truly phenomenal performance improvements. In less than five years, the pulse rate improved by an order and now 100 and 150 kHz systems are widely used (Optech, 2006 and Leica, 2006) and experimental two-pulse systems are also available. More importantly, the ranging accuracy has increased substantially and now stands close to the level of static GPS surveys, i.e., 1-2 cm for hard surfaces, which is practically negligible to the typical navigation error budget. This remarkable performance potential of the newer LiDAR systems, combined with better operational techniques, opened the door toward applications where large-scale or engineering-scale accuracy is required. At this point the georeferencing error budget and, to a lesser extent, the sensor calibration quality, are critical to achieving engineering design level accuracy (few cm). Using ground control is an effective way to compensate for georeferencing and sensor modeling errors. In addition, ground control can provide for independent and highly reliable QA/QC processes.

This paper proposes a method to use road pavement markings as ground control to assess the quality of the LiDAR data as well as to improve the point cloud accuracy by post-processing. Beyond their wide availability, the use of pavement markings is primarily motivated by the fact that they can be rather easily surveyed using GPS VRS (Virtual Reference System) technology; the process is fast, typically it takes one minute to survey a point, and the accuracy, in general, is about 2-3 and 3-6 cm horizontally and vertically, respectively.

## 2. LIDAR ACCURACY AND ERROR CORRECTION TECHNIQUES

The errors in laser scanning data can come from individual sensor calibration or measurement errors, lack of synchronization, or misalignment between the different sensors. Baltsavias (1999) presents an overview of the basic relations and error formulae concerning airborne laser scanning. Schenk (2001) provides a summary of the major error sources for airborne laser scanners and error formulas focusing on the effect of systematic errors on point positioning. In general, LiDAR sensor calibration includes scan angle, range calibration and intensity-based range correction. The LiDAR sensor platform orientation is always provided by a GPS/IMU-based integrated navigation system. The connection between the navigation and LiDAR sensor frames is described by the mounting bias, which is composed of the offset between the origin of the two coordinate systems and the boresight misalignment (the boresight misalignment describes the rotation between the two coordinate systems, and is usually expressed by roll, pitch and heading angles). To achieve optimal error compensation that assures the highest accuracy of the final product, all of these parameters should be calibrated. Since not all of the parameters can be calibrated in a laboratory

---

\* Corresponding author.

environment, a combination of laboratory and in situ calibrations is the only viable option for LiDAR system calibration. Typical anomalies in the LiDAR data indicating system calibration errors are: edges of the strips could bend up or down (scan angle error), horizontal surfaces have a visible mismatch between the known and the LiDAR point-defined surfaces (boresight misalignment or navigation error), vertical coordinates of LiDAR points over flat areas do not match the known vertical coordinate of the area (ranging or navigation error), objects, such as pavement markings made of retro reflective coatings, may show up above the surface level, although they should practically have identical vertical coordinates (lack of intensity correction of the range data), etc.

The techniques to detect and ultimately compensate for errors fall into two broad categories based on whether they use absolute control or not. The first group includes most of the strip adjustment techniques and some of the sensor and boresight calibration methods. The ground control-based techniques encompass comparisons to reference surfaces, such as parking lots and buildings, and methods using LiDAR-specific control targets.

Strip adjustment methods primarily minimize the vertical discrepancies between overlapping strips or between strips and horizontal control surfaces. These strip adjustments can be referred to as one-dimensional strip adjustment methods (Crombaghs et al., 2000; Kager and Kraus, 2001); tie or absolute control features used for this adjustment are flat horizontal surfaces. The problem with this kind of adjustment is that existing planimetric errors are likely to remain in the data. Vosselman and Maas (2001) have shown that systematic planimetric errors are often much more significant than vertical errors in LiDAR data and, therefore, a 3D strip adjustment is the desirable solution minimizing the 3D discrepancies between overlapping strips and at control points. A number of 3D adjustment methods have been published. Kilian et al. (1996) presented a method of transforming overlapping LiDAR strips to make them coincide with each other using control and tie points in a way similar to photogrammetric block adjustment. Burman (2002) treated the discrepancies between overlapping strips as positioning and orientation errors with special attention given to the alignment error between the IMU and laser scanner (Soininen, 2005). Filin (2003) presented a similar method for recovering the systematic errors; the method is based on constraining the position of the laser points to the surface from which it was reflected. Toth et al. (2002) presented a method that tried to make overlapping strips coincide, with the primary objective of recovering the boresight misalignment between the IMU and laser sensor.

LiDAR-specific ground control targets were introduced by Toth and Brzezinska (2005; Csanyi et al., 2005). The proposed technique uses ground control targets specifically designed for LiDAR data to provide quality control for applications that require cm-level, engineering scale mapping accuracy. Simulation results confirmed that the optimal target is rotation invariant, circular-shaped, elevated from the ground and that a flat target with 1 m circle radius can provide sufficient accuracy from a point density of about 5 pts/m<sup>2</sup>. Targets larger than 2 m in diameter will not lead to significant improvements. In addition, a two-concentric-circle design (the inner circle has one-half the radius of the outer circle) with different coatings can produce considerable accuracy improvements in the horizontal position. Details and performance evaluation can be found in (Csanyi and Toth, 2007).

### 3. LIDAR INTENSITY DATA

The introduction of intensity data a few years ago produced unrealistically high initial expectations. On one side, the visualization value provided a major help for interactive processing, and thus, users could immediately benefit from the new source of data, as LiDAR intensity was comparable to optical image type of data that had been missed by practitioners from the early beginning. On the other side, the algorithmic advantages of using intensity data for providing better LiDAR data processing were largely overestimated. While research instantly started to address the exploitation of the new source of information, the problem seemed to be harder than expected. In simple terms, the major difficulty of working with LiDAR intensity data is the relative nature of this signal. For example, different surfaces, data from different flying heights, and different surface orientations can produce exactly the same intensity values. Therefore, techniques to calibrate the intensity and range values with respect to each other started to become more common.

One of the first attempts on using intensity data dates back to the time when LiDAR intensity data were not yet commercially available. Maas (2001) describes the extension of a TIN-based matching technique using reflectance data (LiDAR intensity data) to replace surface height texture for the determination of planimetric strip offsets in flat areas with sufficient reflectance texture. As an extension, Vosselman (2002) offers another solution, kind of a feature-based matching, to avoid interpolation of the data, using linear features, gable roofs, and ditches, modeled by analytical functions that can provide accurate offset determination. Later, research interest steered toward conventional classification use of the intensity data. Song et al. (2002) proposed a technique to use intensity data for land-cover classification. A similar study on using intensity for glacier classification is presented in Lutz et al. (2003). A recent review of more advanced versions of these techniques is offered by Hasegawa (2006). A comprehensive study on processing both range and intensity data is provided by Sithole (2005). Kaasalainen et al. (2005) provides a review on intensity data with respect to calibration. Nobrega and O'Hara (2006) compare two techniques for filtering intensity data for object extraction. Finally, Ahokas et al. (2006) presents the results of a calibration test on intensity data using the Optech ALTM 3100.

Figures 1 and 2 show simultaneously acquired orthoimage and the LiDAR intensity image, respectively, of an intersection. The LiDAR point density was about 4 pts/m<sup>2</sup> with foot print size of 15 cm. Note that the pavement markings in the LiDAR image are quite visible and distinct from the pavement. Consequently, if the approximate location of the pavement markings is known, then their extraction is a fairly straightforward task.

To illustrate that LiDAR elevation and intensity data are correlated and intensity information can indicate the presence of ranging error, Figure 3 shows the elevation data of the same intersection. Note that the pavement markings can be seen quite well, which conflicts with the fact that elevation value of the markings and the pavement around them should be identical (the few mm thickness of the markings is negligible compared to the few cm ranging accuracy of the laser system). This phenomenon is known and correction tables are available to partially compensate for this effect. The importance of this anomaly from our perspective is that during the comparative analysis later, the elevation value of the markings should be replaced by the average elevation of the pavement.

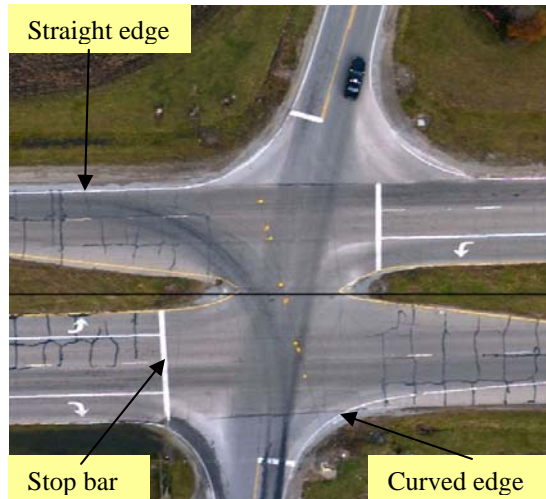


Figure 1. Typical pavement markings at an intersection.



Figure 2. LiDAR intensity image.

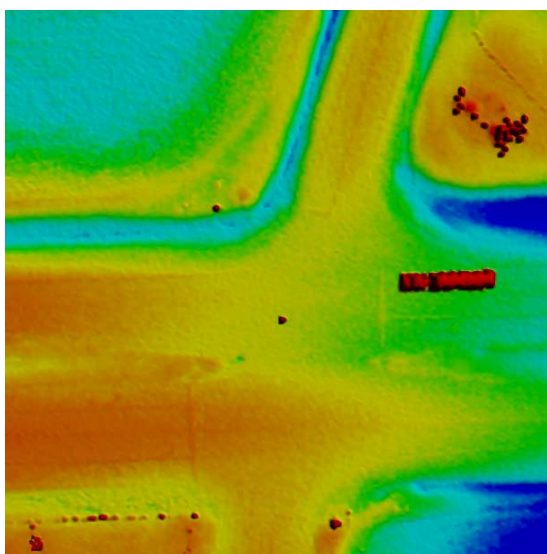


Figure 3. LiDAR elevation data.

#### 4. EXTRACTING PAVEMENT MARKINGS AND USING THEM AS GROUND CONTROL

The concept of the proposed method, including pavement marking extraction as well as parameterization of the marks based on LiDAR intensity data, the comparison with ground truth, and the determination of a transformation to correct the point cloud, analysis of result, etc., is shown in Figure 4. General assumptions are that the survey data of the pavement markings are available a priori and the individual point accuracy, describing the marks, is known at the cm-level. To achieve good performance, sufficient number of pavement markings is required with good spatial distribution. At this point only three types of pavement markings are considered: Stop bars, straight edge lines and curved edge lines; Figure 1 shows the three pavement marking types. The survey data of the pavement markings is provided as point observations along the centerline of the markings. The LiDAR data, including range and intensity components, are assumed to be of reasonable quality; i.e., the point cloud accuracy is better than a meter.

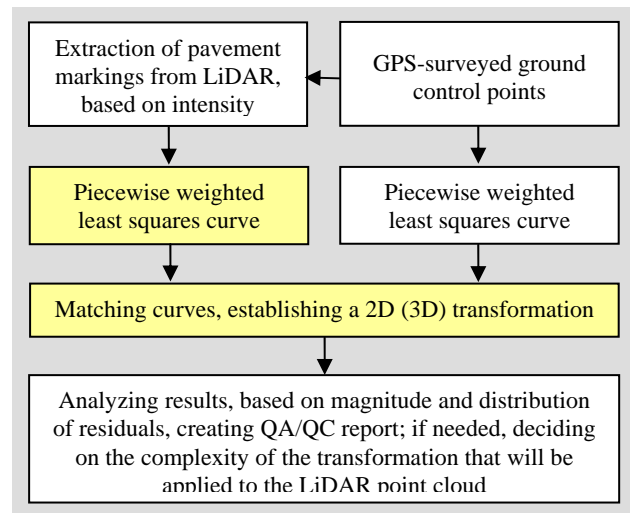


Figure 4. Block diagram of the proposed method.

Based on the comparison of the two descriptions of pavement markings, one obtained from the GPS survey and the other one from LiDAR intensity data, offset and orientation differences can be detected. Depending on the magnitude of the observed differences and their spatial distribution, a variety of corrections can be applied to the LiDAR point cloud to improve the point position accuracy. For example, if there is a similar vertical shift detected at the control features, a common vertical offset correction can be applied. If the amount of vertical shift detected varies by location and/or combined with non-negligible horizontal differences, a more complex model, such as a 3D similarity transformation, can be applied. Note that assessing the horizontal accuracy is difficult, as it is mainly defined by the footprint of the laser pulse, which depends on flying height and beam convergence; in addition, the impact of object surface characteristics could be also significant. The transformation based on the observed differences can be formulated on both, point- and linear feature-based least squares adjustment techniques. The conventional control point-based method is rather straightforward; similar to an absolute orientation of a stereo model with fixed scale. Linear feature-based orientation is less widely used, but could be feasible given the availability of matched linear features. Finally, if the differences are out of



the usual range (gross errors), the process can indicate system malfunctioning.

In our case, the point-based transformation is directly not applicable, as there is no point-to-point correspondence between the two point sets that describe the same linear feature. Assuming that the two representations provide an adequate description of the same shape, the problem is simply how to match two free-shape curves. In the following, the two key components of the proposed method, curve fitting and matching are discussed at detail.

#### 4.1 Curve fitting

The extracted LiDAR points of the pavement markings and their surveyed data should be modeled as linear features in order to be matched with each other. The selected method is an extended version of the algorithm, originally proposed by Ichida and Kiyono in 1977, and is a piecewise weighted least squares curve fitting based on cubic (third-order polynomial) model, which seemed to be adequate for our conditions. To handle any kind of curves, defined as the locus of points  $f(x, y) = 0$  where  $f(x, y)$  is a polynomial, the curve fitting is performed for smaller segments in local coordinate systems, which are defined by the end points of the curve segments. The primary advantage of using a local coordinate system is to avoid problems when curves become vertical in the mapping coordinate system. Figure 5 shows the concept of the local coordinate system used for curve fitting; obviously, the fitting results as well as the fitting constraints are always converted forth and back between the local and mapping coordinate frames.

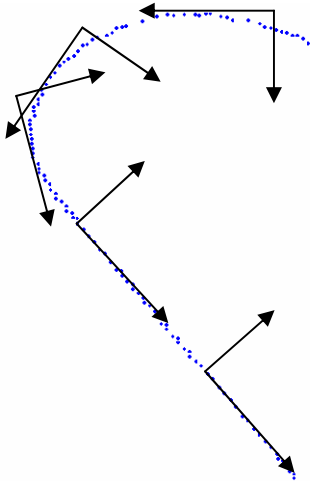


Figure 5. The curve fitting is done in local coordinate system, oriented to curve segment.

The main steps of the piecewise cubic fitting (PCF) process are shortly discussed below; the notation used in the discussion is introduced in Figure 6. To achieve a smooth curve, the curve fitting to any segment is constrained by its neighbors by enforcing an identical curvature at the segment connection points; in other words, PCF polynomial is continuous with its first derivative at connection points  $x=s$ ,  $x=t$ , etc. The equations describing the third-order polynomial and its first derivative are:

$$S_k(x) = y_s + m_s \cdot (x-s) + a_s \cdot (x-s)^2 + b_s \cdot (x-s)^3$$

$$\text{slope} = S'_k(x) = m_s + 2 \cdot a_s \cdot (x-s) + 3 \cdot b_s \cdot (x-s)^2$$

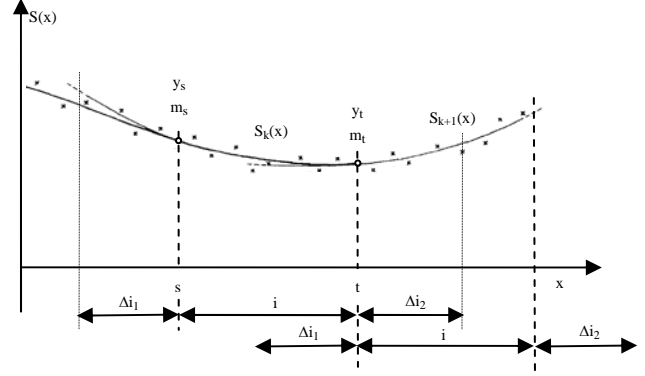


Figure 6. Piecewise weighted least squares curve fitting method.

The core processing includes the following steps: 1)  $a_s$  and  $b_s$ , the coefficients of the second and third order terms of the fitted curve for interval ' $i$ ' are estimated; consider the constant term ( $y_s$ ) and the coefficient of the first order term ( $m_s$ ) fixed, known from the curve fitting from the previous segment. In the adjustment, the points in interval  $\Delta i_2 + i + \Delta i_1$  (past, present, and future data points) are used, 2) the value ( $y_t$ ) and the slope ( $m_t$ ) at  $x=t$  are computed; these values as fixed constraints are used in the curve fitting for the next segment, and 3) step 1 is repeated to process the next segment.

Step 1	$y - y_s - m_s \cdot (x-s) = a_s \cdot (x-s)^2 + b_s \cdot (x-s)^3$ LS for points in interval $\Delta i_1 + i + \Delta i_2 \Rightarrow \hat{a}_s, \hat{b}_s$ $\Rightarrow S_k(x) = y_s + m_s \cdot (x-s) + \hat{a}_s \cdot (x-s)^2 + \hat{b}_s \cdot (x-s)^3$ $\rightarrow x = t$
Step 2	$\hat{y}_t = S_k(t) = y_s + m_s \cdot (t-s) + \hat{a}_s \cdot (t-s)^2 + \hat{b}_s \cdot (t-s)^3$ $\hat{m}_t = S'_k(t) = m_s + 2 \cdot \hat{a}_s \cdot (t-s) + 3 \cdot \hat{b}_s \cdot (t-s)^2$ $\rightarrow y_t = \hat{y}_t \text{ and } m_t = \hat{m}_t$
Step 3	$S_{k+1}(x) - y_t - m_t \cdot (x-t) = a_t \cdot (x-t)^2 + b_t \cdot (x-t)^3$ LS for points in interval $\Delta i_1 + i + \Delta i_2 \Rightarrow \hat{a}_t, \hat{b}_t$

#### 4.2 Matching curves

Iterative registration algorithms are increasingly used for registering 2D/3D curves and range images recently. The well-known Iterative Closest Point (ICP) algorithm (Besl and McKay, 1992; Madhavan et al., 2005) is adopted here to match curves describing pavement markings obtained from LiDAR intensity and GPS measurements. The ICP algorithm finds the best correspondence between two curves (point sets) by iteratively determining the translations and rotations parameters of a 2D/3D rigid body transformation.

$$\min_{(R,T)} \sum_i \|M_i - (RD_i + T)\|^2$$

Where  $R$  is a  $2 \times 2$  rotation matrix,  $T$  is a  $2 \times 1$  translation vector and subscript  $i$  refer to the corresponding points of the sets  $M$  (model) and  $D$  (data). The ICP algorithm can be summarized as follows:

1. For each point in  $D$ , compute the closest point in  $M$
2. Compute the incremental transformation ( $R, T$ )
3. Apply incremental transformation from step (2) to  $D$
4. If relative changes in  $R$  and  $T$  are less than a given threshold, terminate, otherwise go to step (1)

Our 2D ICP was implemented in Matlab and space-scale optimization was incorporated to reduce execution time.

## 5. EXPERIMENTAL RESULTS

To perform an initial performance test of the proposed method, a typical intersection was selected from a recently flown LiDAR survey, where GPS-surveyed pavement markings were available. Figure 7 shows the area with linear pavement markings measured from the LiDAR intensity data as well as the GPS points. Note the clearly visible misfit between the two point sets; the horizontal accuracy of the GPS-surveyed points, provided by the Ohio Department of Transportation VRS system is 1-2 cm.

The LiDAR point-based description of the pavement markings was obtained by filtering. The search space was defined by the GPS control points (pavement markings are assumed to be within  $\pm 1$  m of their true location) and intensity thresholding was used to extract the linear features; the road pavement has low intensity value while the pavement markings exhibit higher intensities. The threshold is adaptively defined by analyzing the histogram of the LiDAR intensity values of the road surface around the surveyed road pavement markings and/or by examining intensity values of road surface profiles (LiDAR scan-lines).

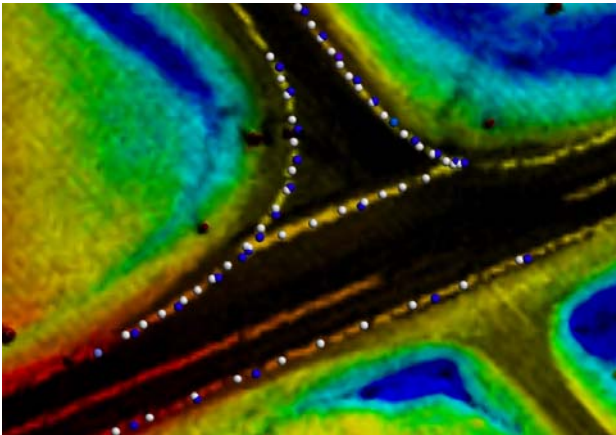


Figure 7. Intersection with pavements markings measured from LiDAR intensity data (white) and GPS-surveyed (blue).

In the curve-fitting step, both representations of the linear features are computed according the algorithm described in 4.1. Figure 8 shows one example of the fitted curves for the west curb line.

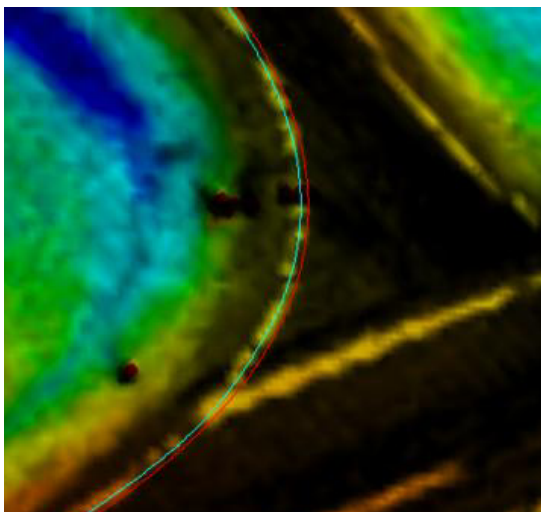


Figure 8. Curve fitting based on LiDAR and GPS points.

The results of the ICP-based curve matching for all the four curve lines is shown in Figure 9. Visually, the transformation shows a good fit; the blue points nicely fall on the GPS-defined curves. Note that the original curve points, derived from LiDAR, moved to the control curve similarly, as opposed to they would move if the individual curves had matched. Figure 10 shows the results of curve matching for the lower straight pavement line, including both the transformation results; as expected the individual transformation implements a perpendicular projection to the control curve.

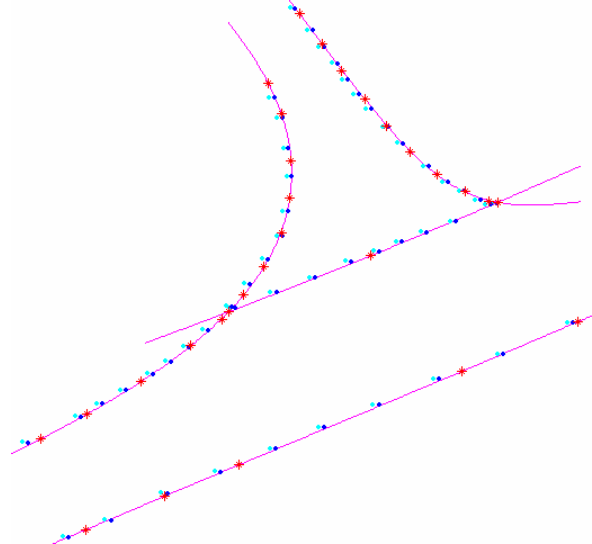


Figure 9. Curve matching based on all the four curves; magenta: curves fitted to control points, red: GPS control points, blue: curve points derived from LiDAR, and cyan: transformed curve points (derived from LiDAR).

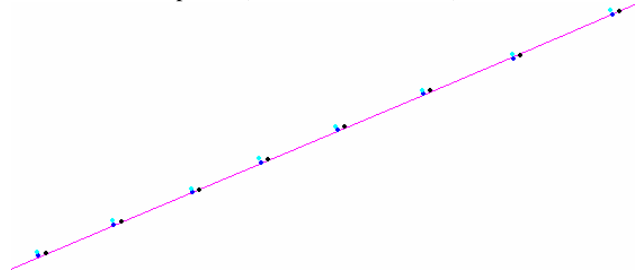


Figure 10. Comparing individual and combined curve fitting to a straight feature; magenta: reference curve, cyan: points derived from LiDAR, blue: transformed points based on single curve matching, and black: transformed points based on matching all the four curves together.

To assess in actual numbers the accuracy of the transformation, obtained by the ICP-based curve matching, correspondence between the LiDAR-derived curve and the control curve were established. Since the two curves in general are not totally identical, even after the final ICP iteration, the transformed LiDAR-derived points are close but not necessarily fall on the control curve. However, the location of the transformed LiDAR-derived points represents the best fit to the control curve in least squares sense. Therefore, these points are projected to the closest points of the control curve, and then they are considered as conjugate points. The transformation parameters between these two point sets (the original LiDAR-derived points and their corresponding points on the control curve) are calculated in a least squares adjustment. In this computation, the transformation parameters for the test data were estimated at  $\sigma_{\Delta X} = \pm 0.013\text{m}$ ,  $\sigma_{\Delta Y} = \pm 0.017\text{m}$ , and  $\sigma_{\text{angle}} = \pm 1.95$  arcmin, indicating that a good match was found with the



ICP method for the spatially well distributed test data set. The numerical values, including the transformation parameters, error terms, and dispersion matrix are listed in Tables I and II.

Transformation parameter	ICP-adjusted results [m, °]	Estimated accuracy [cm, °]
$\Delta X$	0.46	0.013
$\Delta Y$	-0.08	0.017
$\varphi$	-0.09	0.03

Table I. Transformation results (2D).

1.0e-003 *	0.1789	-0.1699	-0.0063
	-0.1699	0.2902	0.0087
	-0.0063	0.0087	0.0003

Table II. A posteriori dispersion matrix.

The ~2 cm horizontal accuracy is reasonable given the fact that the GPS-surveyed points are known at 1 cm-level accuracy and the LiDAR-based pavement marking positioning accuracy is estimated at the few cm range.

## 6. CONCLUSION

The introduced method to automate the use of pavement markings as ground control showed good initial performance. Both the curve fitting and ICP-based matching delivered robust results. Further research will consider the extension of technique to 3D.

### References:

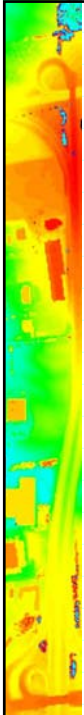

- Ahokas, E., Kaasalainen, S., Hyypä, J. and Suomalainen, J., 2006. Calibration of the Optech ALTM 3100 Laser Scanner Intensity Data Using Brightness Targets, Proceedings of ISPRS Commission I. Symposium.
- ASPRS LiDAR Committee, 2004. ASPRS Guidelines Vertical Accuracy Reporting for LiDAR Data [http://www.asprs.org/society/committees/lidar/Downloads/Vertical\\_Accuracy\\_Reporting\\_for\\_Lidar\\_Data.pdf](http://www.asprs.org/society/committees/lidar/Downloads/Vertical_Accuracy_Reporting_for_Lidar_Data.pdf)
- Baltsavias, E.P., 1999. Airborne Laser Scanning: Basic Relations and Formulas. ISPRS Journal of Photogrammetry & Remote Sensing, Vol. 54: 199-214.
- Besl, P. J. and McKay, N. D. A method for registration of 3-d shapes. IEEE Trans. Pat. Anal. and Mach. Intel. 14(2), pp 239-256, Feb 1992.
- Burman, H. ,2002. Laser Strip Adjustment for Data Calibration and Verification. International Archives of Photogrammetry and Remote Sensing, 34 (Part 3A): 67-72.
- Crombaghs, M. J.E., R. Brügelmann, E.J. de Min, 2000. On the Adjustment of Overlapping Strips of Laseraltimeter Height Data. International Archives of Photogrammetry and Remote Sensing, 33, (Part B3/1):224-231.
- Csanyi N, Toth C., Grejner-Brzezinska D. and Ray J., 2005. Improving LiDAR data accuracy using LiDAR-specific ground targets, ASPRS Annual Conference, Baltimore, MD, March 7-11, CD-ROM.
- Csanyi, N. and Toth, C., 2007. Improvement of LiDAR Data Accuracy Using LiDAR-Specific Ground Targets, Photogrammetric Engineering & Remote Sensing, Vol. 73, No. 4, pp. 385-396.
- Filin, S., and Vosselman, G., 2004. Adjustment of Airborne Laser Altimetry Strips. International Archives of Photogrammetry, Remote Sensing and Spatial Information Sciences 34 (Part B) pp. 285-289.
- Hasegawa, H., 2006. Evaluations of LiDAR Reflectance Amplitude Sensitivity Towards Land Cover Conditions, Bulletin of the Geographical Survey Institute, Vol. 53.
- Ichida, K. and Kiyono, T.1977. Curve Fitting with One-Pass Method with a Piecewise Cubic Polynomial, ACM Transactions on Mathematical Software, Vol. 3, No. 2, pp. 164-174.
- Kager, H. and Kraus, K., 2001. Height Discrepancies between Overlapping Laser Scanner Strips. Proceedings of Optical 3D Measurement Techniques V, Vienna, Austria: 103-110.
- Kaasalainen, S., Ahokas, E., Hyypä, J. and Suomalainen, J., 2005. Study of Surface Brightness from Backscattered Laser Intensity: Calibration of Laser Data, IEEE Geoscience and Remote Sensing Letters, 2(3):255-259.
- Kilian J., Haala, N., Englich, M., 1996. Capture and Evaluation of Airborne Laser Scanner Data. International Archives of Photogrammetry and Remote Sensing, 31 (Part B3):383-388.
- Leica Geosystems, ALS50, <http://gis.leica-geosystems.com>
- Lutz, E., Geist, Th. and Stötter, J., 2003. Investigations of Airborne Laser Scanning Signal Intensity on Glacial Surfaces - Utilizing Comprehensive Laser Geometry Modeling and Orthophoto Surface Modeling (A Case Study: Svartisheibreen, Norway), proceedings of ISPRS Commission III, WG 3.
- Maas, H.-G., 2001. On the Use of Pulse Reflectance Data for Laserscanner Strip Adjustment. International Archives of Photogrammetry, Remote Sensing and Spatial Information Sciences, 33 (Part 3/W4): 53-56.
- Madhavan, R., Hong, T., Messina, E. Temporal Range Registration for Unmanned Ground and Aerial Vehicles, Journal of Intelligent and Robotic Systems, Volume 44, Number 1 / September, 2005, pp. 47-69.
- Nobrega, R. and O'Hara, C., 2006. Segmentation and Object Extraction from Anisotropic Diffusion Filtered LiDAR Intensity Data.
- Optech, ALTM 3100AE, 2006, [www.optech.ca/pdf/Brochures/ALTM3100EAWspecsfnl.pdf](http://www.optech.ca/pdf/Brochures/ALTM3100EAWspecsfnl.pdf)
- Schenk, T., 2001. Modeling and Analyzing Systematic Errors in Airborne Laser Scanners. Technical Notes in Photogrammetry, vol. 19. The Ohio State University, Columbus, USA.
- Sithole, G., 2005. Segmentation and Classification of Airborne Laser Scanner Data, Publication of Geodesy 59, Nederlandse Commissie voor Geodesie, Delft (184 pages).
- Song, J-H., Han, S-H., Yu, K, and Kim, Y., 2002. Assessing the Possibility of Land-Cover Classification Using LiDAR Intensity Data, International Archives of Photogrammetry, 34. pp. 4.
- Toth C., Csanyi N. and Grejner-Brzezinska D. 2002. Automating the Calibration of Airborne Multisensor Imaging Systems, Proc. ACSM-ASPRS Annual Conference, Washington, DC, April 19-26, CD ROM.
- Toth, C. and Grejner-Brzezinska, D., 2005. Geo-referenced Digital Data Acquisition and Processing Systems Using LiDAR Technology – Final report, ODOT State Job No. 147990.
- Vosselman, G., and Mass, H.-G., 2001. Adjustment and Filtering of Raw Laser Altimetry Data. Proc. OEEPE Workshop on Airborne Laserscanning and Interferometric SAR for Detailed Digital Elevation Models. OEEPE Publication 40, Stockholm, Sweden. pp. 62-72.
- Vosselman, G., 2002. On the Estimation of Planimetric Offsets in Laser Altimetry Data. International Archives of Photogrammetry and Remote Sensing, 34 (Part 3A): 375-380.
- Vosselman, G., 2002. Strip Offset Estimation Using Linear Features. 3rd International LIDAR Workshop, October 7-9, Columbus, <http://www.itc.nl/personal/vosselman/papers/vosselman2002.columbus.pdf>



## **APPENDIX B**

### **Project Review Presentation**

ASPRS WGLR/EGLR Joint Summer Meeting, June 13, 2008

# Quality Assessment of LiDAR Data by Using Pavement Markings

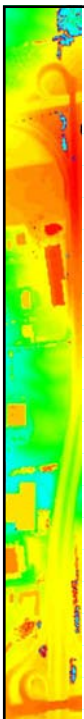

Charles Toth

Center for Mapping  
The Ohio State University

toth@cfm.ohio-state.edu

ASPRS WGL/EGL Joint Summer Meeting  
June 13, 2008

1

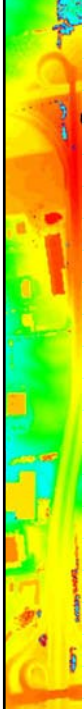



# Motivation


- ❖ Engineering-scale mapping effort at ODOT
- ❖ LiDAR product characterization, accuracy reporting
  - QA/QC process
  - General expectations vary
  - Object space characteristics frequently ignored
- ❖ Direct georeferencing
  - Extrapolation, different error characteristics
  - No direct redundancy (strip overlap with different samples!)
- ❖ Ground control is needed as independent validation
  - Dedicated targets vs. natural or man-made objects such as **reflective pavement markings**: less labor-intensive, requires limited surveying and imposes less restrictions in normal field operations existing features
  - Finding conjugate entities (points, linear features)

ASPRS WGL/EGL Joint Summer Meeting  
June 13, 2008

2



## Objectives



---

Exploit the good/distinct reflective characteristics of road pavement markings for LiDAR QA/QC


- ❖ Develop algorithms to automatically extract road pavement markings from the LiDAR intensity data
- ❖ Develop methods to create best-fit lines/curves to the extracted LiDAR points
- ❖ Perform a comparison of the control points to the best-fit curve of the features

Apply results to LiDAR data


- ❖ Improve both horizontal and vertical accuracy of the LiDAR data
- ❖ Provide a measure of the horizontal accuracy
- ❖ Evaluate the horizontal accuracy of LiDAR data as well as quantify the horizontal and vertical product accuracies

ASPRS WGL/EGL Joint Summer Meeting  
June 13, 2008

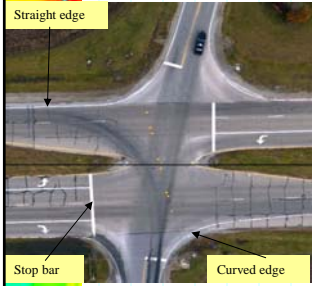
3




## Pavement Marking as Ground Control



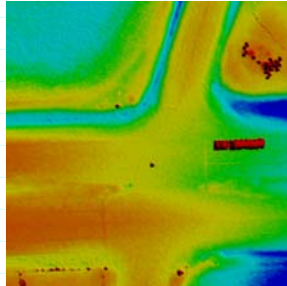
---



Optical image



LiDAR intensity



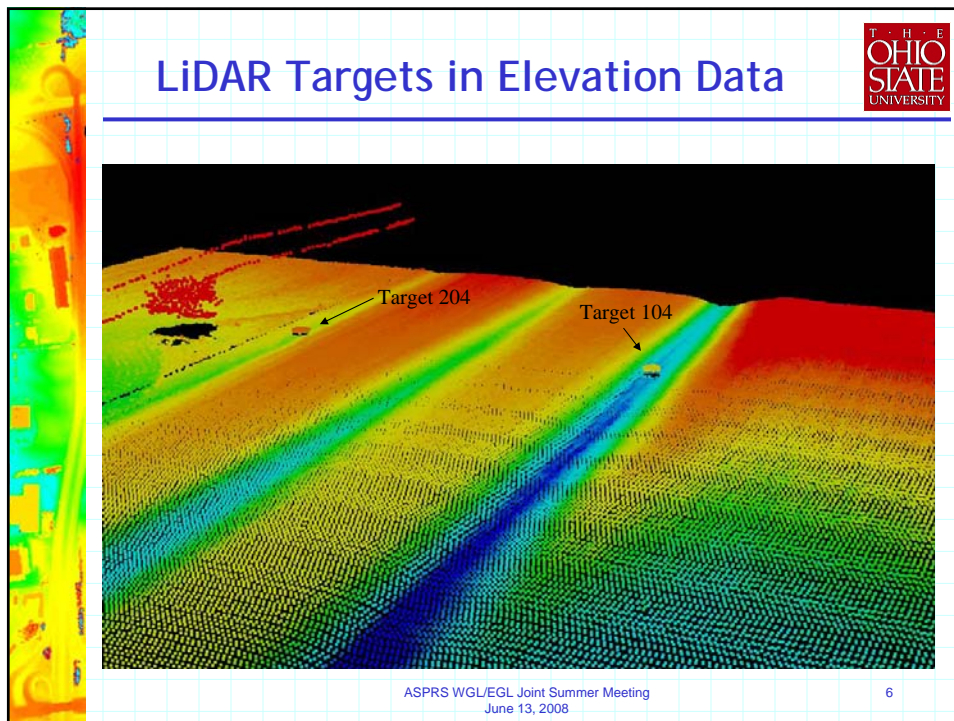
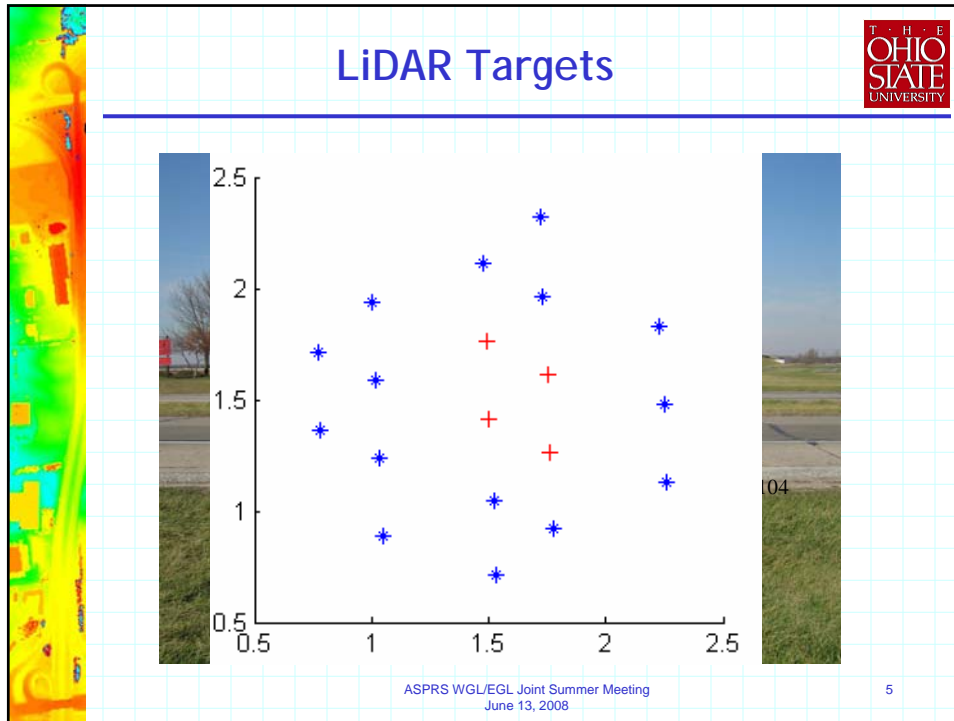
LiDAR elevation

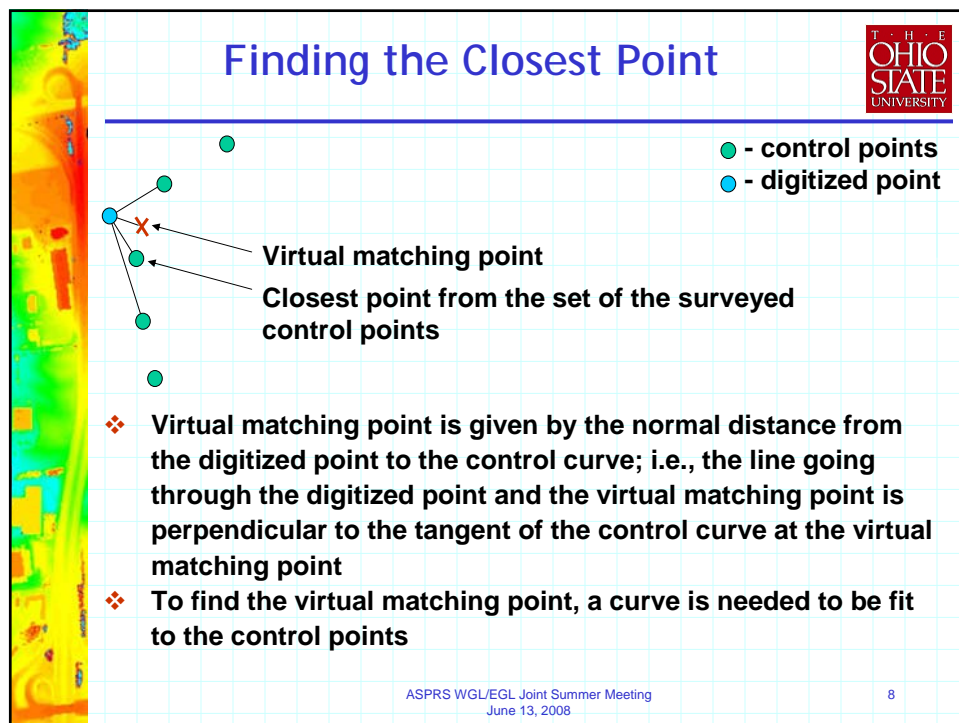
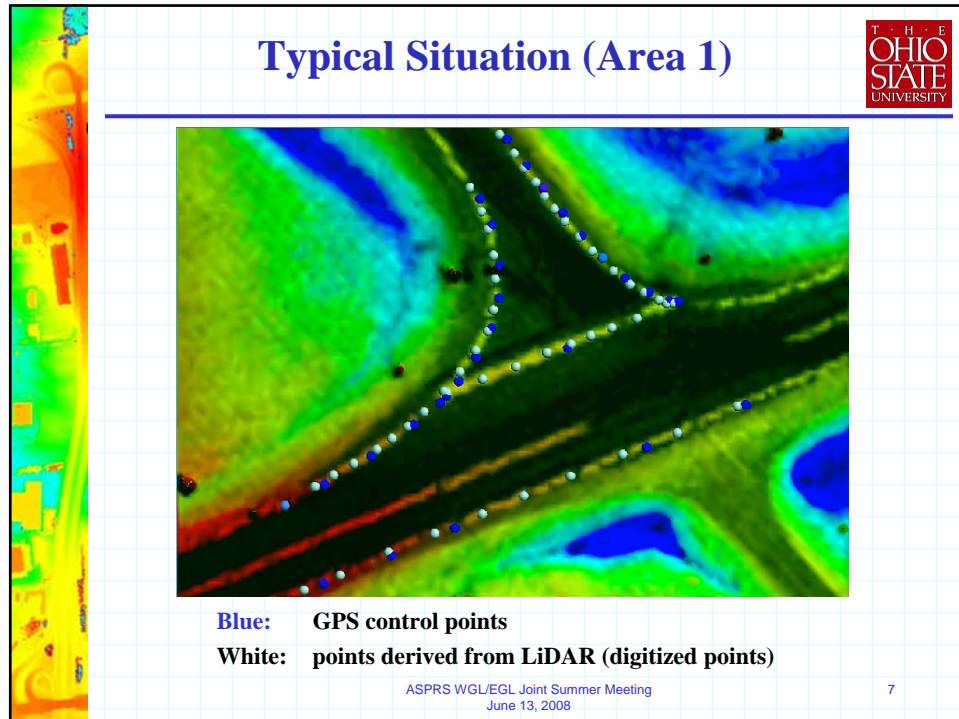
**Problems:**

- ❖ How to measure and characterize features from LiDAR
- ❖ How to find correspondence between measurements based on LiDAR and GPS-surveyed ground control

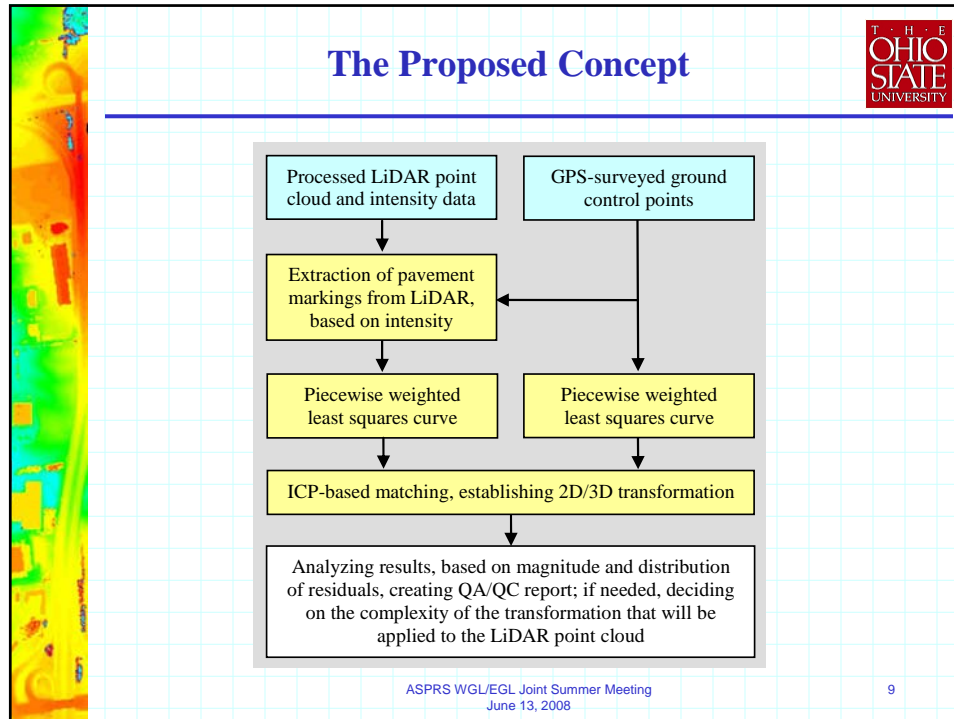
ASPRS WGL/EGL Joint Summer Meeting  
June 13, 2008

4









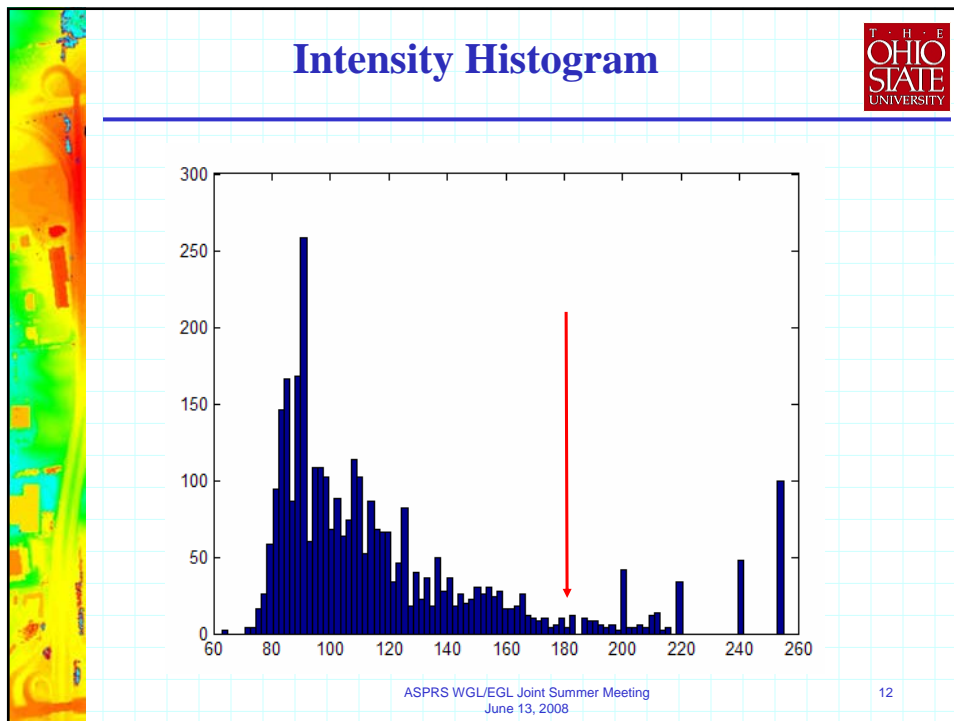
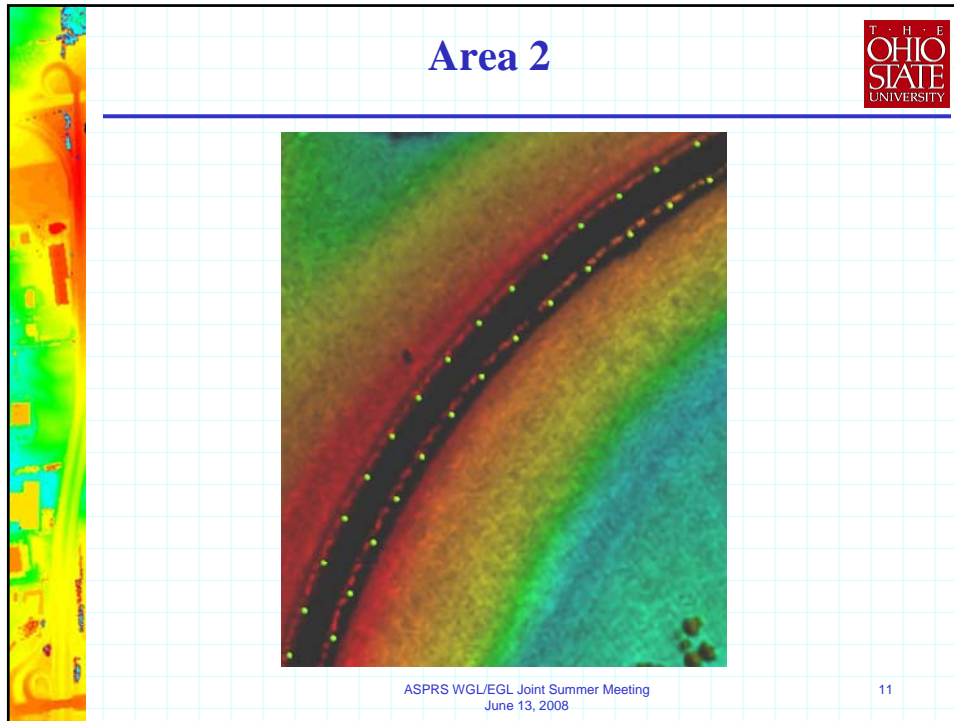
## Automated Feature Extraction from LiDAR Intensity Data Based on Intensity Thresholding

- ❖ **Extraction of LiDAR points reflected from the GPS-surveyed pavement markings based on intensity thresholding**
- ❖ **Feasible where the intensity values of pavement markings are well-separable from intensity values of the surrounding features (pavement markings can be well-distinguished from pavements, especially from dark pavement, but e.g. soil has similarly high intensity values as pavement markings). Automatically extracting road edge lines very close to soil field is a challenge, sometimes not feasible.**

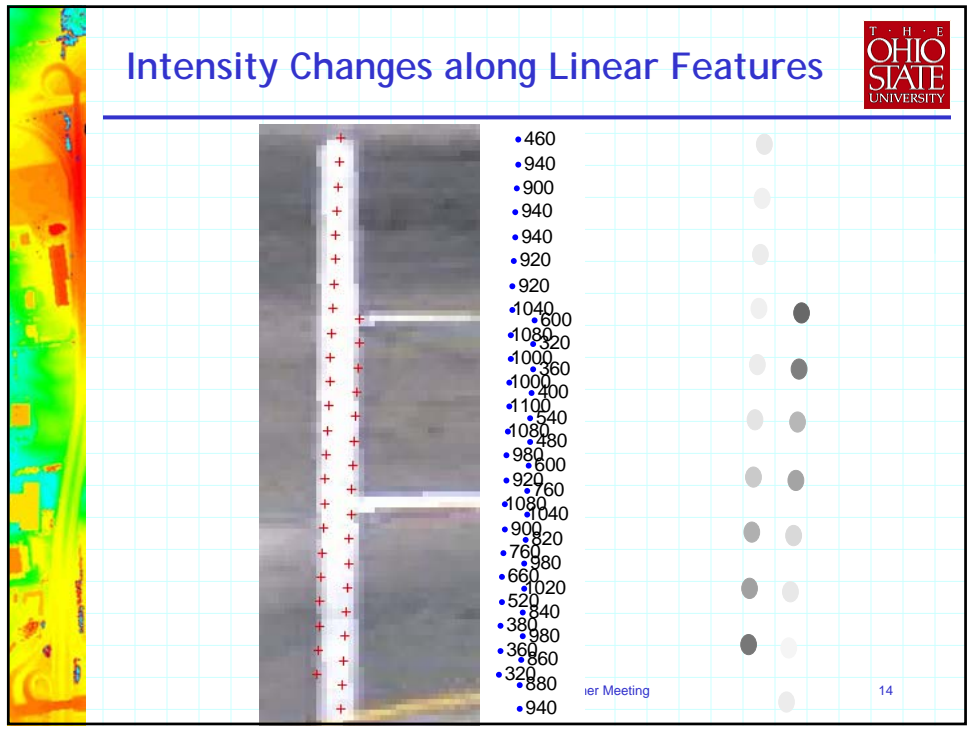
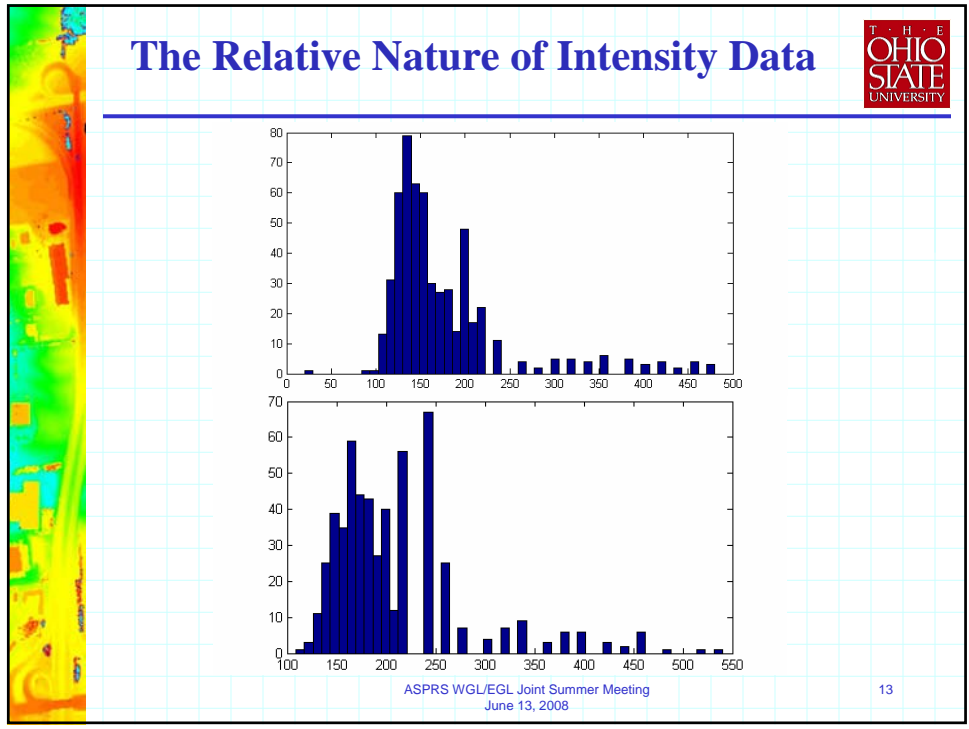
THE OHIO STATE UNIVERSITY

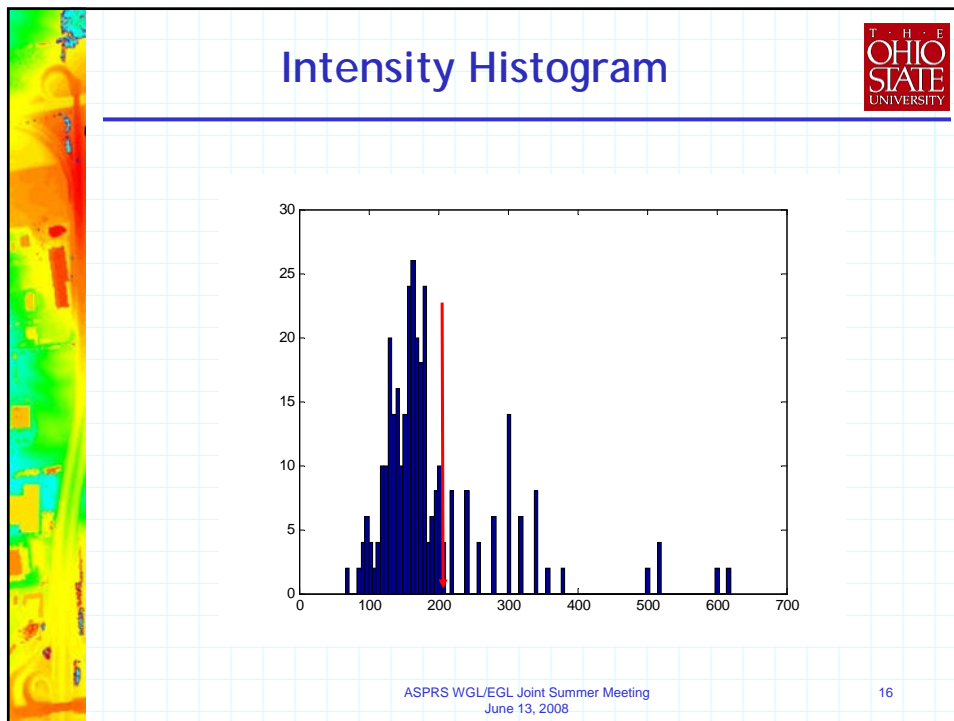
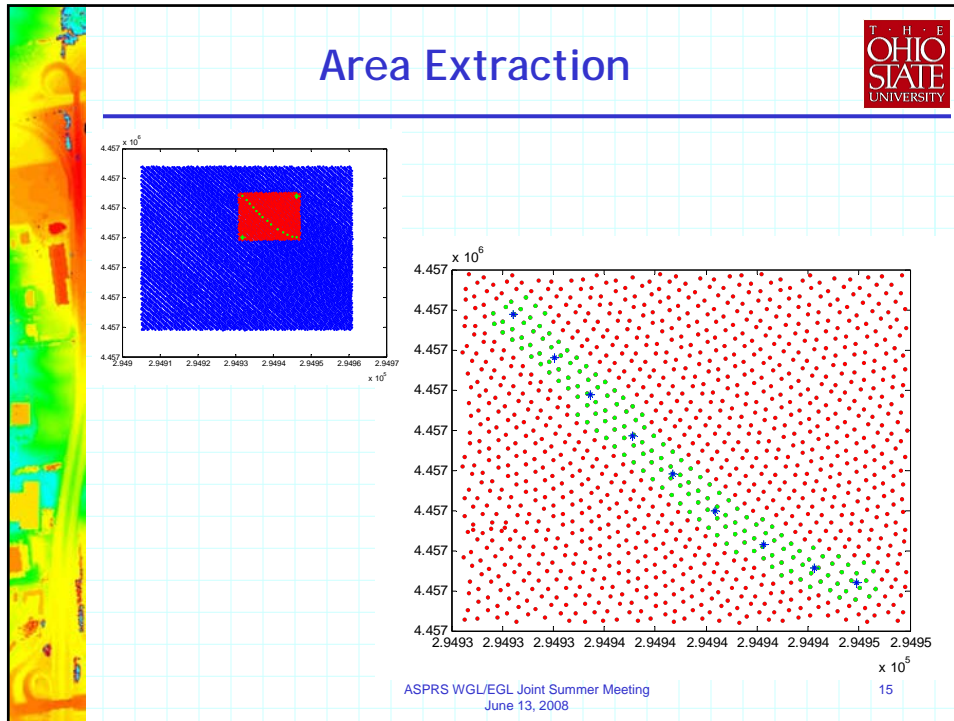
ASPRS WGL/EGL Joint Summer Meeting  
June 13, 2008

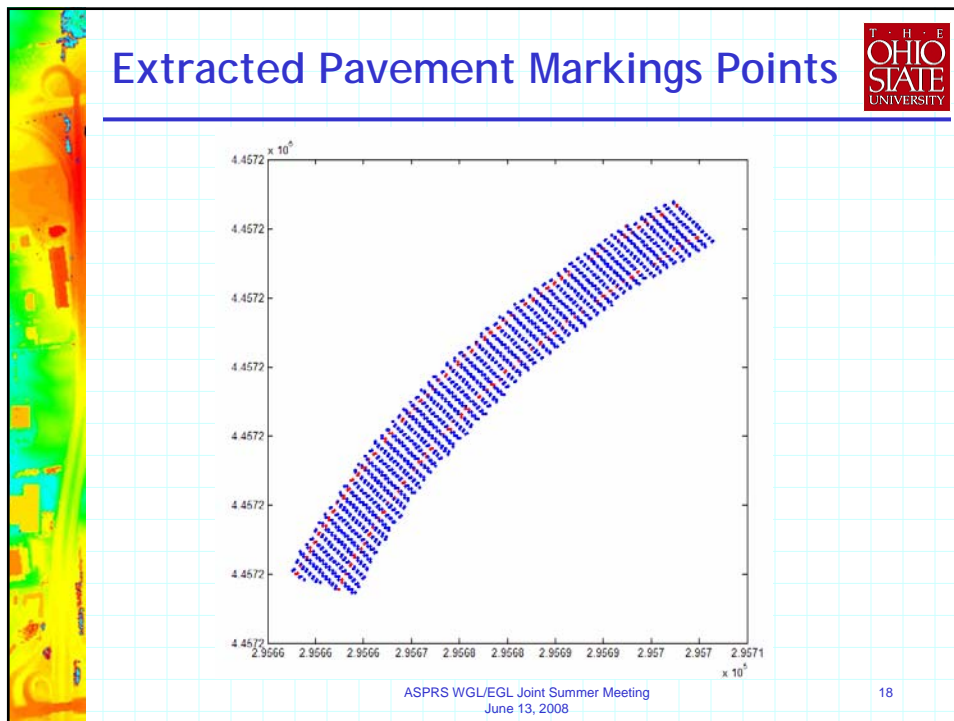
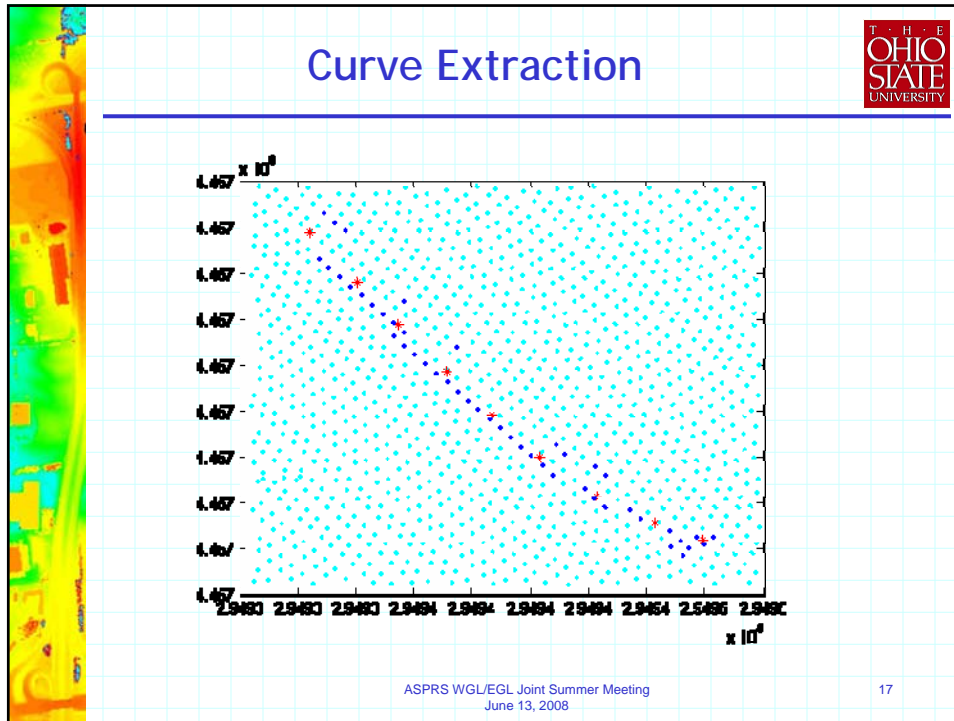
10






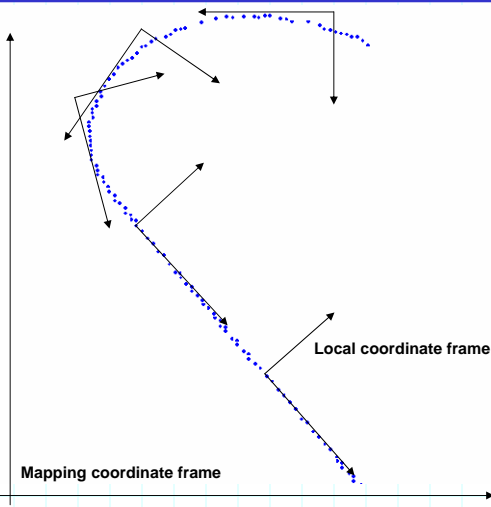






## Piecewise Curve Fitting






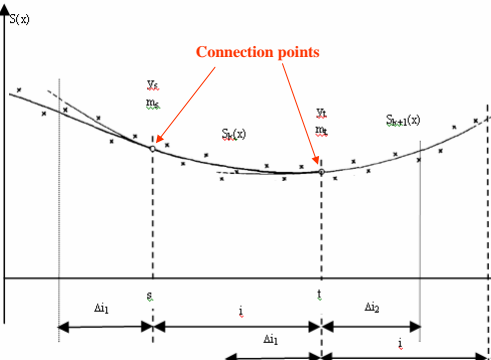
Curve fitting in small sections to allow for free-form curve shapes

ASPRS WGL/EGL Joint Summer Meeting  
June 13, 2008

19

## Piecewise Curve Fitting (Third-order Polynomial)





**Continuous with its first derivative at the connection points**

$$S_k(x) = y_s + m_s \cdot (x-s) + a_s \cdot (x-s)^2 + b_s \cdot (x-s)^3$$

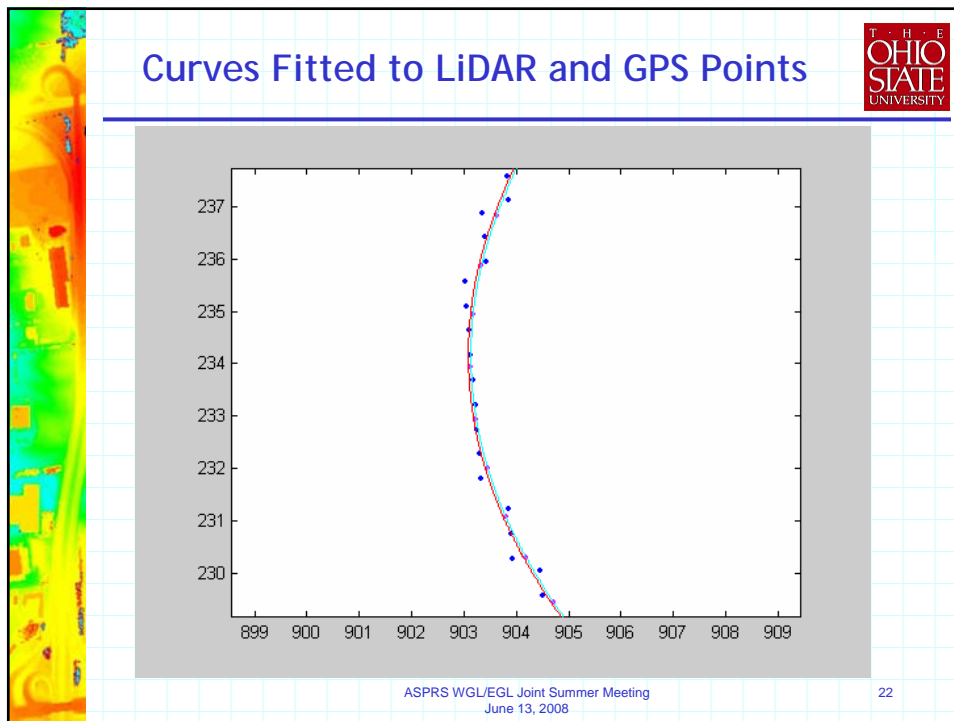
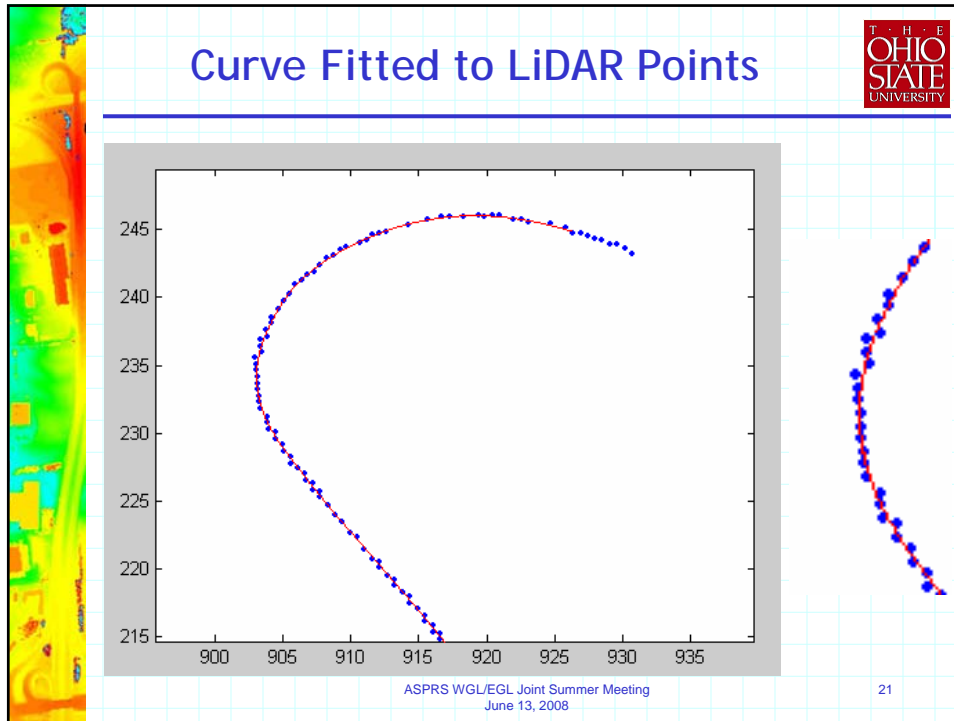
$$\text{slope} = S'_k(x) = m_s + 2 \cdot a_s \cdot (x-s) + 3 \cdot b_s \cdot (x-s)^2$$

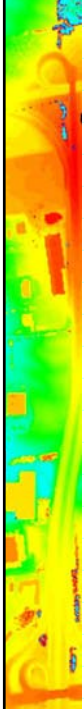
$$S_k(x=s) = y_s$$

$$S'_k(x=s) = m_s$$


Step 1	$y - y_s - m_s \cdot (x-s) = a_s \cdot (x-s)^2 + b_s \cdot (x-s)^3$ LS for points in interval $\Delta i_1 + i + \Delta i_2 \Rightarrow \hat{a}_s, \hat{b}_s$ $\Rightarrow S_k(x) = y_s + m_s \cdot (x-s) + \hat{a}_s \cdot (x-s)^2 + \hat{b}_s \cdot (x-s)^3$ $\rightarrow x = t$
Step 2	$\hat{y}_t = S_k(t) = y_s + m_s \cdot (t-s) + \hat{a}_s \cdot (t-s)^2 + \hat{b}_s \cdot (t-s)^3$ $\hat{m}_t = S'_k(t) = m_s + 2 \cdot \hat{a}_s \cdot (t-s) + 3 \cdot \hat{b}_s \cdot (t-s)^2$ $\rightarrow y_t = \hat{y}_t \text{ and } m_t = \hat{m}_t$
Step 3	$S_{k+1}(x) - y_t - m_t \cdot (x-t) = a_t \cdot (x-t)^2 + b_t \cdot (x-t)^3$ LS for points in interval $\Delta i_1 + i + \Delta i_2 \Rightarrow \hat{a}_t, \hat{b}_t$

ASPI





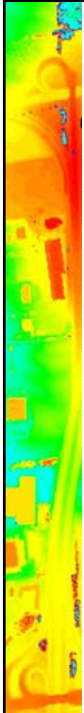
## Matching Curves (Point Sets)




- ❖ The objective of the matching process is to find conjugate points from linear features in LiDAR intensity data (automatically extracted or manually digitized) to the control (surveyed) points and then establish an adequate transformation between them
- ❖ The transformation parameters between the two point sets to be found through least squares adjustment
- ❖ A rigid body transformation between two point sets is established without having corresponding point pairs in the two point sets
- ❖ Proposed solution: Iterative Closest Point (ICP)
  - ICP is applied in 2D/3D to find the best correspondence between the two curves (point sets).
  - With least squares adjustment, the 3D transformation parameters between the matching point sets are obtained

ASPRS WGL/EGL Joint Summer Meeting  
June 13, 2008

23



## Curve Matching Based on Iterative Closest Point Method (ICP)



The ICP algorithm finds the best correspondence between two curves (point sets) in 2D/3D by iteratively determining the translations and rotation parameters of a 2D/3D rigid body transformation

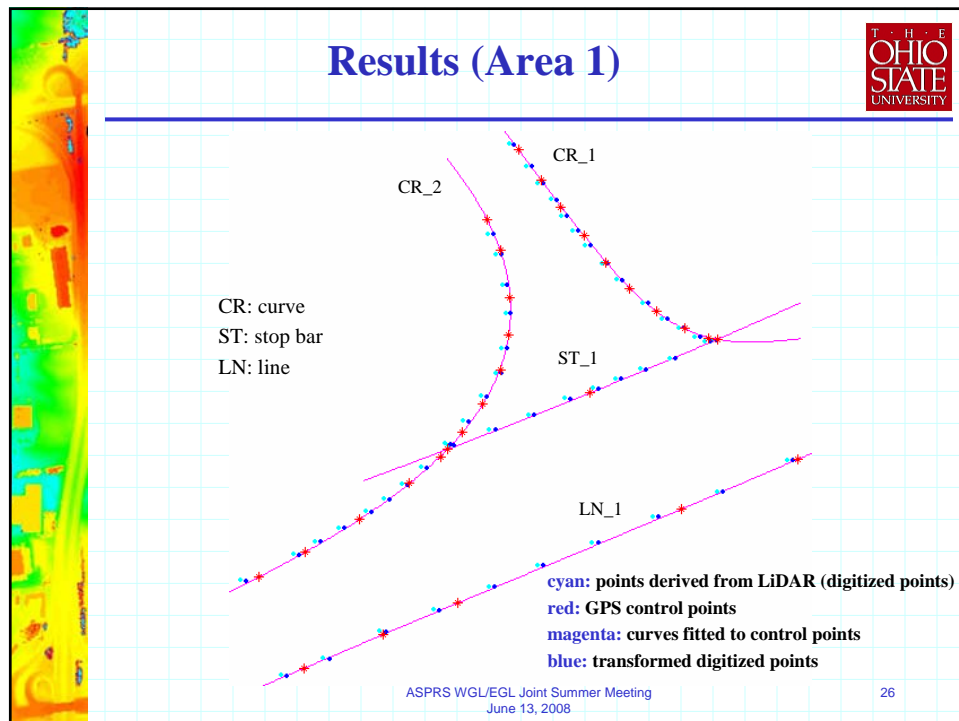
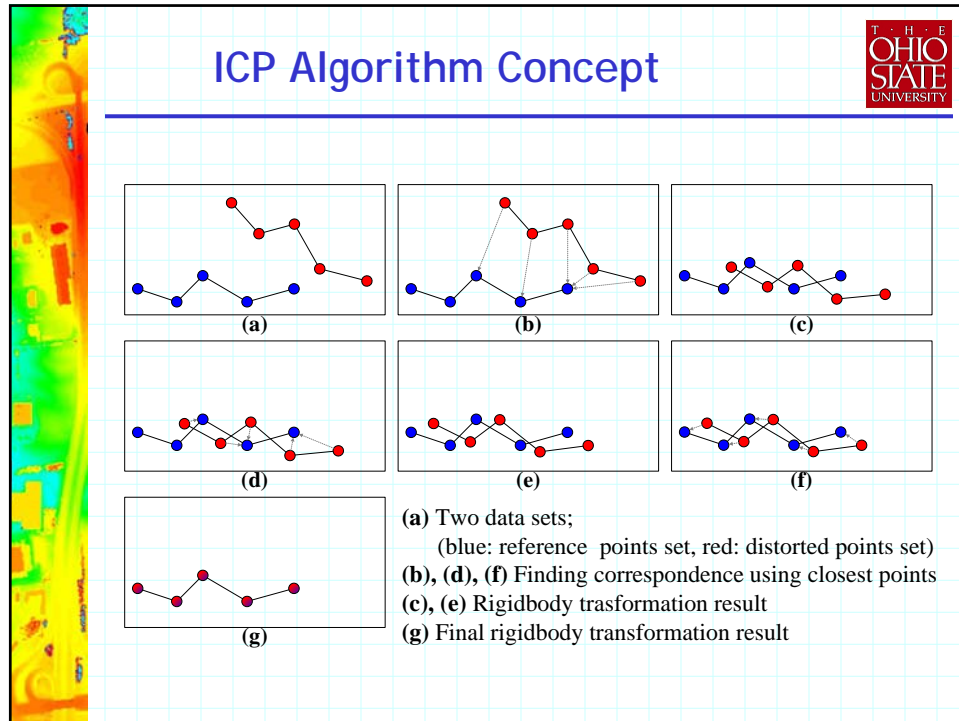
The ICP algorithm works in three phases:

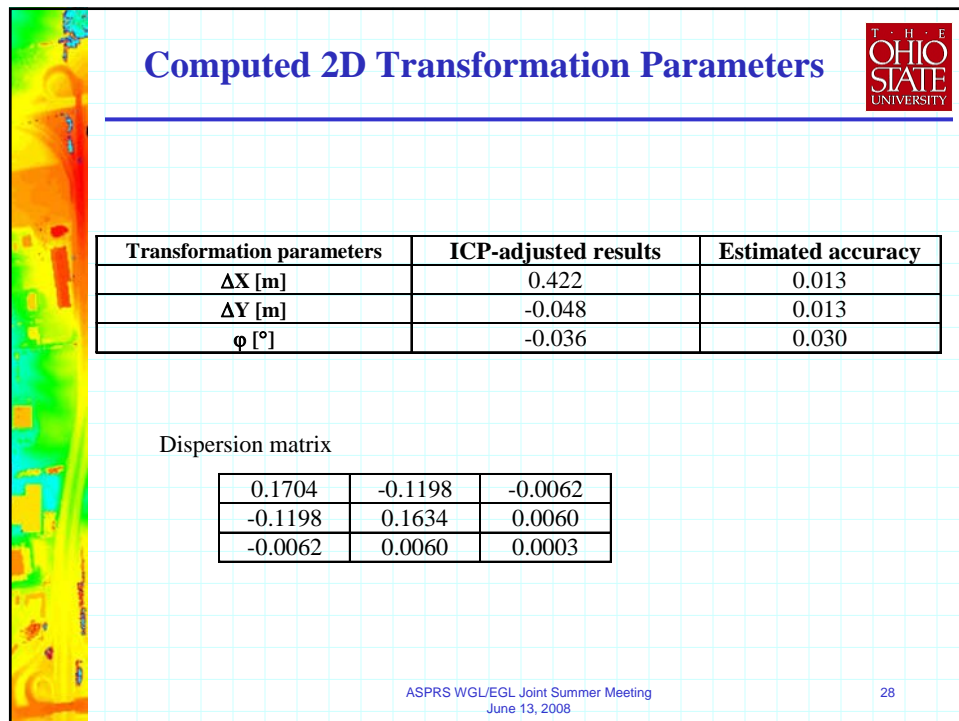
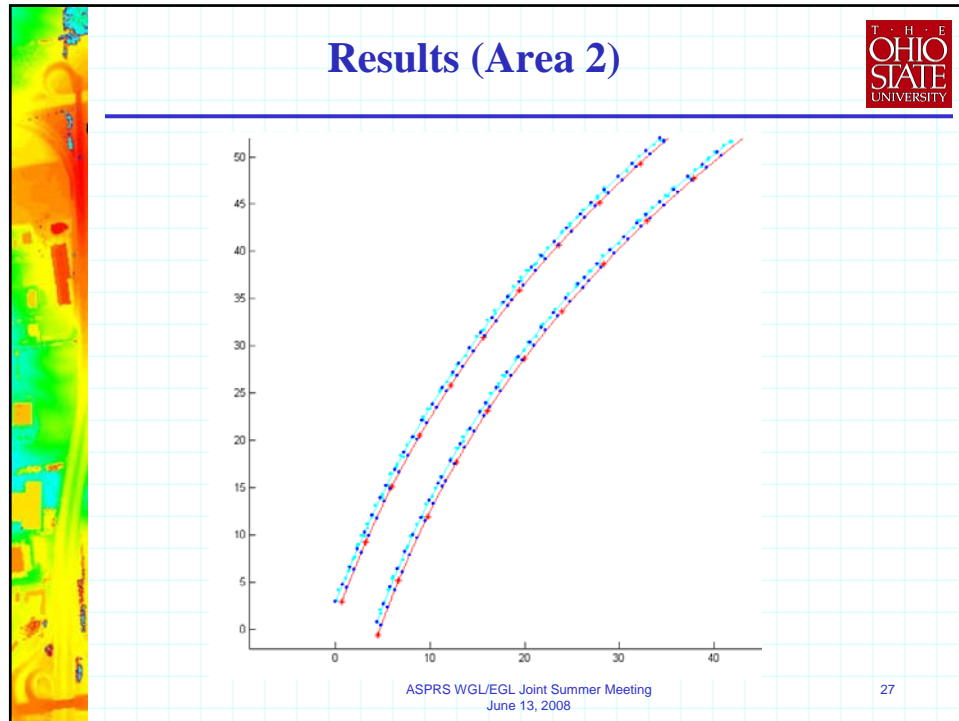
- 1) Establish correspondence between pairs of features based on proximity (for each point in D compute the closest point in M)
- 2) Estimate the rigid transformation that best maps the first member of the pair onto the second and then
 
$$\min_{(R,T)} \sum_i \|M_i - (RD_i + T)\|^2$$

Where  $R$  is a 2\*2 rotation matrix,  $T$  is a 2\*1 translation vector and subscript  $i$  refer to the corresponding points of the sets M (model) and D (data).
- 3) Apply that transformation to all features in the first structure, repeat steps 1-2 until convergence is reached

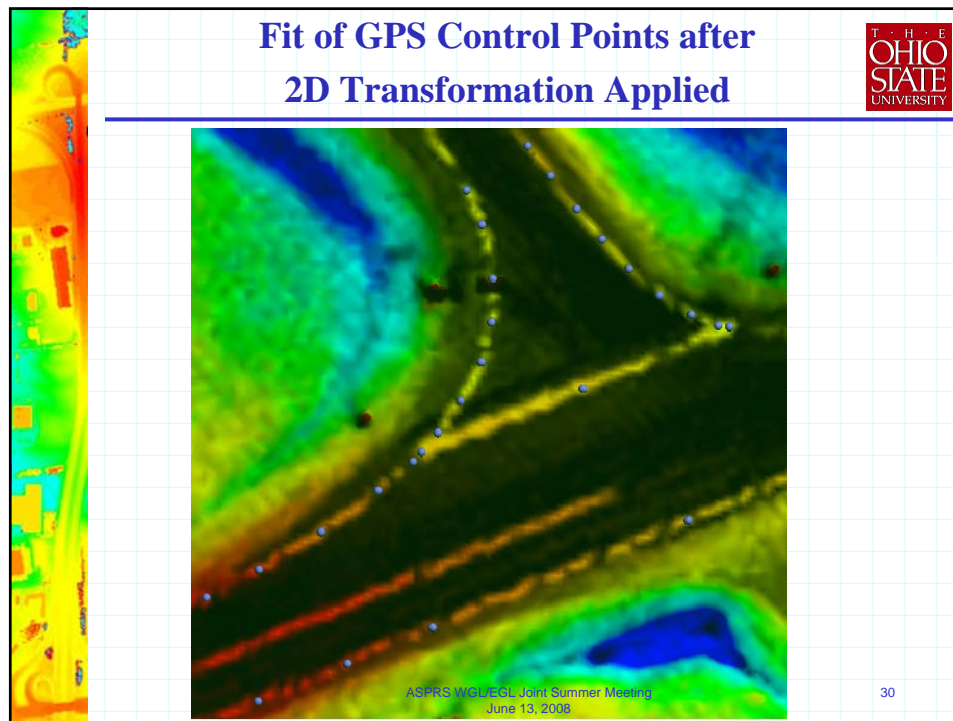
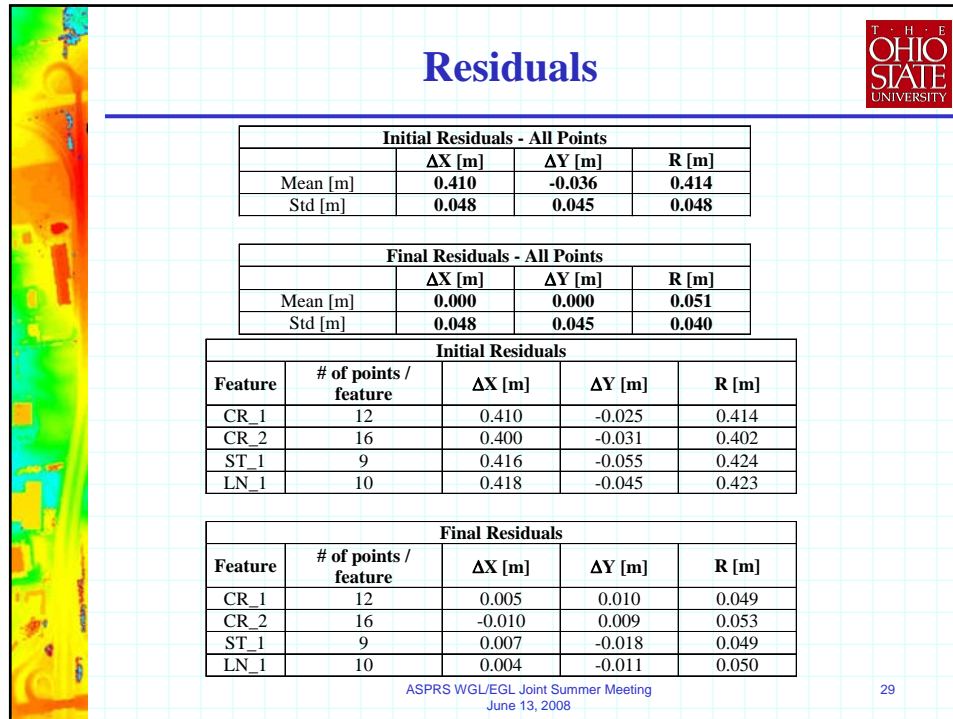
ASPRS WGL/EGL Joint Summer Meeting  
June 13, 2008

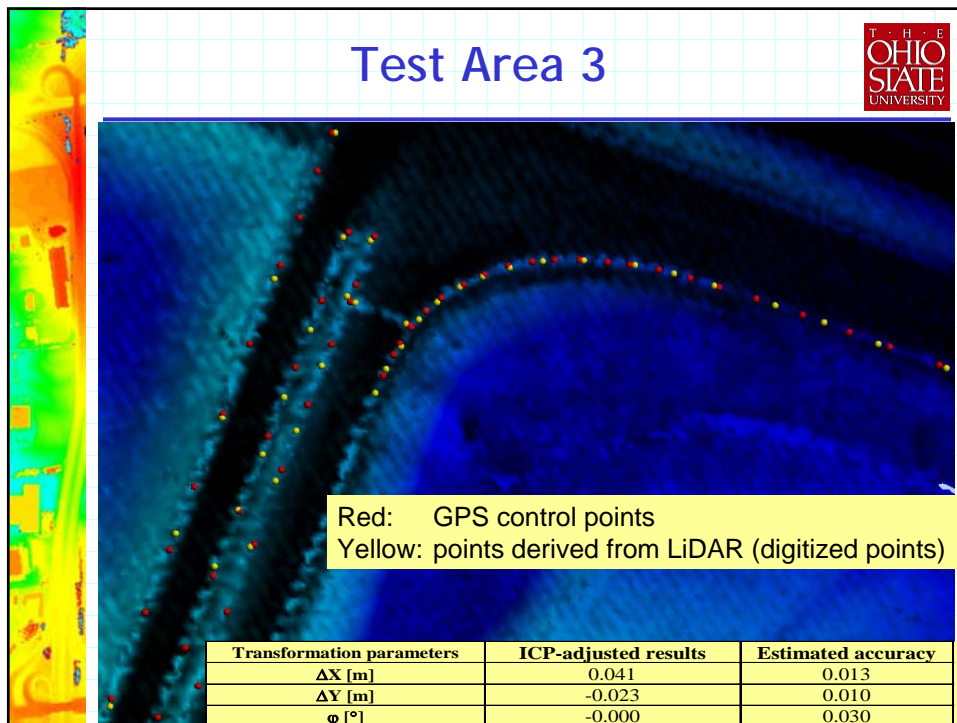
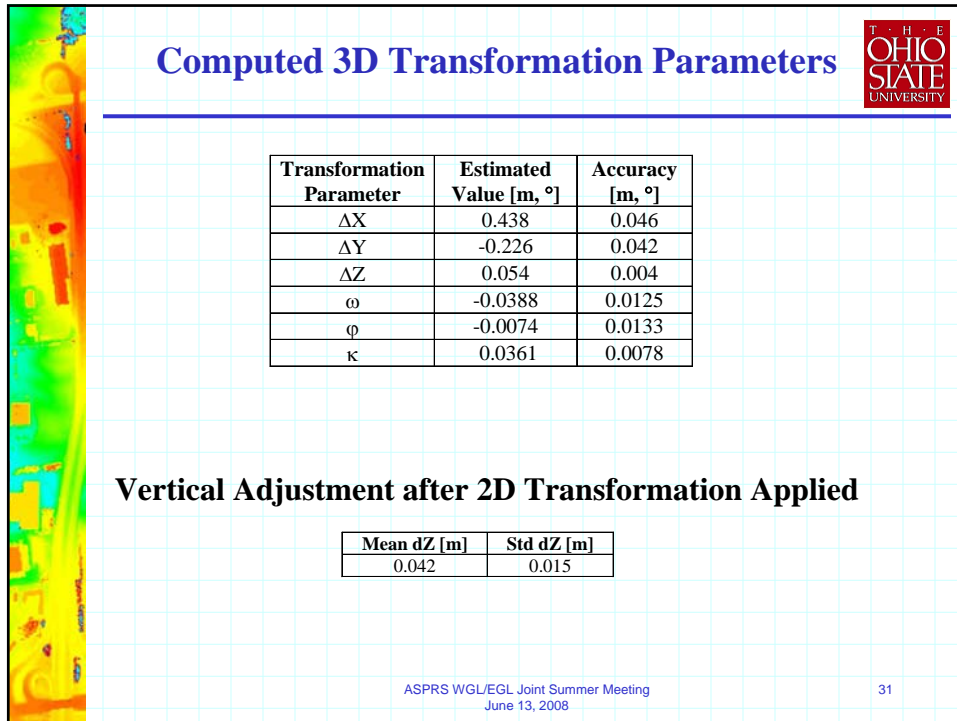
24











## ICP Performance Analysis (Area 2)



ICP input data	ICP-adjusted transformation parameters		
	$\Delta X$ [m]	$\Delta Y$ [m]	$\phi$ [°]
Both, LiDAR and GPS points are curve-fitted	0.153	-0.114	0.000
No fitting of LiDAR points, GPS points curve-fitted	0.150	-0.114	0.000
No fitting of GPS points, LiDAR points curve-fitted	0.158	-0.116	0.000

Case	Differences/Residuals							
	X [m]				Y [m]			
	Before		After		Before		After	
	mean	Std	mean	std	mean	std	mean	Std
1	0.16	0.02	0.00	0.02	-0.11	0.02	0.00	0.02
2	0.16	0.10	0.00	0.10	-0.12	0.09	0.00	0.09
3	0.16	0.02	0.00	0.02	-0.12	0.01	0.00	0.01

## OSU/GeoCue Interface



- ❖ GeoCue provides access to data from their environment (general LiDAR project management, import/export data, visualization/editing, point measurements, etc.)
- ❖ The communication between GeoCue and OSU is defined by the FMAS (Feature Matching and Adjustment System) protocol description.
- ❖ OSU linear feature extraction module is called from GeoCue
  - Command line executable is provided by OSU
  - Parameter passing is via XML format, including GPS-surveyed coordinates of the linear features, and their equivalent (virtual LiDAR points) determined by OSU
- ❖ The workflow is designed to seamlessly integrate manual and automated (OSU) feature extraction and matching
- ❖ The analysis of the transformation results is performed in the GeoCue environment
- ❖ If the correction of LiDAR data is needed, it will be executed in batch mode in GeoCue

## Conclusion



### **Using pavement markings as ground control should**

- ❖ **Improve both horizontal and vertical accuracy of the LiDAR data**
- ❖ **Provide a measure of the horizontal accuracy**
- ❖ **Result in shorter processing time that translates into faster delivery of the data to the end user**
- ❖ **Decrease, or eventually eliminate, the need for using LiDAR-specific ground targets in the vast majority of the projects, and thus, increase safety and efficiency of the survey personnel**
- ❖ **Improve the in-house understanding of the overall LiDAR data error budgets, and thus, help to advance ODOT mapping requirement and specification developments, and**
- ❖ **Result in reduced cost not only within map production, but for the users of the LiDAR data; the accuracy of the surface data will be better**



## **APPENDIX C**

### **FMAS Interface Design**

# LIDAR Featuring Matching & Adjustment System (FMAS) Project

GeoCue Interface Concept  
prepared for  
Office of Aerial Engineering,  
Ohio Department of Transportation

Revision 2.0

*Lewis Graham*  
GeoCue Corporation  
9668 Madison Blvd., Suite 101  
Madison, AL 35758  
256-461-8289  
April 07, 2007  
[www.geocue.com](http://www.geocue.com)

## Table of Contents

1	References.....	3
2	Introduction.....	4
2.1	Overview of the Integration Concept.....	4
2.2	The GeoCue Implementation Concept.....	5
2.3	Summary of the GeoCue SOW Tasks .....	6
3	System Concept Overview.....	7
3.1	Mission Planning .....	8
3.2	Data Acquisition .....	8
3.3	Initial Geocoding .....	9
3.4	Project Data Adjustment.....	10
3.5	FMAS Flow .....	12
3.6	Downstream Processing.....	15
3.7	Summary.....	15
4	Detail of Processing Steps .....	16
4.1	Control Feature Design (GeoCue, OAE).....	16
4.2	Control Feature Import and Display .....	16
4.3	Digitize Conjugate Features.....	16
4.4	Extract Conjugate Features (Phase II) .....	17
4.4.1	Interface .....	18
4.4.2	Input Data.....	19
4.4.3	Output Data.....	19
4.5	Conflation .....	20
4.5.1	Interface .....	22
4.5.2	Input Data.....	22
4.5.3	Output Data.....	23
4.6	Statistics Display, Generate Transformation Parameters.....	23
4.7	Apply Transformation Parameters.....	24
5	Issues/Discussion Points .....	25
5.1	Processing Order.....	25
5.2	Lack of Orthogonality between Horizontal and Vertical.....	25
5.3	Planimetric Dispersion.....	25
5.4	Feature Coding.....	26
5.4.1	Geometry.....	26
5.4.2	Feature Type .....	26
5.4.3	Topology.....	26
5.5	Data Formats.....	26
5.5.1	Features.....	27
5.5.2	Image Data .....	27
5.5.3	LIDAR Data.....	27
5.5.4	Coordinate Systems .....	27
5.5.5	Metadata.....	27
5.6	Software Interface.....	28
5.7	Distributable Architecture.....	28

6	Project Deployment and Schedule .....	29
7	Summary .....	30



## 1 References

1. *Airborne LiDAR Reflective Linear Feature Extraction for Strip Adjustment and Horizontal Accuracy Determination, PS-07-10, Center for Mapping, Ohio State University, August 15, 2006*
2. *Ohio Department of Transportation, Office of Aerial Engineering; Scope of Work for Feature Matching - GeoCue Integration, July 05, 2006*
3. *Quotation for Feature Matching – GeoCue Integration (Q07012402), GeoCue Corporation, January 24, 2007*

## 2 Introduction

The Office of Aerial Engineering (OAE) of the Ohio Department of Transportation (ODOT) is contracting with The Center for Mapping, Ohio State University (OSU) to develop LIDAR<sup>1</sup> Feature Matching Algorithms (FMA) for use in analyzing the relative and absolute horizontal accuracy of LIDAR data and performing subsequent adjustments based on these analyzes. While the algorithms can be generalized to full three dimensional analysis, the work associated with this project will be restricted to horizontal analysis and adjustment.

The Office of Aerial Engineering uses the commercial software package GeoCue with the application module, LIDAR 1 CuePac, as the data and algorithm management system for its LIDAR production operations. The OAE has contracted with GeoCue Corporation to have the Feature Mapping Algorithms integrated into their existing GeoCue LIDAR processing system to facilitate the use of these new algorithms directly and efficiently in day-to-day LIDAR production.

### 2.1 Overview of the Integration Concept:

GeoCue is a general purpose geospatial workflow management system that is designed to accommodate software tools from disparate vendors, integrating these tools into a common enterprise environment. It is an integration framework that provides high level features such as:

- Graphical display of processing elements (such as LIDAR sources, image data, etc.)
- Distributed file management
- Multiuser data access control
- Production auditing
- Dispatched/distributed processing of certain commands
- Checklist-driven production
- Direct user modification of workflow steps

The OAE uses GeoCue as the workflow manager for LIDAR data processing, data analysis and derivative product generation such as LIDAR orthos. The new LIDAR Feature Matching Algorithms are to be integrated into the existing workflow such that they can be seamlessly used by production operators from the GeoCue user interface. Figure 1 depicts the GeoCue interface showing an OAE LIDAR project in Ashtabula County, Ohio.

---

<sup>1</sup> Note that GeoCue consistently uses LIDAR (rather than LiDAR or lidar) as the acronym for Light Detection and Ranging. This is based on the fact that the original acronym for Radio Detection and Ranging was RADAR, not RaDAR.

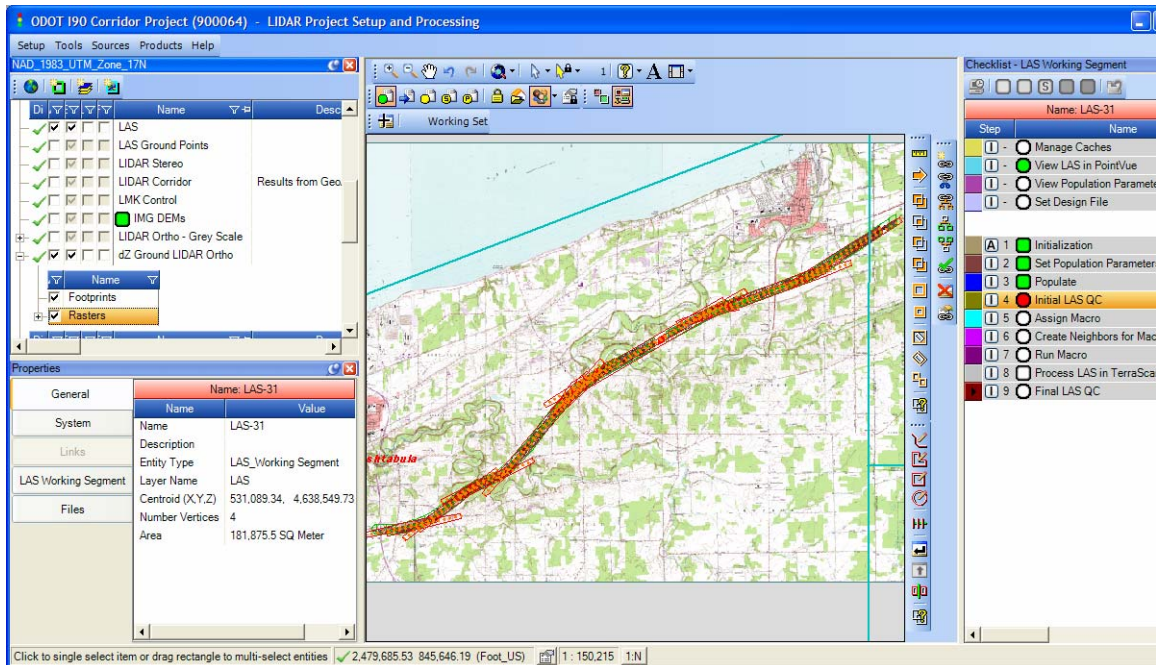


Figure 1 LIDAR project in GeoCue

The integration concept is to design a generalized interface within GeoCue that the researchers at the Center for Mapping can use to design the Feature Matching Algorithm interface. The second stage of development will be the integration and testing of the integrated system at both the Center for Mapping and the OAE.

The end result of this work will be a system that:

- Facilitates measuring horizontal control in LIDAR intensity images
- Generates statistical reports of the goodness of fit
- Provides the user the ability to adjust the LIDAR data horizontally to minimize the fit residuals<sup>2</sup>

## 2.2 The GeoCue Implementation Concept

Our approach to the integration task is to work closely with personnel at the Center for Mapping to mutually design a generalized interface for the OAE GeoCue system that will allow rapid integration of the Feature Matching Algorithms. The interface will be such that it can accommodate changes to software developed by the Center for Mapping without requiring further custom modifications to the core GeoCue software.

<sup>2</sup> As a matter of convenience, we will also include the ability to perform an absolute Z shift when applying the horizontal adjustments to the LIDAR data.

We will package the resultant GeoCue components of the software as a Commercial off the Shelf (COTS) “CuePac”, thus meeting the OAE’s requirement to support the resultant software under standard commercial software maintenance practices.

### **2.3 Summary of the GeoCue SOW Tasks**

GeoCue has been generally tasked with the following items under our components of the project:

1. We will conduct an on-site visit at either the Center for Mapping or the Office of Aerial Engineering (TBD) to develop the overall project plan. This initial meeting will be held as quickly as possible following authority to proceed<sup>3</sup>.
2. We will provide a preliminary Project Schedule within 45 days of authority to proceed.
3. We will develop a design concept for the generalized GeoCue program interface to be used in integrating the Feature Matching & Adjustment System (FMAS). This design concept will be reviewed with Center for Mapping staff and accepted comments will be incorporated into the design<sup>4</sup>.
4. We will take delivery of previously developed algorithms from the Center for Mapping to use as sample code for testing the GeoCue generalized program interface.
5. We will deliver an Initial Operational Capability (IOC) software delivery to the Center for Mapping that contains the generalized interface.
6. We will incorporate feedback from Center for Mapping personnel regarding the IOC delivery into a Final Operational Capability (FOC) system.
7. We will accept the initial delivery of the Feature Mapping & Adjustment System from the Center for Mapping and integrate these algorithms into the GeoCue system.
8. We will deliver the integrated product to the Center for Mapping and provide installation assistance via telephone conferencing.
9. We will incorporate feedback from the Center for Mapping into the final software version.
10. We will deliver the integrated software package to the Office of Aerial Engineering and provide the workflow portions of training (the Center for Mapping will provide algorithm use training). This will be a two day trip to the OAE.

---

<sup>3</sup> This meeting was held on April 12, 2007 at the Center for Mapping, OSU.

<sup>4</sup> This document

### 3 System Concept Overview

The general concept behind the Feature Matching and Adjustment System (FMAS<sup>5</sup>) is to use LIDAR return intensity images to extract two dimensional linear features. These extracted features are correlated with the LIDAR source strips (e.g. if the system is in strip extract mode, then feature  $k$  can be associated with Strip  $n$ ). Externally collected *control* features are fed to the algorithms as *targets*. Much as in aerial imaging block bundle adjustments, features that tie between strips can be used for relative adjustments whereas external control features can be used for absolute adjustment. While the algorithms developed by CFM can, in theory, be used for full three dimensional feature extraction and subsequent sensor modeling, this project will limit the implementation to detecting horizontal deviations and minimizing those deviations by horizontally adjusting the LIDAR data.

The OAE has an existing workflow procedure for relative adjustment using the Terrasolid<sup>6</sup> product, TerraMatch. TerraMatch, in concert with the LIDAR editing program TerraScan, provides capabilities for relative adjustment of LIDAR flight lines<sup>7</sup> as well as absolute vertical adjustments. It does not provide tools for absolute horizontal accuracy assessment and adjustment.

We recommend a two phase approach where the first phase introduces external control for absolute horizontal accuracy assessment and correction but uses interactively collected *match* features for analysis and adjustment. The second phase will add the automatic feature extraction algorithms being developed by the CFM. We are recommending this approach because the OAE has a desire to rapidly deploy a horizontal assessment/adjustment tool. This two phase deployment will allow OAE to deploy an interactive system early in the project and add the automatic feature extraction algorithms into the production flow when they become available.

The first phase deployment will include algorithms to match (*conflate*) hand-digitized image recognizable linear features<sup>8</sup> to externally provided control. The horizontal errors between the measured features and the control features are then used to set parameters of an adjustment algorithm (12 parameter transform with Z held fixed). Finally, this adjustment algorithm is applied to the LIDAR data to effect a correction. The application of the adjustment will be encoded in GeoCue to allow us to take advantage of distributed processing.

---

<sup>5</sup> We are not attempting to name the system – this is a place holder for this document.

<sup>6</sup> Terrasolid OY, Helsinki, Finland ([www.terrasolid.com](http://www.terrasolid.com))

<sup>7</sup> Most TerraMatch adjustments are on a pre-flight line basis. There is one adjustment that operates intra-line.

<sup>8</sup> While our emphasis is on linear features we believe the system should also include a provision for signaling LIDAR data with targets. These features would be polygons or attributed points.

The second phase of the project will incorporate automatic detection of match features to a set of control features by the CFM algorithms.

There are, of course, a number of issues and questions associated with these steps that will have to be decided. An initial discussion of these is provided in a separate section of this document.

An overview of the envisioned processing is contained in the following sections.

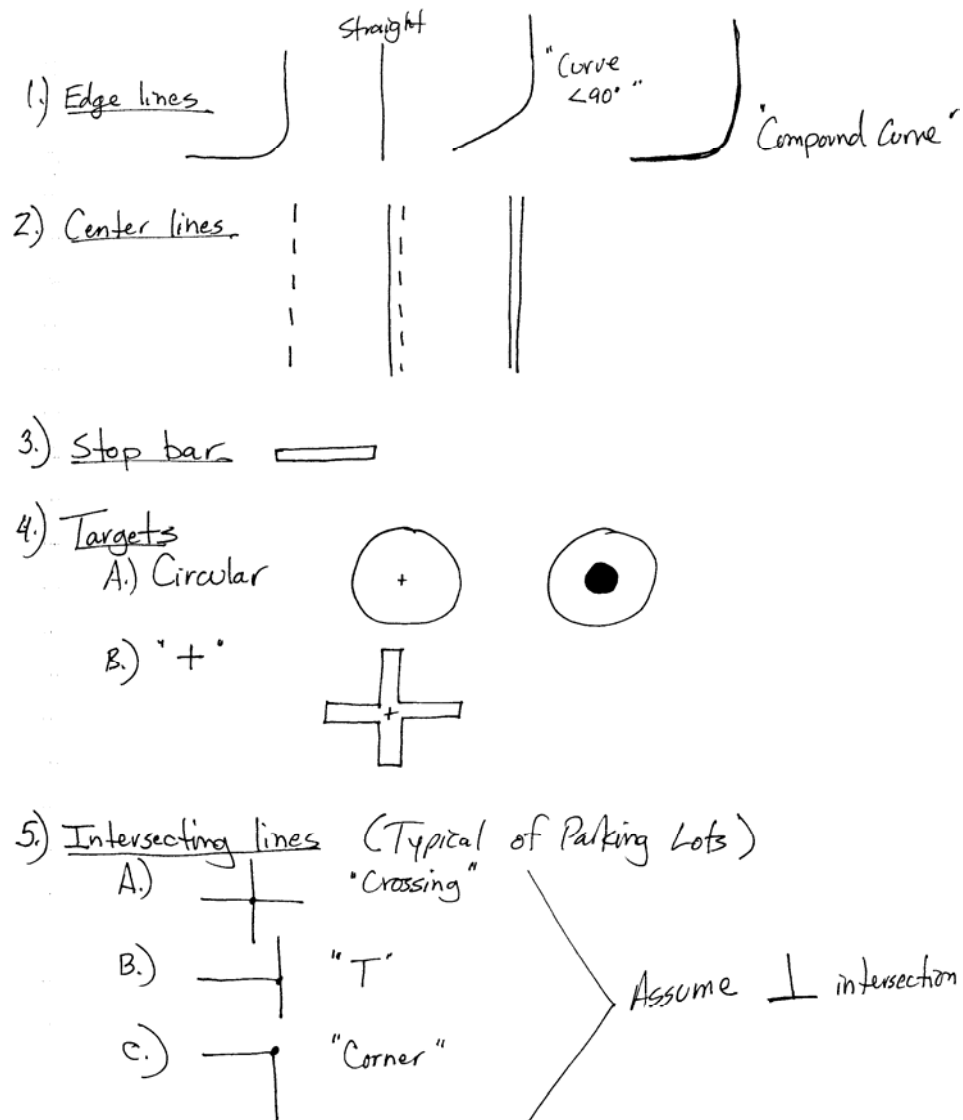
### **3.1 Mission Planning**

The first step in a project is planning the data collect. Note that this includes both the plan for aerial data acquisition (flying the LIDAR unit) as well as planning the collection of ground control. If the project is to be signalized then the location and schedule for target panels must also be considered.

### **3.2 Data Acquisition**

Data acquisition involves actually flying the LIDAR mission as well as collecting the planned ground control. Note that some projects may include signalized control. In this case targets must be placed prior to data collection. Surveying of control does not, of course, have to be done prior to the LIDAR acquisition but, in the case of targets, should be accomplished in a timely enough manner to reduce the risk of target disturbance between aerial acquisition and control acquisition.

Some examples of linear features that can be used for the FMAS are depicted in Figure 2. Note that part of this project will be devising a canonical method of encoding the descriptions of linear features.

Figure 2 Linear Feature Examples<sup>9</sup>

### 3.3 Initial Geocoding

Initial geocoding is the processing of raw laser pulse and time data to X, Y, Z tagged points. The processing is generally:

1. Reduction of GPS/IMU data (OAE uses the Applanix application POSpac for this process). This produces a Trajectory data set<sup>10</sup>.

<sup>9</sup> From John Ray's notes from the 24 January 2007 meeting at ODOT



2. Ensuring sensor calibration data are correctly set (lever arms, etc.)
3. Correlating/interpolating the Trajectory data to the time encoded laser data pulses to form a geocoded point cloud. Since OAE uses an Optech LIDAR unit, this process is conducted using the Optech proprietary software package REALM. These data are output in an industry standard file format (LAS), with one flight line per data file.

### 3.4 Project Data Adjustment

In the current OAE workflow, the LIDAR data are next checked (and adjusted, if necessary) for geometric accuracy using the Terrasolid package, TerraMatch. TerraMatch relies on vertical data for detecting data “block” anomalies but the adjustments are made in all three dimensions (X, Y and Z). TerraMatch uses a modeling approach rather than heuristic approach to data adjustment in that it incorporates a generalized sensor model of the LIDAR system. A heuristic system would simply attempt to adjust data based on a generalized mathematical model such as rational functions.

Figure 3<sup>11</sup> depicts a profile view of four overlapping LIDAR flight lines (each line being shown in a different color). Note that if the flight direction were from left to right, the major anomaly being depicted would be a pitch error (typically caused by a lever arm parameter error). Figure 4 shows the effect of corrections to the data.

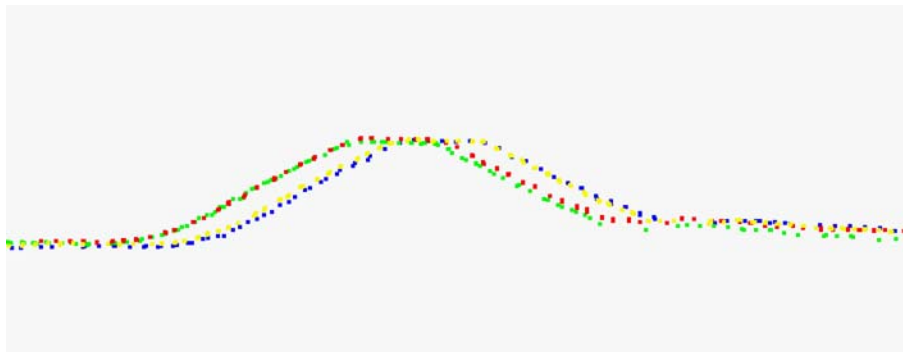
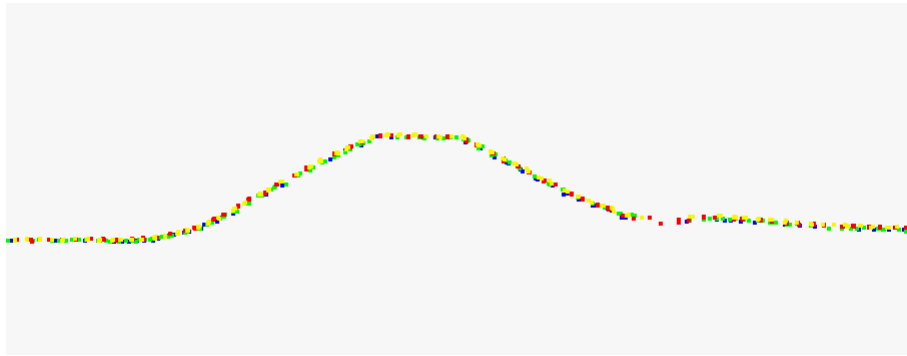


Figure 3 An uncorrected LIDAR profile

<sup>10</sup> For an Applanix system, this is a Smoothed, Best Estimated Trajectory (SBET) data set in the form of a disk resident file.

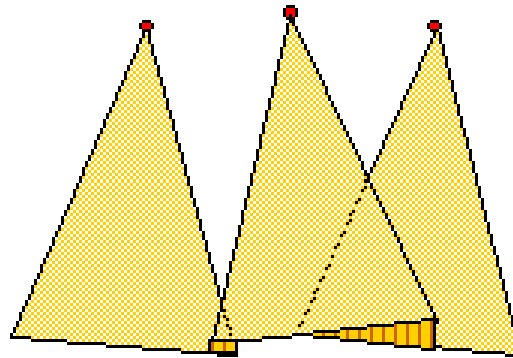
<sup>11</sup> A number of the figures in this section are taken from Terrasolid training material.



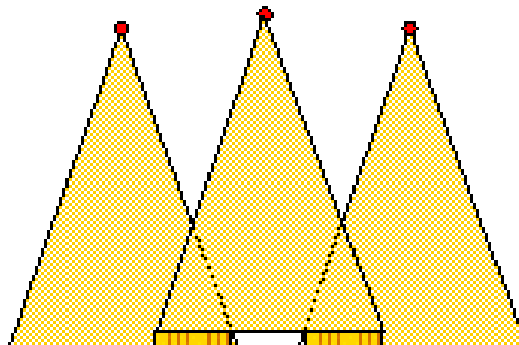


**Figure 4 After correction**

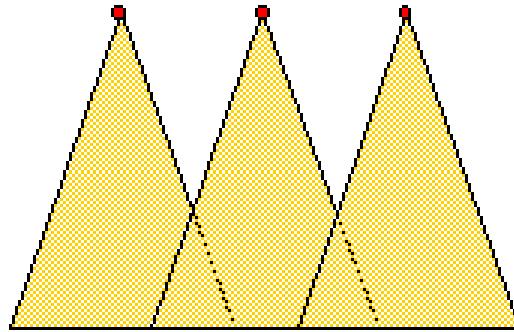
Figure 5, Figure 6 and Figure 7 depict the typical sequence of correcting a LIDAR lift using TerraMatch. Figure 7 depicts the relative Z correction of strips following correction for other factor (roll, pitch, yaw, etc.). Note that a final step is applied to the data in which all strips are corrected for absolute Z. This requires being able to identify at least 1 control point in the project.



**Figure 5 General multi-strip mission**



**Figure 6 Roll Correction**



**Figure 7 Strip-wise Z correction**

Note that after the above procedures have been applied, the data can still have a bias in X and Y (horizontal shift). Detecting and correcting such a potential horizontal shift is the crux of the FMAS.

It should be noted that, like aerial block adjustment algorithms, TerraMatch relies on overlapping data from multiple flight lines to measure anomalies in the geometry of the LIDAR data. Unfortunately, the strong component of measurement is in LIDAR strip side lap. While this works quite well for area projects, it can be a problem for the corridor flight patterns typical of transportation work.

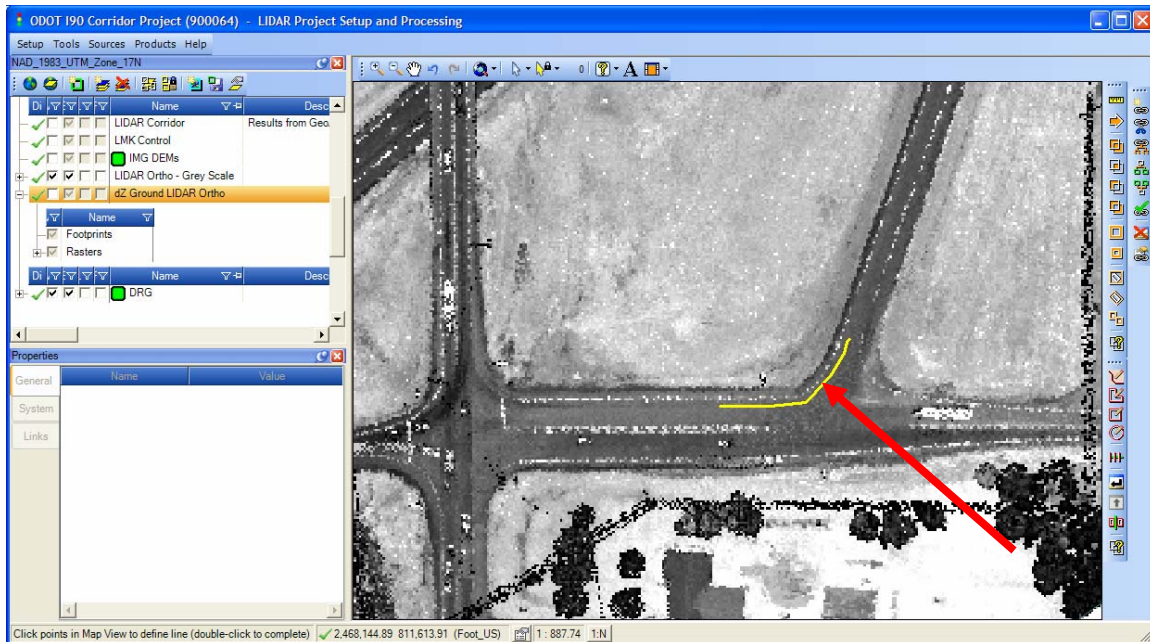
### **3.5 FMAS Flow**

This is the new section of processing that is used to measure and correct for horizontal shifts in the data. Whereas the corrections made using TerraMatch rely primarily on profile views of overlapping LIDAR data, the FMAS will rely primarily on LIDAR intensity. An example of a LIDAR intensity image is depicted in Figure 8.



**Figure 8 LIDAR Intensity example**

The general idea with FMAS is to compare known control features to LIDAR Intensity Image identifiable features. This is depicted (simulated) in Figure 9. Here the control (known measured feature) is shown as a yellow line. The matching LIDAR feature is the white line along the edge of pavement. This simulation shows that the LIDAR data are horizontally shifted up and to the left. In other words, if the LIDAR data were shifted down and to the right, the edge of pavement feature in the LIDAR data would overlie the control line.



**Figure 9 Simulation of a linear feature for FMAS**

The general flow for FMAS will be (all interactive operations are performed within the GeoCue Client Map View interface):

1. Generate LIDAR orthos
2. Import control features such that they display in the GeoCue Map View
3. Manually inspect each feature to ensure that a conjugate feature is present within the LIDAR data. (optionally) Remove features that are inappropriate for matching.
4. Pass control features to CFM algorithm for automatic extraction from the LIDAR Intensity Image. Note that GeoCue will also pass LIDAR patches that are bounding boxes of LAS data that enclose the feature.
  - a. Alternatively, a user could interactively digitize match features using GeoCue.
5. Receive back from CFM algorithms a set of conjugate feature definitions (one per intersecting strip) and goodness of fit parameters.
6. Graphically depict the conjugate features in the GeoCue Map View
7. Call a (CFM supplied) *conflation* algorithm that matches image derived features to the control features and provides fit statistics.
8. Provide a tabular list of the “goodness of fit” parameters (residuals)
9. Allow the user to compute the components of a *fit* matrix
10. Compute fit residuals in the statistics table
11. Allow user to iterate through the withhold, fit steps.
12. Apply corrections to the actual LIDAR data

### **3.6      *Downstream Processing***

Downstream processing is the normal TerraScan (or similar application) editing and product generation.

### **3.7      *Summary***

Note in the above scheme that the horizontal adjustment process slots into the current GeoCue workflow. In fact, a user could elect, based on a manual inspection, to bypass either vertical adjustment, horizontal adjustment or both.

## 4 Detail of Processing Steps

This section provides the initial details of the FMAS. It will be further definitized in detailed design notes.

### 4.1 Control Feature Design (GeoCue, OAE)

GeoCue and OAE will develop a standard for encoding the features to be used in FMAS. This will probably be an ASCII encoded text file<sup>12</sup> containing the information listed in Table 1. Note that we also need to handle *targets*. We will probably reserve special feature codes for targets that reference a target library.

Table 1 Feature Coding

<i>Feature ID</i>	<i>Parent ID</i>	<i>Feature Code</i>	<i>Coordinates</i>	<i>Notes</i>
A unique integer that identifies this feature	The feature ID of the parent feature if this is a child feature (0 if this is the top of the tree)	A text string (e.g. CURB) or a coding number to indicate the feature type	X,Y coordinate pairs that are in topographical order	

### 4.2 Control Feature Import and Display

A new command will be written for the FMAS GeoCue environment to import the control features. This import will create *entities* in GeoCue that will contain database attributes of the feature definitions. Users will be able to modify the display symbology of the features using the *Symbology* tool in Environment Builder.

### 4.3 Digitize Conjugate Features

Digitize conjugate (match) features will allow a user to digitize, from the GeoCue Map View, features in the LIDAR ortho image that match the input control features. This mode allows manual collection of features for generating matching statistics. This will be useful for the phase I deployment (prior to integration of the CFM feature extraction code) and for cases in which the automatic feature matching algorithms fail.

<sup>12</sup> We would prefer XML but this would require new workflows for the survey group of OAE.

This capability will function as:

1. The user digitizes a feature
2. The user *links*<sup>13</sup> the newly digitized feature to its control conjugate
3. A checklist step is executed on the digitized feature that attributes the feature based on its linked control feature

#### **4.4 Extract Conjugate Features (Phase II)**

The Locate Conjugate Features step passes the control features along with LAS extractions to the CFM automatic feature extraction routine. The Feature Extraction algorithms extract control conjugate features from these LAS data sets.

The Locate Conjugate Features function will operate in two modes:

1. Extract from LIDAR flight line
2. Ignore flight lines

The LAS data structure contains a Source ID field that is used to identify the source of each point within the LAS point cloud. When the data are first generation merged data from LIDAR flight lines, the Source ID represents the flight line number. In the flight line extraction mode, the extraction code will treat each flight line independently, providing an extracted feature per Source ID. This mode is used to enable relative horizontal accuracy analysis.

In the *ignore flight line* mode, the extraction algorithm will not differentiate between flight lines, treating an LAS source as homogeneous. This mode is used when relative accuracy is not needed or when the density of the LIDAR data is not sufficient, when used in single strip mode, to support feature extraction.

Note that we have divided the feature extraction operations into two distinct executable programs; Extraction and Conflation. This differentiation allows the same conflation code to be used regardless of the source of the extracted features (interactive digitizing or automatic feature extraction).

The general feature extraction sequence is as follows:

1. Linear features are extracted from the LIDAR data using well known image extraction techniques. These features would have to be encoded as to the source ID (SID) of the LIDAR flight line from which they originated. We assume that the resultant features would be hierarchically connected (Figure 10). These algorithms would function totally within the CFM segments of code. The techniques for actual feature extraction will be documented by CFM and thus are not part of this design concept document.

---

<sup>13</sup> GeoCue contains an *associativity* system that will be used for this operation



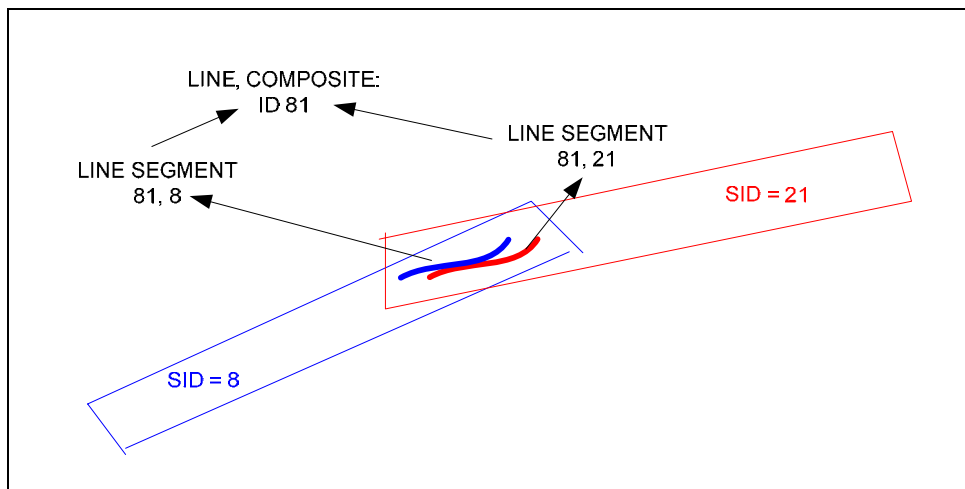


Figure 10 Composite Linear Feature

2. The CFM feature extraction code will pass back to the GeoCue:
  - a. Composite line definitions
  - b. Adjustment parameters for each flight line
  - c. Residuals
3. GeoCue will display the extracted line segments. We assume that these would be feature coded in some manner as to type of feature (center line stripe, edge of pavement and so forth)

#### 4.4.1 Interface

The interface to the feature extraction routine will be via command line. The exact specification will be defined in a design note but the general format will be:

##### *ExtractFeatures*

<b>-s</b>	This flag indicate strip-wise extraction. If not present, extraction will be aggregated
<b>-l "Control library path"</b>	Full path to the control feature library
<b>-i "LAS input path"</b>	Full path to the input LIDAR data (LAS files). May be repeated <i>n</i> times where <i>n</i> is the number of LAS files from which to extract features
<b>-c "control path"</b>	Full path to a control feature definition file
<b>-o "output path"</b>	Full path to the location/filename for the output feature(s)

Note that our scheme is to call the function (actually an executable program) for each feature rather than to pass a collection of features. This method will allow distributed processing of the extraction process.

#### 4.4.2 Input Data

The input data are defined in Table 2:

**Table 2 Extract Features Input Data**

<i>Data</i>	<i>Mode</i> <sup>14</sup>	<i>Format</i>	<i>Notes</i>
Control Feature Library	R	XML (content to be defined by GeoCue and OAE)	This file contains the definitions of all of the standard features used within the FMAS project.
LIDAR data files	R	LAS 1.0	This is an extraction of project data in a buffered region surrounding the control feature. The size of the buffer is defined in the Control Feature Library. If more than one file is passed, the CFM code must merge the files prior to extraction.
Control Feature file	R	XML – format to be determined by GeoCue and CFM	This file defines the specific instance of a control feature that is to be extracted from the LAS data.

#### 4.4.3 Output Data

The input data are defined in Table 3

**Table 3 Extract Features Output Data**

<i>Data</i>	<i>Mode</i>	<i>Format</i>	<i>Notes</i>
Extracted Feature file	C	XML – format to be determined by GeoCue and CFM	This file contains the extracted feature(s)

The extracted feature will contain both the feature definition (for example, the X, Y, Z coordinates of nodes) as well as the goodness of fit statistics. For example, if the extracted feature were a line string composed of a set of X, Y, Z coordinates, the output would also include the variance of each node as well as the overall fit statistics.

<sup>14</sup> C = Created by this function (implies Write), W = Write access, R = Read access

Note that the process of *matching* an extracted feature to a control feature will be available as a separately callable CFM routine. This *Conflation* routine (see next section) will allow the FMAS to use digitized features in lieu of automatically extracted features for generating horizontal fit statistics.

The format of the extracted feature data are to be determined by GeoCue and the Center for Mapping. Some general ideas are discussed in the following chapter.

## 4.5 Conflation

In general, conflation is the process of merging data sets from multiple sources where the features to be merged generally are not identical. This is a common operation for merging high resolution map insets into a lower resolution map and maintaining correct topography. The process involves matching two sets of features where the geometry of the match features is not the same.

In the FMAS, *conflation* refers to the process of matching extracted features to control features through a solid body transformation (TBD). The result (output) of the conflation is a set of matching transformations as well as the fit statistics.

It is important to note (and this may entail additional discussions between CFM and GeoCue) that we consider the process of statistically extracting a conjugate feature and the conflation process to be two distinctly separate operations with different sets of statistics. In the case of feature extraction, the returned statistics may mean how well the extracted raw feature data (say intensity pixels) map to a predefined geometric shape (for example, a curve). This is illustrated in Figure 11. Note that the *location* of the control feature did not come into play in this segment of modeling, only the characteristic of the feature. Thus the statistics here would mean how well the extracted pixels match the geometric constraint of the control feature.

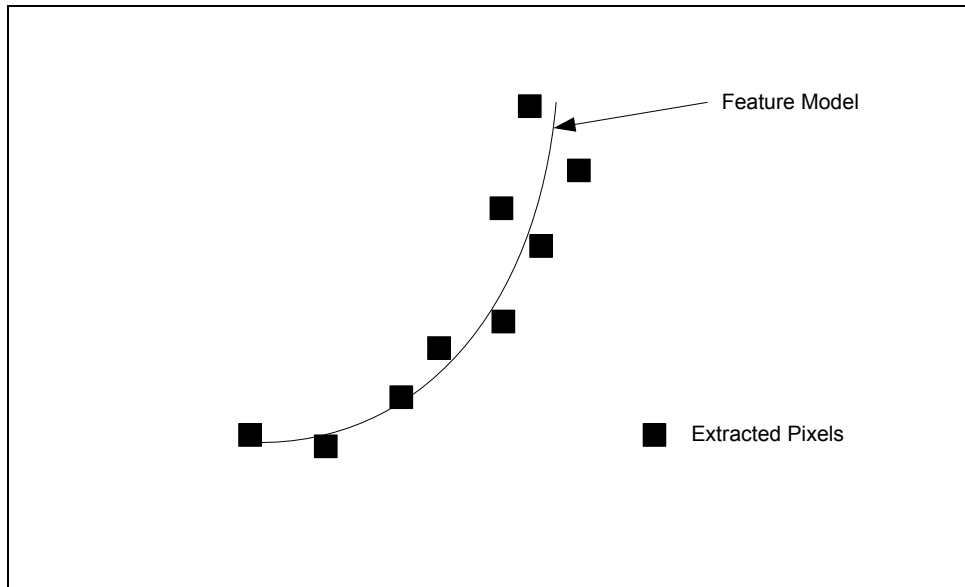


Figure 11 Fitting to a feature model

Figure 12 illustrates the *conflation* process. Here an extracted conjugate feature is being matched to the control feature. The statistics on this fit are quite different that those associated with the actual feature extraction. Here the statistics relate to the goodness of fit following a rigid body transformation (for example).

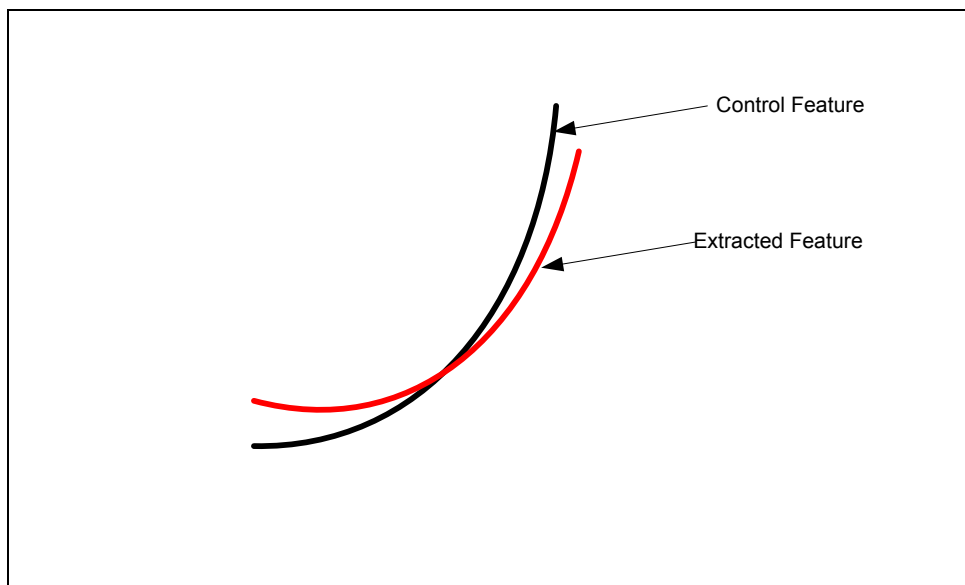


Figure 12 Comparing the extracted feature to the control feature

### 4.5.1 Interface

The interface to the conflation routine will be via command line. The exact specification will be defined in a design note but the general format will be:

#### *Conflate*

**-l** "*Control library path*" Full path to the control feature library  
**-c** "*control path*" Full path to a control feature definition file  
**-f** "*feature path*" Full path to the extracted feature file  
**-o** "*output path*" Full path to the location/filename for the output file

Note that our scheme is to call the function (actually an executable program) for each feature rather than to pass a collection of features. This method will allow distributed processing of the conflation process.

### 4.5.2 Input Data

The input data are defined in Table 2:

**Table 4 Extract Features Input Data**

<i>Data</i>	<i>Mode</i>	<i>Format</i>	<i>Notes</i>
Control Feature Library	R	XML (content to be defined by GeoCue and OAE)	This file contains the definitions of all of the standard features used within the FMAS project.
Control Feature file	R	XML – format to be determined by GeoCue and CFM	This file defines the specific instance of a control feature that is to be conflated with the extracted feature
Extracted Feature file	R	XML – format to be determined by GeoCue and CFM	This file defines the specific instance of an extracted feature that is to be conflated with a control feature

### 4.5.3 Output Data

The output data are defined in Table 5

**Table 5 Conflation Output Data**

<i>Data</i>	<i>Mode</i>	<i>Format</i>	<i>Notes</i>
Conflation parameters and Statistics	C	XML – format to be determined by GeoCue and CFM	This file contains the conflation parameters and fit statistics

The format of the conflation data are to be determined by GeoCue and the Center for Mapping. Some general ideas are discussed in the following chapter.

## 4.6 Statistics Display, Generate Transformation Parameters

GeoCue will provide a tabular display of the conflation statistics. This display will allow a user to examine both relative and absolute horizontal fit residuals and withhold features from the fit operations. This section of the FMAS will also generate the transformation parameters.

FMAS will allow a global adjustment of the horizontal and vertical components of data via a 12 parameter transformation matrix as depicted in Table 6.

**Table 6 Global Adjustment Matrix**

$C_{0,0}$	$C_{0,1}$	$C_{0,2}$	$C_{0,3}$
$C_{1,0}$	$C_{1,1}$	$C_{1,2}$	$C_{1,3}$
$C_{2,0}$	$C_{2,1}$	$C_{2,2}$	$C_{2,3}$
$0$	$0$	$0$	$1$

For the FMAS system, all parameters in Z except the Z translation term ( $C_{2,3}$ ) will be zero. The user interface will allow input of a constant Z shift. This provides the ability to adjust the absolute vertical bias of the data set.

The adjustment interface will be similar to the current Entity Manager interface (Figure 13). This interface has a two-way connection with graphics in the GeoCue Map View. Selecting in the Map View causes rows in Entity Manager to select and selecting rows in Entity Manager causes the associated graphic elements to become selected in the Map View.

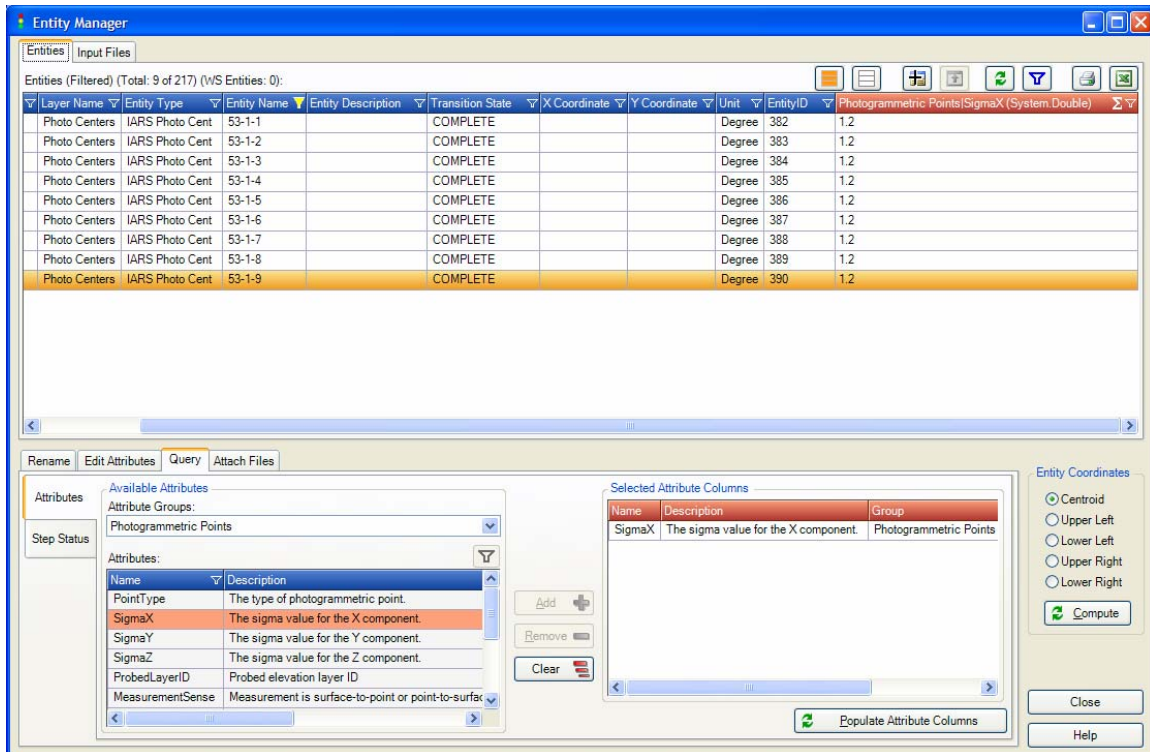


Figure 13 Example List view in GeoCue

## 4.7 Apply Transformation Parameters

This final step in the FMAS flow applies the transformation of Table 6 to all LIDAR data in the project. It will be possible to use the Command Dispatch System within GeoCue to distribute this processing across multiple processing nodes.

## 5 Issues/Discussion Points

This section contains, in no particular order, a list of issues and discussion points that the FMAS team will have to decide.

### 5.1 *Processing Order*

The geometric correction of LIDAR data involves corrections in three dimensions. The FMAS addresses horizontal corrections only. This raises the question of processing precedence – is vertical corrected prior to horizontal or vice versa? This is coupled with the next issue; the fact that horizontal and vertical are correlated.

The FMAS implementation will that the data are fully adjusted *relatively* using TerraMatch (or some other tool) and then the horizontal corrections are applied using FMAS. We also permit absolute Z to be adjusted as part of the FMAS transformation.

### 5.2 *Lack of Orthogonality between Horizontal and Vertical*

Obviously the horizontal and vertical components of adjustment of LIDAR data are highly coupled. For example, a shift in X, Y or both moves a sample horizontally with respect to the measurement location. If the terrain is not level, the Z accuracy is effected. Obviously the proper way to address this problem is a simultaneous adjustment of X, Y and Z using a rigorous sensor model. This is just an observation – no action is required.

### 5.3 *Planimetric Dispersion*

The uncertainty of location of a LIDAR “point” is much larger in X, Y than in Z for near nadir returns. This effect is caused by beam divergence. The effect of this for LIDAR intensity images is similar to low pass filtering. This means that the spatial resolution of the horizontal components of the LIDAR “pixel” will be limited regardless of increases in LIDAR coverage density. The primary factors affecting spot size are flying height and off-nadir angle.

The summary of this point is that beam divergence may provide an effective Ground Sample Distance of  $d$  for a given flying height that cannot be improved by increasing the scan rate of the sensor or decreasing the forward velocity of the sensor platform.



## 5.4 *Feature Coding*

We think it will be very important to include feature coding in the system. By this we mean the inclusion of attributes with the linear features. The important attributes (at least initially) appear to be:

### 5.4.1 *Geometry*

Geometry indicates the geometric description of the feature. It seems that we need to encode the basic geometry type (we think we should include: point, 2D line, 3D line and perhaps polygon for certain target panels).

### 5.4.2 *Feature Type*

Feature type is the name of the object physically represented by the feature. Examples might be:

1. Edge of Pavement
2. Center line, single stripe
3. Top of curb
4. LIDAR Target, Type 205

We can expand the attributes as needed. It seems that it would be ideal to use existing DOT feature codes, if possible.

### 5.4.3 *Topology*

*Topology* provides the relationship of one feature to another. We need this to identify the segments of the same *parent* feature in two or more LIDAR strips. GeoCue contains an associativity system that can be used to accomplish this at the GeoCue level. We will need to devise a simple coding scheme to convey this to the CFM routines.

## 5.5 *Data Formats*

Data format is how we convey information back and forth between the GeoCue sections of code and the CFM sections. We propose the following:

### 5.5.1 Features

Based on a meeting held on April 12, 2007 at the Center for Mapping, the feature definition scheme was changed from Shape to XML. GeoCue will work with CFM to define the schema for these data. The general content will be:

- Descriptor (e.g. Line, Curve, Polyline, etc.)
- Coordinates
- Feature Code
- Feature ID
- Parent ID (0 if no parent is associated)
- Statistics (e.g. if this is a control feature that has been RTK collected as point nodes, then the statistics are  $\sigma_x$ ,  $\sigma_y$ ,  $\sigma_z$  for each node)
- Standard buffer zone - if this is a control feature, the standard distance for a buffer for LIDAR data

### 5.5.2 Image Data

Tiled TIFF with tfw files

### 5.5.3 LIDAR Data

LAS 1.0. Note that the LIDAR data passed to CFM algorithms will have mixed flight line data in each file. Individual flight line can be determined on a per-point basis by LAS coding bits.

### 5.5.4 Coordinate Systems

While GeoCue will support a mixed configuration of coordinate systems within a project, we propose that features and image data be transformed to a common system (within GeoCue) prior to passing to the CFM algorithms.

### 5.5.5 Metadata

We propose passing metadata such as statistics tables as extensible markup language (XML) files with schemas defined by the project needs.

### **5.6      *Software Interface***

GeoCue contains a generalized ability to call executable programs that use a scheme of command line parameters passed at invocation time, for example:

```
Cmd.exe -r"801", -if "\\Cyclops\data\histogram.xml", -of "\\Ulysses\output\stats.xml",  
...
```

We recommend that all interfaces between GeoCue and the CFM algorithms be of this form. This will allow the OAE to reconfigure the deployed system without the need to resort to programming.

### **5.7      *Distributable Architecture***

Wherever possible, executable programs should be designed such that they can participate in distributed (parallel) processing schemes. Parallel processing can be completely handled by GeoCue if the executable program is designed such that it does not need to span operations across multiple entities.

## 6 Project Deployment and Schedule

We recommend a multiphase deployment as recommend in Table 7:

**Table 7 Project Schedule**

<i>Phase</i>	<i>Capability</i>	<i>Deliverables</i>
GeoCue I	<ul style="list-style-type: none"> <li>• Ability to import control features</li> <li>• Ability to digitize conjugate features</li> <li>• Ability to construct a set of transform statistics based on the <i>conflation</i> call to CFM code</li> <li>• Ability to apply a transform to the LIDAR data</li> </ul>	GeoCue FMAS CuePac, IOC
CFM I	<ul style="list-style-type: none"> <li>• GeoCue-CFM Interface</li> <li>• Conflation algorithm</li> <li>• Passing (from CFM to GeoCue) a conflation results XML file</li> </ul>	CFM IOC
CFM II	<ul style="list-style-type: none"> <li>• Ability to extract 2D linear conjugate features from LIDAR data based on a control feature</li> </ul>	CFM, GeoCue FOC

## 7 Summary

In today's LIDAR data processing as implemented at the OAE, the ability exists to:

- Perform a quick assessment of relative LIDAR accuracy (GeoCue dZ images)
- Perform a quick assessment of absolute Z accuracy if control are available (GeoCue Z Probe and/or TerraScan)
- Perform a relative data adjustment in three dimensions (TerraScan)
- Perform an absolute vertical data adjustment (TerraScan)

The capability that is missing is the ability to assess and adjust the absolute horizontal accuracy of the LIDAR data. The new GeoCue-CFM system will provide a solution to this deficit. This capability will be delivered early in the project as a manual system. It will be followed by the CFM algorithms to automatically extract conjugate features to the supplied control features.

The delivered system will be fully integrated with the OAE workflow system that is in place today, minimizing the need for training outside of the operations of this inserted capability. This means that the OAE can expect to be immediately productive with enhanced metric accuracy.

## ACRONYMS

AOI	Area of Interest
CC	Custom Code
CCB	Configuration Control Board
CFM	The Center for Mapping (of the Ohio State University)
CI	Custom Integration (refers to setting up system components using Environment Builder)
CIR	Color Infrared – typically the NIR band, the Blue band and the Green band (i.e. the Red band of RGB is replaced by the NIR band).
CM	Change Management
CORS	Continuously Operating Reference Station
CORS96	NAD83(CORS96) A version of the NAD83 reference system – has a direct mathematical mapping to ITRF
COTS	Commercial-off-the-Shelf
CR	Change Request
DEM	Digital Elevation Model – see DTM
DSM	Digital Surface Model – first surface (rooftops, trees, ...) elevation model
DTM	Digital Terrain Model – typically a terrain model of bare earth
ECO	Engineering Change Order
FMA	Feature Matching Algorithms
FMAS	Feature Matching and Adjustment System
FOC	Final Operational Capability
GPS	Global Positioning System
GUI	Graphical User Interface
IMS	Inertial Measurement System – combines an IMU with a computer to provide an interpolated navigation system. Applanix and Leica add a GPS receiver to reduce drift errors and provide X, Y, Z reset. These systems are called “Aided IMS”
IMU	Inertial Measurement Unit – provide roll, pitch, yaw and (usually) X, Y, Z accelerations.
INS	Inertial Navigation System – see IMU
IOC	Initial Operational Capability
ITRF	International Terrestrial Reference Frame

---

JPEG	Joint Photographic Expert's Group, a standards group for image compression. Note: JPEG typically refers to the (old but most common) discrete cosine transform algorithm whereas JPEG2000 refers to the (new) wavelet-based compression algorithm. The two formats are not interchangeable.
LL	Lower Left
LR	Lower Right
LUT	Look-up Table
MABR	Minimum Area Bounding Rectangle – An MBR rotated such as to form the minimum area necessary to enclose an object by a rotated rectangle.
MBR	Minimum Bounding Rectangle (always aligned to the coordinate system)
NAD	North American Datum
NIR	Near-Infrared
OAE	Office of Aerial Engineering (of the Ohio Department of Transportation)
ODOT	Ohio Department of Transportation
OSU	The Ohio State University
QC	Quality Check
RGB	Red-Green-Blue
RRDS	Reduced Resolution Data Sets (same as Image Overviews or Image Pyramids)
RTK	Real Time Kinematic
SID	Source Identifier
TEC	Topographic Engineering Center (of the United States of America, Army Corps of Engineering)
TIFF	Tagged Image File Format
TIN	Triangulated Irregular Network (this is a generic term. There is no common, interchangeable TIN standard)
TR	Trouble Report
TTN	Triangulated Topographical Network – A proprietary, closed Intergraph TIN format
TTC	Tonal Transfer Curve – a lookup table to convert <i>n</i> bit data to <i>m</i> data. For example, to convert 12 bit per pixel image data to 8 bit per pixel image data. These curves generally build in contrast and gamma correction.

UL	Upper Left
UR	Upper Right
USACE	United States Army Corps of Engineering
WGS-84	World Geodetic System of 1984
XML	Extensible Markup Language





## **APPENDIX D**

### **Software Developments (Included only in the digital version)**

1. Matlab macros used to implement all the functions developed in this project
2. CurveFitting, ICP and PavementExtraction Processing Software, User's Manual
3. Microsoft VC++ source code
4. Java source code used to implement XML data conversion

## APPENDIX D

### D.1. Matlab code for pavement extraction

The basic program input and output definition is provided in Table A.1.

<b>Pavement marking extraction (PavMarkExtract_main)</b>	
<b>Input</b>	<ul style="list-style-type: none"> <li>• LiDAR strip points</li> <li>• Control point</li> <li>• Boundary value</li> <li>• Threshold for residuals</li> <li>• Threshold for mean residuals</li> <li>• Intensity step</li> </ul>
<b>Output</b>	<ul style="list-style-type: none"> <li>• Selected Lidar pavement marking points</li> </ul>
<b>Embedded macros/functions</b>	<ul style="list-style-type: none"> <li>• BoundaryExtract.m</li> </ul>

Table D.1: Program input/output specification.

## D.2. Matlab code for for ICP-based matching, curve fitting and QA/QC computation

The basic program input and output definition is provided in Table A.2.

<b>Main program (ICP_MAIN)</b>	
<b>Input</b>	<ul style="list-style-type: none"> <li>• Control points</li> <li>• Extracted LiDAR pavement marking points</li> </ul>
<b>Output</b>	<ul style="list-style-type: none"> <li>• Transformation parameters between control points and extracted LiDAR pavement marking points:               <ul style="list-style-type: none"> <li>○ Local shift</li> <li>○ Global shift</li> <li>○ Rotation angles</li> <li>○ Rotation matrix 3x3</li> </ul> </li> <li>• Statistics:               <ul style="list-style-type: none"> <li>○ Aposteriori dispersionmatrix of transformation parameters</li> <li>○ Residuals: original and final, mean and standard deviation</li> </ul> </li> </ul>
<b>Embedded macros/functions</b>	<ul style="list-style-type: none"> <li>• transform2D</li> <li>• iterative_adjustment_transform2D</li> <li>• curve_fit</li> <li>• ItCPmultiplecurves_measofconv_ends_checkrange_</li> <li>• resolution_curve</li> <li>• search_np</li> <li>• eukldist</li> <li>• nearestpoint_ends_search_checkrange</li> <li>• pcf2</li> <li>• pcf2_controls_valueconstraint</li> <li>• pcf2_linearinterpolation</li> <li>• residuals</li> </ul>

Table D.2: Program input/output specification.